RADC-TR-69-253
Final Technical Report
September 1969

NANOSECOND RADAR - OVERSIZE WAVEGUIDE SYSTEM (NAROWS)

General Electric Company

Rome Air Development Center
Air Force Systems Command
Griffiss Air Force Base, New York

NANOSECOND RADAR - OVERSIZE WAVEGUIDE SYSTEM (NAROWS)

C. Younger
J. P. Quine
J. W. Maurer
A. E. Blume
General Electric Company

FOREWORD

The work described in this report was performed by Cousby Younger, John P. Quine, John W. Maurer, Alan E. Blume and Theodore W. Dietze at the Research and Development Center of the General Electric Company in Schenectady, New York, under Contract F30602-69-C-0066, Project 4506, Task 450602. The period covered was 15 October 1968 to 15 May 1969. The work was administered under Requisition No. EH 61747 of the Heavy Military Electronics Systems of the General Electric Company in Syracuse, New York. Mr. Frank E. Welker and 1st Lt Tracy B. Gardner III (EMATP) were the Rome Air Development Center project engineers.

This technical report has been reviewed by the Office of Information (EMLS) and is releasable to the Clearinghouse for Federal Scientific and Technical Information.

This report has been reviewed and is approved.

Tracy B. Gardner III

Approved: TRACY B. GARDNER, III, 1st Lt, USAF
Project Engineer

Alfred W. Barker

Approved: LEO W. SULLIVAN
Colonel, USAF
Chief, Surveillance & Control Division

FOR THE COMMANDER: Irving J. Gabelman
for IRVING J. GABELMAN
Chief, Advanced Studies Group

Abstract

This report summarizes the results of a six-month study to determine optimum configurations for the components required for a feed system for a high-power nanosecond-pulse high-resolution S-band radar system. The system employs 8.00 x 5.36-inch oversize rectangular waveguide. System components including power combiners, load switches, straight waveguides, H-plane bends, horn radiators, horn radomes, duplexers, rotary joints and sampling couplers are described.

Table of Contents

Table of Contents (cont.)

List of Illustrations

List of Illustrations (cont.)

EVALUATION

NANOSECOND RADAR-OVERSIZE WAVEGUIDE SYSTEM

This is a technical evaluation of Item A001, Contract F30602-69-C-0066 which is the final report of a design study of the NAnosecond Radar Oversize Waveguide System (NAROWS).

The design study of the NAROWS was implemented in order to obtain the best high power, low dispersion RF transmission system for the NAnosecond Radar Laboratory (NARAL). This study precedes the actual building of the NAROWS as set forth in the contract.

The contractor has presented the NARAL with a comprehensive analysis of the microwave components to be incorporated into the NAROWS. The study covered the combiner, load switch, straight runs, H-plane bends, radiating horn, horn radome, duplexer, rotary joints and signal monitors.

The knowledge gained from the study led the contractor to propose an engineering change to upgrade the duplexer from a breadboard model to an experimental model. This duplexer is an improvement in the NAROWS which greatly increases the capability of the NARAL. It allows the NARAL to receive radar signals independently of a second antenna and simplifies the signal processing.

Although the contract calls for delivery of a hardware oversize waveguide system, this is the only final report that will be received.

Tracy B Gardner III

TRACY B. GARDNER, III
1/Lt., USAF
Project Engineer

1.0 Introduction and General System Considerations

1.1 Introduction

This report summarizes the results of a six-month study phase to determine the optimum configurations of the oversize waveguide components to be developed under the present program for a high-power nanosecond-pulse high-resolution radar system. This system is to be installed at the Floyd Test Site, Griffiss Air Force Base. The components that will be developed will form the feed system from the output of the S-band tube to the input of a developmental-model horn radiator. The horn will also be developed under the present program.

The use of oversize waveguides offers two important advantages in this application: (1) increased power handling and (2) lower dispersion. The concepts to be employed in the design of the oversize waveguide components were developed under previous programs sponsored by the Rome Air Development Center [1], [2], [3]. The components to be developed will be compatible with oversize rectangular waveguide having width a = 8.00 inches and height b = 5.36 inches and carrying the TE_{10} mode polarized with the electric field parallel to the b dimension. This waveguide size was established, during the present study, as an optimum compromise between power handling capability and spurious-mode control. The 5.36-inch dimension was close to the optimum value based on the above two considerations, and was chosen specifically to be compatible with a previously developed [3] duplexer tube design.

Two classes of components (developmental and breadboard) will be developed under the present program. The developmental model components are:

1. Power Combiner
2. Load Switch
3. Straight Lengths of Oversize Waveguides
4. H-plane Bends

5. Horn Radiator

6. Horn Radome

The breadboard model components are:

1. Duplexer

2. Rotary Joint

3. Signal Sampling Coupler

A layout of the oversize waveguide system is shown in Fig. 1.1. The initial developmental model system, without the breadboard model duplexer, would extend vertically from the tube to the exit port in the ceiling, as indicated by the dashed lines above the load switch, and the bend and horn that complete the system would be located to the left of the position shown. The WR-430 flexguide shown is not included in the components to be designed and fabricated on this contract; however, the protection to the tube provided by this flexible coupling makes it essential.

The addition of the duplexer to the system is complicated by the duplexer length and the large radius of curvature required for bends. Several duplexer configurations were considered; the one shown is the best in terms of space required and accessibility, even though a second port is required in the ceiling. The uppermost part of the 180° bend in the duplexer is approximately 32 inches below the ceiling.

Design approaches for realizing the required system components are described in Sections 2 to 8 of this report. Some general system considerations are discussed in the following parts of Section 1.

1.2 Pressurization

The system will be operated with sulfur hexafluoride (SF_6) at 2 atmospheres gauge as the dielectric in the waveguide. This internal pressure is not unusually high for waveguide systems; however, because of the relatively large dimensions of the oversize-waveguide components, a consideration of the material and structural aspects is required.

SF_6 is a heavy, inert, colorless, odorless, non-toxic gas. It has a density about 5 times that of air. Therefore, the system can be filled with SF_6 by simply displacing the air, with little mixing. Since a relatively large amount of air mixed with the SF_6 has little effect on the breakdown strength, it is not necessary to evacuate the air from the system before filling it with the SF_6. The major problem with contaminant gases arises from the possible recombination with decomposition products to form compounds which may be very corrosive. Thermal decomposition does not occur until the temperature exceeds 150° C, and thus is not expected to occur in the present application. Decomposition is also caused by arcing, which hopefully will not occur under normal operating conditions. Decomposition caused by arcing may result in the formation of extremely poisonous gases; therefore precautions should be taken when venting a system in which arcing has occurred. While decomposition is not expected normally, those decomposition products that may form under abnormal conditions can be removed by use of a filter in a recirculating system. Recirculation also has the advantage of providing a homogeneous gas mixture and of preventing the formation of hot spots (regions of low gas density and therefore low power-handling capability) near areas of localized heating.

Gas connections will be provided at the lowest and the highest available points in the waveguide system, to allow filling the system and connection of a gas recirculating pump and return. The detailed design of the waveguide

system components will include consideration of the possibility and relief of air entrapment.

1.3 Support System

Preliminary estimated weights of the developmental system components, based on 0.25-inch average wall thickness of copper and nickel, are as follows:

Combiner	425 pounds
Load Switch	900
Straight Waveguide	250
50-inch Radius 90° Bend	200
Tapered Horn	1500

Each waveguide component will be provided with mounting brackets or other means of attachment to allow supporting it independently of other components.

The installation area for the oversize waveguide system should have an adjustable frame mounted to the ceiling, from which the components of the system can be suspended. It is recommended that the lowest component in the system, the combiner, be supported from a structure having its support base as near to that of the tube as possible, to minimize the amount of stress transferred to the tube because of thermal or mechanical expansion and contraction effects.

2.0 Developmental-Model Power Combiner

An E-plane combiner will be used to combine the four WR430 waveguide outputs of the high-power klystron into one oversize rectangular waveguide. Figure 2.1a shows the original concept of the output waveguide configuration of the high-power klystron. This configuration can be combined, as shown in Figure 2.2, using tapers to change the waveguide cross section and E-plane and H-plane offsets to interweave the waveguides in the E-plane. The common walls between the stacked waveguides will be gradually removed as described later to combine all the power into one oversize waveguide.

The dispersion of the combiner is held to a minimum by using the widest feasible waveguide width for the E-plane and H-plane offsets and by tapering as quickly as possible to a width of 8.00 inches ($a/\lambda = 2.27$). The 8-inch width results in a phase deviation from linearity which is at least an order of magnitude lower than for an equal length of standard-width waveguide (see Figure 2.1 of Technical Report RADC-TR-67-534, Reference [4]). The peak power handling capability is maintained as close to that of the four WR430 waveguide outputs of the tube as is consistent with reasonable design practices. The individual components making up the combiner are designed for low VSWR and for low mode conversion to avoid echoes and distortion of the pulse shape. Design goals of -35 dB reflection coefficient (VSWR = 1.036) and -35 dB mode conversion at mid-band have been established based on pulse distortion specifications.

The first high-power klystron will not have the desired output waveguide configuration of Fig. 2.1a, but instead will have the waveguide configuration shown in Fig. 2.1b. Waveguide twists will be used to change from this configuration to the desired configuration. The following net twist angles are required: 135° CCW in waveguide run #1, 45° CCW in waveguide run #2, 45° CW in

waveguide run #3, and 135° CW in waveguide run #4. In order to insure that the four twists have equal electrical path lengths, each twist would consist of one 90° twist and one 45° twist with the twist directions chosen to give the above net twist angles.

One possibility that has been considered is to use the alternate output waveguide structure of Figure 2.1c and to correct the polarity by making the path lengths of waveguide runs 1 and 3 differ from the path lengths of waveguide runs 2 and 4 by one-half wavelength. The polarity could also be corrected by using simple 90° twists, for instance 90° CCW twists in waveguide runs 1 and 3 and 90° CW twists in waveguide runs 2 and 4. The use of twists to correct the polarity is preferred since the differential-path-length technique is inherently bandwidth limited.

2.1 Twist Design

The feasibility of twisting the WR430 (4.30 inches x 2.15 inches) waveguide was considered. Analysis shows that the cross-polarized TE_{01} mode and the TE_{30} mode are the principal spurious modes excited in an oversize waveguide twist. The waveguide modes which propagate in WR430 waveguide within the operating band (3.1-3.6 GHz) are the dominant TE_{10} mode and the spurious TE_{01}, TE_{11}, TM_{11}, and TE_{20} modes. Therefore the only mode excited by a twist which will propagate in WR430 waveguide is the TE_{01} mode. Approximate calculations show that for a 90° twist in WR430 waveguide the TE_{01} mode conversion will be of the order of -15 dB at the upper and lower frequency limits ($f_o \pm 7.5\%$) for twist lengths equal to 9.00 inches, 20.13 inches or 30.75 inches (roughly 1, 2, or 3 beat wavelengths). For 45° twists in WR430 waveguide the TE_{01} mode conversion at the band edges will be of the order of -20 dB for twist lengths equal to 10.06 inches, 20.62 inches, or 31.07 inches (roughly 1, 2, or 3 beat wavelengths).

Since the above values of mode conversion are not considered acceptable, even for the longest lengths examined, twists in WR430 waveguide do not appear feasible.

Instead of twisting WR430 waveguide it was decided that the twists should be performed in a waveguide having a cross section in which all modes excited by the twist geometry, the cross-polarized TE_{01} mode and the TE_{30} mode, are below cutoff ($a/\lambda < 1.5$, $b/\lambda < 0.5$). Further the waveguide size should be made as large as possible to maximize power handling capability of the twist. Gradual single-mode twists have essentially the same power handling capability as straight waveguide of the same cross section [5]. The largest possible cross section in which neither the TE_{01} mode nor the TE_{30} mode can propagate at the high frequency end of the band (3.6 GHz) is approximately 4.89 inches x 1.63 inches (only the TE_{10} and the TE_{20} modes can propagate). This size waveguide should be adequate since it has a theoretical power handling capability about 88% that of WR430 waveguide.

Twists that rotate the polarization 90° in a length of $2\lambda_g$ or more will generally have a VSWR less than 1.1 [6]. Lewin [7] has set up the wave equations in helical coordinates and calculated λ_g in terms of $1/\ell$ where ℓ is the length in which the guide cross section has rotated a full 360°. However, the correction term is small for guides with a cross section aspect ratio of 2:1 or greater and with twists many times longer than the guide width.

The twist designs recommended for use with the klystron output waveguide configuration of Fig. 2.1b are shown in Figs. 2.3a, 2.3b, 2.3c, and 2.3d. These designs are based on a constant twist rate of 5° per inch (90° in 18 in.). The 90° section is about 4.8 guide wavelengths long and should have a VSWR less than 1.05. These figures show the outside dimensions of the mandrels which would be used assuming the twists will be electroformed. Flanges would be

"grown-on" during the electroforming process so that the twists can be inserted into the combiner at plane B-B of Fig. 2.

2.2 Compound Input Taper

Linear tapers will be used to transition from the WR430 waveguide outputs of the tube (4.30 inches x 2.15 inches) to the 4.89-inch x 1.63-inch cross section of the twists. Fig. 2.2 shows the taper design which has been selected based on considerations discussed below. Only the TE_{10}, TE_{11}, TM_{11}, TE_{20} and TE_{01} modes can propagate at the taper input, and only the TE_{10} and TE_{20} modes can propagate at the output. A symmetrical, linear, E-plane taper will excite the composite TE_{12}/TM_{12} mode (LSE_{12} mode) with an amplitude coupling coefficient given by [1]:

$$C_{10}^{12} = \frac{b_2(b_2-b_1)}{\pi\lambda L} , \qquad (2.1)$$

where

b_1 = waveguide height at taper input

b_2 = waveguide height at taper output

L = taper length

λ = wavelength .

A symmetrical, linear, H-plane taper will excite the TE_{30} mode with an amplitude coupling coefficient [1]:

$$C_{10}^{30} = 0.375 \frac{a_2(a_2-a_1)}{\pi\lambda L} \qquad (2.2)$$

where

a_1 = waveguide width at taper input

a_2 = waveguide width at taper output

L = taper length

λ = wavelength .

Since neither the LSE_{12} mode nor the TE_{30} mode can propagate at either end of this taper, only the TE_{10} mode VSWR need be considered in the taper design.

Johnson [8] considers the problem of a linear double taper connecting two uniform rectangular waveguides of arbitrary dimensions and propagating the TE_{10} mode. He gives expressions, in good agreement with experiment, (Eqs. 12, 13, 15, 16 and 17) which can be used to calculate VSWR versus taper length at a selected frequency. Once a length is selected, the same expressions can be used to calculate VSWR versus frequency. Using the above equations it was shown that a 13.5-inch long taper from WR430 waveguide to the 4.30-inch x 2.15-inch waveguide should have a VSWR less than 1.020 over the 15% operating frequency band (3.1 to 3.6 GHz) and that a 9.75-inch long taper should have a VSWR less than 1.025 over the same band. A VSWR of 1.025 corresponds to a reflection coefficient of -38 dB which is adequately low. Hence it is recommended that the compound input taper be made 9.75 inches long.

2.3 E Plane Offsets

The E-plane offsets of the combiner (see Fig. 2.2) are used to stagger the waveguides in the E-plane as indicated in sectional view C-C so that they may be interleaved to form an E-plane bifurcation by means of the H-plane offsets which follow. A double offset design employing four E-plane bends in series is used to make sure the electrical path lengths through all the offsets are identical. Figures 2.5a and 2.5b show the design details.

It was shown in Section 2.1 that a waveguide cross section of a = 4.89 in. x b = 1.63 inches is optimum for the twists which will be inserted at plane B-B of Fig. 2.2. It was also found, as discussed in Section 2.4, that 4.89 inches is a good choice for the width of the waveguide of the H-plane offsets (waveguide height b does not affect the H-plane offset design).

Quine [9] has shown how to design E-plane bends for oversize waveguides. E-plane bends tend to couple energy from the TE_{10} mode to TE_{1n}, TM_{1n} degenerate mode pairs for n odd. However, for waveguide with a = 4.89 inches and b = 1.63 in. only the TE_{10} and TE_{20} modes will propagate and the radii of the E-plane bends making up the E-plane offsets can be chosen on the basis of TE_{10} mode VSWR alone. An inside bend radius consistent with low VSWR [10], 6 inches, will allow the required offsets to be performed in a reasonable overall length, about 13.9 inches.

2.4 H-Plane Offsets

Figure 2.6a shows the geometry of the H-plane offsets and the design dimensions selected. The offset consists of two H-plane bends each having a bend angle, θ, connected as shown. Two mode bend analysis (Eqs. (2)-(7) of reference [9] was used to analyze the bends making up the offset. This analysis is valid for $a/\lambda < 1.5$ and is approximate for a/λ slightly greater than 1.5. With center line bend radius, R, and waveguide width, a, given, the center line bend length, $R\theta$, may be chosen so that the power which is incident at port 1 in the TE_{10} mode couples over to some degree to the TE_{20} mode and then back to the TE_{10} mode at port 2 to give a 1-cycle (n = 1) bend. If the center-line bend length is doubled, a 2-cycle (n = 2) bend results. At $\lambda = \lambda_o = 3.52324$ inches the center-line bend lengths for 1-cycle and 2-cycle bends were calculated as a function of radius, R, for a = 4.89 inches (a/λ_o=1.388) and a = 5.75 inches (a/λ_o = 1.632) for 1-cycle and 2-cycle bends. From these calculations the radii, R, which gave S/2 = 4.419 inches were selected. Also the maximum power coupled to the TE_{20} mode was calculated. Table 2.1 summarizes the results.

The following conclusions are drawn from Table 1:

(1) The use of 2-cycle bends to make up the H-plane offset results in prohibitively long overall lengths with either a = 5.75 inches or a = 4.89 inches.

Table 2.1

Properties of Possible H-Plane Bends
for H-Plane Offset with S/2 = 4.419",
at $\lambda = \lambda_o = 3.52324"$

Waveguide Width a	No. of Cycles n	Bend Radius R	Bend Angle θ	Centerline Bend Length Rθ	$R\theta/\lambda_{beat}$	Maximum Power Coupled to TE_{20} Mode $P_{2\ max}$	Overall Axial Length of Offset (L = 2R sin θ)
4.89"	1	47.853"	17,4819°	14.6007"	0.9921	0.01573	28.7"
	2	195.478	8.62314	29.4198	1.9990	0.000957	58.7
5.75	1	105.955	11.7223	21.6776	0.9944	0.01107	40.4
	2	429.467	5.81439	43.5825	1.9993	0.000681	86.8

(2) Offsets in the full width waveguide, a = 8.000 inches, also appear to be out of the question since the centerline bend length required is approximately $\lambda_{beat} = \lambda_{20}\lambda_{10}/(\lambda_{20}-\lambda_{10}) = 45.37$ inches (offset length L ≈ 90 inches).

(3) The overall length of a 1-cycle H-plane offset using bends with a = 4.89 inches would be 28.7 inches, about 30% shorter than an offset using bends with a = 5.75 inches.

The above indicates that making the H-plane offsets in waveguide with width a = 4.89 inches would result in a reasonable length and consequently this width is preferred. Figure 2.6b shows that the spurious mode amplitude as a function of wavelength are also adequately low. The solid curve shows the spurious mode amplitude of one of the two bends making up the offset. Within a 15% frequency band centered at $f_o/f = \lambda/\lambda_o = 1$ the TE_{20} mode amplitude of a single bend is at least 26 dB below the TE_{10} mode.

Connecting two bends together in the configuration of the offset results in spurious mode cancellation within the operating bandwidth in the manner shown by the dashed curve in Fig. 2.6b. Thus the H-plane offset in 4.89-inch wide waveguide should have a spurious mode at its output, port 3, which is at least 30 dB below the TE_{10} mode over the 15% operating bandwidth.

2.5 H-Plane Taper

H-plane tapers will be used immediately following the H-plane offsets to increase the waveguide width from 4.89 inches to 8.00 inches in as short a length as possible. The 4.89-inch width is below cutoff for the TE_{30} mode (the mode excited by a symmetrical H-plane taper). Equation (2.2) can be used to calculate the mode conversion at the wide end of a linear taper connecting the two waveguide widths. It is found that an undesirably long taper length of about 47 inches is required to keep the mode conversion below -35 dB. A more

desirable length of about 18 inches would have an unacceptable mode conversion of about -27 dB.

One method of obtaining low mode conversion with a short linear taper is to place mode compensating elements at or near the source of the mode conversion. In this case metal wedges could be used at the wide end of the H-plane taper. This technique was demonstrated experimentally with the H-plane tapers of a -3 dB side-wall multi-hole directional coupler developed on Contract AF30(602)3682, Reference [2]. However, this technique is undesirable because considerable experimental effort is required to arrive at a suitable wedge configuration.

Analysis has shown that a second method employing a double angle H-plane taper configuration as shown in Fig. 2.7 will give low mid-band mode conversion with an overall taper length, L, of about 18 inches. By making L_2 equal to one-half beat wavelength and choosing θ_2 to give the same magnitude of mode conversion that is produced by θ_3, the TE_{30} mode excited at 2 will cancel the TE_{30} mode excited at 3. Since the average beat wavelength in a tapered region is approximately equal to the geometric mean of the beat wavelengths at the ends of the region, L_2 can be determined by:

$$L_2 = \frac{\lambda_{B\,avg}}{2} \approx \frac{\sqrt{\lambda_{B_2}\,\lambda_{B_3}}}{2} \qquad (2.3)$$

The mode conversion at 2 is made equal to that at 3 by letting:

$$\theta_2 = \frac{a_3}{a_2}\,\theta_3 \qquad (2.4)$$

Then $\theta_1 = \theta_2 + \theta_3$ determines the length L_1. Overall taper length $(L_1 + L_2)$ for mode cancellation at 3.35 GHz is plotted in Fig. 2.7b as a function of a_2. The mode conversion which results at the edges of the operating frequency band is also plotted as a function of a_2. A value of $a_2 = 7.25$ inches has been selected. From Fig. 2.7b the resulting overall taper length which gives complete mode

cancellation at 3.35 GHz is 17.44 inches. The mode conversion is below -31 dB at both the upper and lower ends of the operating frequency band.

2.6 E-Plane Bifurcation

The four 8.00-inch x 1.63-inch waveguides at the output of the H-plane taper will be combined by means of tapered E-plane bifurcations as indicated in Fig. 2.8. The tapered bifurcating plates willbe employed for two reasons. The first is to reduce the tendency for breakdown to occur at the edges of the bifurcating plates in the event that the amplitudes of the TE_{10} mode incident in the four 8.00-inch x 1.63-inch waveguides are not equal. The edges will be radiused or chamfered.

The second reason for employing tapered bifurcating plates is to reduce the VSWR that would result due to the 0.100-inch plate thickness. Because of the high degree of symmetry that is employed, only the LSE_{1n} modes having n equal to or greater than 8 will be excited by the bifurcating plates. The TE_{30} mode will also be generated by the tapered plate, but the amplitude of this mode is expected to be negligible.

2.7 E-Plane Taper

An E-plane taper will be used at the output of the E-plane bifurcation as indicated in Fig. 2.8 to reduce the waveguide height from 6.92 inches to 5.36 inches, the full oversize waveguide height selected for maximum compatibility with the oversize waveguide duplexer (see discussion in Section 8). The LSE_{12} mode will be generated at both ends of the E-plane taper with magnitudes determined by Eq. (2.1). For example, at Section C-C where b = 6.92 inches, the mode conversion is -25.6 dB. By spacing the ends of the taper one beat wavelength ($\approx$ 18 inches) the mode conversion will be small over the bend.

3.0 Developmental-Model Load Switch

A switch will be provided at the output of the Developmental-Model Power Combiner to switch the transmitter output from the radiating system to a dummy load (see Fig. 1.1). Since the switch is not required to switch under power or between pulses, a mechanical type of waveguide switch is suitable. However, pressurization must not be lost during switching. The switch and the dummy load should handle the full peak and average power output of the tube. Since it will be located at least 18 feet above the floor level, the switch will be either motor or pressure driven so that it can be operated remotely.

3.1 Load Switch Configuration

Two basic types of mechanical waveguide switches were considered for use in the full oversize waveguide system: (1) the conventional rotary motion waveguide switch, and (2) a transverse motion waveguide switch. The conventional rotary motion waveguide switch employs either a 90° E-plane or a 90° H-plane bend in a cylinder which rotates 90° so as to switch microwave power from one input port to either of two diametrically opposed output posts. This study has shown that a rotary motion type switch in full oversize waveguide (a = 8.00 inches, b = 5.36 inches) would require an H-plane bend having a radius of 50 inches to minimize mode conversion within the operating band. This would make the rotating cylinder about 100 inches in diameter. A second large bend would be required at the output of the switch to enable the switch to be inserted into a vertical waveguide run. This approach would result in an undesirably large overall switch insertion length of at least 200 inches. Further, since each bend contributes a small amount of mode conversion*, it is desirable to minimize the number of oversize-waveguide bends used in the system between the combiner and the horn.

---

* Mode conversion of a 90° bend with a 50-inch radius would be about -15 dB at the edges of a 15% frequency band.

The transverse motion type of waveguide switch shown in Fig. 3.1 was selected as the most desirable type for use in the oversize waveguide system since it does not insert any oversize-waveguide bends between the combiner and the horn, and because it results in an insertion length of only about 3 feet, which includes a straight length of waveguide to which a sampling coupler will be attached. The switching action is accomplished by means of a sliding section which either inserts a straight-through waveguide section between the combiner and the horn or connects the combiner to the dummy load through a 90° waveguide bend. It should be noted that the bend design in this case is not critical, because of the extremely low back scattering of gradual oversize-waveguide bends. An H-plane bend having a center line radius of about 12 inches will be employed. Nearly all of the energy converted to higher-order modes will travel in the forward direction and be absorbed by the multimode load. The load will be attached to the sliding section and will move with it.

The central moving section which includes the straight-through waveguide section, the H-plane bend and the multimode dummy load will be moved by means of a drive shaft passing through an O-ring pressure seal. The entire volume within the fixed housing of the switch will be pressurized both inside and outside the central moving section. If necessary, holes will be provided in the waveguide walls of the moving section to facilitate filling the housing with SF_6. Vent valves will be provided to allow trapped air to escape during the filling process.

Chokes will be provided, as discussed in Sect. 3.2, to allow a small gap to be used between the moving and fixed parts of the load switch. The choke grooves may be cut either in the fixed housing as indicated in Fig. 3.1 or in the flanges attached to the straight-through and H-plane bend waveguides.

3.2 Motional Choke Joints Configurations

Reference [11] gives detailed discussions of choke designs for standard-size waveguides. Similar considerations apply in the case of chokes for oversize waveguides. The design procedure for obtaining low reflection and low leakage with an oversize-waveguide choke is similar to that for a standard-size waveguide choke, and will not be discussed here. The question of spurious mode resonances, however, will be discussed in some detail.

Figures 3.2 and 3.3 show two possible configurations for the choke grooves for the developmental-model load switch. Both of these configurations employ choke grooves along the top and bottom walls in order to efficiently reflect the currents associated with the desired TE_{10} mode. It may be advantageous to bend these grooves inwards at both ends as shown in order to compensate for "diffraction effects" near the side walls. In this way, the insertion loss for the desired TE_{10} mode may be reduced somewhat. The configuration of Fig. 3.2 also employs choke grooves along the side walls in order to prevent leakage of diffracted energy into the region beyond, whereas in the configuration of Fig. 3.3 this energy is dissipated in absorbing material. It is believed that the insertion loss for the desired TE_{10} mode is approximately the same for both configurations because the energy reflected back into the waveguide in the case of the configuration of Fig. 3.2 is largely in the form of higher order modes.

As an approximation, it appears reasonable to assume that the frequencies of the spurious mode resonances in the choke region correspond roughly to the cutoff frequencies of an equivalent waveguide of width a' equal to half the average perimeter between the grooves and waveguide edge. For the configurations shown in Figs. 3.2 and 3.3 , a' is approximately

$$(8.00" + 5.36") + \lambda/2 = 13.36" + 1.76" \approx 15"$$

The cutoff wavelengths λ_{cm} for this equivalent waveguide are given by

$$\lambda_{cm} = 2a'/m \tag{3.1}$$

Table 3.1 lists values of λ_{cm} and the corresponding cutoff frequencies f_{cm} for several values of m.

Table 3.1

Values of λ_{cm} and f_{cm} for a' = 15"

m	λ_{cm} (Inches)	f_{cm} (GHz)
6	5.00	2.36
7	4.29	2.75
8	3.75	3.15
9	3.33	3.55
10	3.00	3.94
11	2.73	4.32

It is seen from the data in Table 3.1 that two resonant frequencies may fall within the desired operating frequency band from 3.1 to 3.6 GHz; these correspond to m = 8 and 9.

Equation (3.1) gives a crude estimate of the frequencies of the spurious mode resonances in the choke region. However, observable resonance effects (i.e., high VSWR and insertion loss, electric-field breakdown and heating effects) may not occur at any of these resonant frequencies. In order for strong resonance effects to occur at a particular resonant frequency, the coupling between the incident TE_{10} mode and the resonant mode in the choke region must have a value reasonably close to the critical value determined by the amount of dissipation experienced by the resonant mode. If the coupling is too high or too small relative to the critical value, only weak resonance effects will be observed.

The use of finite length grooves as in Figs. 3.2 and 3.3 changes the values of the resonant frequencies and also introduces dissipation as a

result of coupling to other modes in the choke and waveguide regions and as a result of radiation into the region beyond the grooves. It is also believed that the rectangular shape of the oversize waveguide and groove perimeter leads to considerable coupling among modes, with the result that the resonant modes are considerably damped. This may be especially true in the case of oversize waveguides having a large number of propagating modes. Certainly the configuration shown in Fig. 3.3 should be expected to provide a high degree of damping for the resonant modes. However, the configuration of Fig. 3.2 may have the advantage of greater simplicity.

Some experiments were performed at X band with an available choke joint in 2.8 inch x 2.5 inch waveguide. This choke is described in detail in Section 4.0 of [12]. The choke was designed to be used in conjunction with a 0.005-inch mica sheet to form a pressure window. The choke employed two continuous 0.100-inch wide grooves having a depth of 0.300 inches corresponding approximately to one-quarter free-space wavelengths and 0.100-inch spacing between waveguide edge and first groove and between first and second grooves corresponding to somewhat less than one-quarter wavelength in mica dielectric.

Figure 3.4 shows measured values of the transmission and reflection coefficients for the double-groove choke joint. These data were obtained with a 0.050-inch gap between the grooved choke flange and a plane (ungrooved) flange. It is seen that the insertion loss is not measurable (i.e., < 0.1 dB) and the reflection is below -30 dB from 8.5 to 10 GHz. Note that there are no signs of any choke resonances within this frequency range. Appreciable insertion loss and reflection occurs at frequencies below approximately 8.0 GHz. This is believed to be due to the relatively small (0.100 inch) spacing between grooves employed in this particular design. The frequency range from 8.5 to 10 GHz over which low insertion losses and low reflections were measured

corresponds to approximately a 15 percent frequency band as required for the present S-band application.

Data were also obtained with gap sizes up to 0.350 inch. A slow deterioration of the reflection and transmission characteristics was observed as the gap size was increased. It appears that good performance can be obtained with gap sizes of 0.050 inch or less at X band. This corresponds to a 0.150-inch gap at S band.

Data are presented in [12] of the peak-power-handling capability of the above double-groove choke joint with a 0.005-inch mica sheet inserted between the grooved flange and a plane (ungrooved) flange. These data indicate that this configuration has nearly the same power-handling capability as the 2.8 inch x 2.5 inch straight waveguide.

These experimental results are encouraging and indicate that a successful (i.e., resonant free) choke design for the developmental-model load switch can be realized with either of the configurations shown in Figs. 3.2 and 3.3 .

3.3 Load Configuration

The multimode dummy load must be capable of dissipating at least 1 Kw of average power and should not degrade the peak-power-handling capability of the oversize waveguide system appreciably. A microwave absorbing material capable of withstanding high temperature, temperature gradients, and thermal shocks is indicated by the average power level requirement. One material which is considered suitable for this application consists of finely divided iron suspended in a ceramic base fixed at a temperature of about 2400° F. To avoid peak-power-handling degradation and to achieve a low VSWR, the material will be gradually introduced into the waveguide in a tapered fashion. Figure 3.6 shows an outline of a possible load configuration employing doubly tapered wedges introduced into the waveguide from the corners. The taper length will

be made as long as possible consistent with available load material (about four wavelengths) to take advantage of the broad band, low VSWR characteristics of a gradual taper. The maximum VSWR of the load was not specified and it is considered not to be critical. A VSWR of 1.1 has been established as a design goal, but a VSWR as high as 1.2 is considered acceptable.

4.0 Straight Waveguides

The principal questions concerning the straight waveguides required for the developmental system relate to the wall thickness, the surface finish, and the method of fabrication.

The large cross-sectional size and the relatively small quantity required makes the drawing process normally used to form waveguides unfeasible. Fabrication by brazing or welding would be possible; however, this method has several potential problems. The distortion caused by the heating of the joining and flanging processes, and the uniformity and integrity of the finished seams cannot be predicted accurately, so that several attempts may be necessary to obtain satisfactory waveguide sections. Electroforming leads to the best dimensional accuracies and surface finishes. Expendable aluminum mandrels, which can be machined conveniently, are required. Lengths up to six feet long can be accommodated in the available electroforming tanks. It is estimated that the total cost for fabrication by electroforming will be comparable to that for a welded or brazed assembly, and the dimensional accuracy obtained will be appreciably better.

Several mandrels with lengths totaling approximately eight feet will be machined. The lengths will be chosen to allow easy substitution of the experimental model components at a later time. Flanges will be grown on during the electroforming process.

The surface finish to be specified depends on its effect on power handling capacity, dissipative losses, and the cost of fabrication. Calculation of the reduction of peak power capability by surface roughness indicate that a 300μ inch surface finish would be tolerable at 3 atmospheres of pressurization. The waveguide surface current density for the fundamental mode will be relatively low because of the large cross section, thus the use of a coarse surface finish

would not result in excessively high dissipative losses in the oversize waveguide system. However, in order to test the waveguide for high power handling capability, cavities will be formed with the oversize waveguide components, and the dissipative losses here will limit the peak voltage build-up that can be obtained. A 32μ inch surface finish, about 0.7 of one skin depth, appears to be a suitable compromise between the increase of surface loss and the cost of mandrel fabrication. This finish will increase the surface resistivity about 20% above the theoretical value.[13]

To verify the validity of the expressions for deflection with electroformed waveguides, the deflections and the pressure at which the yield strength is exceeded were calculated and measured for an electroformed rectangular waveguide having inside dimensions 8 x 1.34 inch. The wall thickness of this waveguide was thinnest at the center of the wide faces, with increasing thickness toward the corners, as is usual with an electroformed section of this shape. At eight points, spaced 1 in. apart in a transverse plane, the minimum wall thickness measured was 0.143 inch and the maximum was 0.240 inch. The average wall thickness was 0.165 inch. Similar values were obtained on both broad walls of the waveguide. Assuming a value for the elastic limit, s, of electroformed copper of 9000 psi, the pressurization, p, beyond which the waveguide is permanently distorted was computed to be 8.3 psi, using the expression [14]

$$p = \frac{2st^2(a + b)}{a^3 + b^3} \tag{4.1}$$

with 0.165 inch as the thickness. a and b are the inside waveguide width and height, respectively. At this pressure, the deflection of the broad wall was computed to be 0.023 inch, using [14]

$$\Delta y = \frac{p}{E}\frac{a^2}{t^3}\left[\frac{5a^2}{32} - \frac{a^3 + b^3}{8(a + b)}\right] \tag{4.2}$$

where E is the modulus of elasticity. A value of 1.7×10^6 psi was used for E. The measured results were in excellent agreement with the computed values, the deflection increasing linearly to 0.023 inch at 8 psi and non-linearly at higher pressures. A maximum pressure of 12 psi was applied, resulting in a deflection of 0.043 inch and a residual deflection of 0.009 when the pressure was removed.

The calculated wall thickness of 8 x 5.36 inch ID waveguide required to keep the wall stress less than the elastic limit is shown below for the two materials commonly used for electroformed waveguide, copper and nickel.

Pressure	Copper s=9000 psi	Nickel s=45000 psi
30 psi	0.288 in.	0.129 in.
40 psi	0.332	0.149

The deflection of both the broad wall and narrow wall for a range of wall thicknesses of 8 in. x 5.36 in. waveguide made of copper or nickel is shown in Fig. 4.1. The solid lines indicate the range over which the stress in the material does not exceed the elastic limit. A modulus elasticity of 16×10^6 and 3×10^6 psi was used for the copper and nickel respectively, for this calculation.

It would be possible to use reinforcing ribs with thinner waveguide walls. However, the additional work required in the fabrication of the electroformed waveguide with ribs either grown in or applied later would increase the cost of the waveguide appreciably more than the reduction in wall thickness would decrease it. The waveguide design to be used will therefore be based on the use of a sufficiently strong non-reinforced wall thickness. An assumed pressurization of 40 psi will give about 30% safety factor and the specification of the minimum wall thickness, instead of an average, will give about 20% additional safety factor.

The waveguide wall design tentatively selected will be a composite layer. Approximately 0.025 in. of copper will be used on the inside to obtain high

conductivity, and then approximately 0.175 in. of nickel will be electroformed over this to obtain the strength required. The copper will contribute very little to the strength of the wall, hence, from Fig. 4.1, the wall deflections will be about + 0.045 in. on the broad wall and -0,010 in. on the narrow wall. Since these deflections will develop in a gradual manner away from the flanges, they are not expected to result in significant mode conversion.

5.0 Developmental Model Bends

A 45° and a 90° H-plane bend will be provided at the throat of the developmental model horn radiator in order to obtain two discrete radiation directions, i.e., nearly horizontal and at 45° from the horizon.

The bends will be designed with an average radius R equal to 6.25a where a is the waveguide width. In the present case a = 8.00 inches, resulting in R = 50 inches. The characteristics of these bends are discussed in Section 8.3 of this report where it is shown that the mode conversion from the TE_{10} mode to the TE_{20} mode is below approximately -15 dB at the ends of a 15 percent operating band. The average mode conversion over the operating band is therefore approximately -21 dB. This performance is considered satisfactory for the interim developmental model system.

6.0 Developmental Model Horn Radiator

The horn radiator has been considered in detail during the study phase. The original specifications called for a one meter square horn to illuminate a movable reflector. RADC also desired to use the horn initially without a reflector. The horn length should be kept to a minimum to make the weight and bulk as small as possible.

During the study phase the idea of using a folded-horn paraboloid as an optimum radiator for the ultimate system was advanced by the Research and Development Center, and approved by Rome Air Development Center. This type of antenna has several advantages. The rotating joints* would be part of the folded-horn paraboloid past the radome and would be much simpler to implement than rotating joints placed in the waveguide runs. The shielding effect of the horn paraboloid would reduce wide-angle radiation. Thus it was decided to make the horn compatible with a future folded-horn paraboloid. The developmental model horn would essentially be the input end of the future horn paraboloid.

The developmental model horn, therefore, must be basically a conical horn with the total flare angle of 25° desired for the folded-horn paraboloid. Its aperture would be compatible from the power standpoint with the one meter square aperture required for the initial developmental model system. It would be fed from the oversize rectangular waveguide run.

6.1 Recommended Design

The recommended configuration of the horn is shown in Figs. 6.1 and 6.2. It is essentially a conical horn of 25° total flare angle, but starts from a rectangular throat of 8 inch x 5.36 inch inside dimensions, the same as the rectangular waveguide. The horn at the throat is then basically a pyramidal horn, but gradually changes over its entire length into a conical horn.

---

* See Section 9.3.

Instead of the gradual full-length horn transition from a rectangular to a round cross section, a rectangular-to-round waveguide transition could have been used in conjunction with a simple conical horn. However, the amplitudes of the higher order modes generated in the throat of a conical horn may be considerably greater than those in a comparable pyramidal horn. For example, the $TE^{\square}_{10}$ mode in rectangular waveguide scatters most strongly into the $LSE^{\square}_{12}$ mode in a pyramidal taper. For the horn of Fig. 6.1, the throat amplitude coupling coefficient, C^{12}_{10}, is -12.4 dB. This value is obtained from Eq. (10) in [15], with the numerator of the right-hand side changed to $b_1(b_2 - b_1)$. With round waveguide feeding a conical taper, the dominant TE°_{11} mode scatters most strongly into the TM°_{11} and TE°_{12} modes. For 8 inch diameter waveguide and a 25° total flare angle, the amplitude coupling coefficients, $C^{TM_{11}}_{TE_{11}}$ and $C^{TE_{12}}_{TE_{11}}$ are -6.0 and -8.3 dB, respectively. These values are obtained from the equations in [16]. Thus the use of the initial pyramidal flare would result in an increase in gain of roughly 2 dB. It should be pointed out that reference [17] gives values for the coupling from the TE°_{11} mode to the TM°_{11} mode which are less than those in [16] and are roughly equal to the values for the conversion from the $TE^{\square}_{10}$ mode to the LSE_{12} mode.

A rectangular-to-round waveguide transition may not be straightforward. Trouble may be experienced with higher order modes which have cutoff frequencies within the operating frequency band and are generated in the transition. Thus, because of the possibility of larger spurious modes at the throat of a purely conical horn and the disadvantages of a waveguide transition, the decision was made to use a full length transition from a rectangular waveguide input to a round radiating aperture.

A complete analysis has not been made to determine the mode conversion caused by the gradual transition from a rectangular to a round cross section. From a consideration of the symmetry of the transition, however, it appears

that the modes corresponding to the $LSE^{\square}_{12}$ and $TE^{\square}_{30}$ modes in rectangular waveguides and the modes corresponding to the TM^{o}_{11}, TE^{o}_{12}, TM^{o}_{12} and TE^{o}_{13} modes in circular waveguides are excited along the transition. These are the same sets of spurious modes generated respectively by purely pyramidal and purely conical tapers. The results of a qualitative study indicate that the mode conversion of the rectangular to circular tapered transition will probably be intermediate between the values quoted in a preceding paragraph for the purely pyramidal and purely conical tapers.

The following equations [18] can be used to check the relative power handling of a square and circular aperture. They give the peak breakdown power, P_{max}, as a function of the peak breakdown field intensity, E_{max}.

For the $TE^{\square}_{10}$ mode, $$P_{max}(kw) = 0.662 \times 10^{-6} ab \frac{\lambda}{\lambda_g} E^2_{max} \qquad (6.1)$$

For the TE^{o}_{11} mode, $$P_{max}(kw) = 0.498 \times 10^{-6} D^2 \frac{\lambda}{\lambda_g} E^2_{max} \qquad (6.2)$$

Since, at the mouth, λ/λ_g for both modes will be very close to 1, λ/λ_g will be set equal to 1. Also, let E_{max} in the first equation equal to E_{max} in the second equation. Then

$$\frac{P^{\square}_{max}}{P^{o}_{max}} = \frac{0.662\ ab}{0.498\ D^2} = \frac{0.52\ ab}{0.498 \frac{\pi}{4} D^2} \qquad (6.3)$$

For equal areas, the breakdown power of a pyramidal horn is therefore 5% greater than that of a conical horn.

The conical horn will be made in two pieces, as shown in Fig. 6.1. The throat section will be electroformed and the mouth section will be fabricated. Flat flanges will be used at the ends of the throat section and the small end of the mouth section. The large end of the mouth section has a flange to which the radome will be attached.

6.2 Horn Patterns

The calculation of conical horn patterns with large flare angles is very difficult. Reference [19] gives an elaborate method of calculation using the modes of a cone, but the results still do not agree well with experiment for large flare angles. Reference [20] has equations for calculating the near field of conical horns; results check well with experiment and the equations could be extended to far field calculations, but the procedure is extremely complicated. The most direct method, then, appears to be the extrapolation of measured data.

The only sources of measured conical horn patterns in the literature appear to be two articles, [21] and [22]. The patterns in [22] have been reproduced in [23]. References [21] and [22] have patterns for conical horns of varying aperture size and flare angle.

The basic principle in extrapolating conical horn patterns is the use of the phase deviation to relate patterns. The phase deviation of a conical horn is the difference in wavelengths between the slant length and axial length, both measured from the apex. Conical horns with the same phase deviation should have approximately the same patterns, normalized to the peak, with $(d/\lambda)\sin\theta$ as the abscissa, where d is the mouth diameter and θ is the angle from the horn axis.

Figure 3(f) of [22], which is essentially the same as Fig. 10·12(f) of [23], is for a horn with a phase deviation of 0.66λ. The horn of Fig. 6.1 of this report has a phase deviation of 0.69λ at center frequency. At the low end of the frequency band the phase deviation would be 0.639λ. Thus a phase deviation of 0.66λ is well within the frequency band.

The pattern given in Fig. 6.3 of this report is taken from Fig. 3(f) of [22]. The ordinates have been changed from relative amplitude to decibels and the angles have been converted from those for a 4.1λ aperture to a 12.6λ aperture (44.4 inches at center frequency) by using the relationship

$$\frac{d}{\lambda} \sin\theta = \frac{d_1}{\lambda_1} \sin\theta_1 \qquad (6.4)$$

Note the "hole" on-axis in the E-plane pattern of Fig. 6.3. The on-axis relative gain is 4.4 dB below the E-plane peak. Thus, if the horn is used as a radiator, it will have maximum relative gain about $\pm$ 4.5° off the axis in the E-plane.

An estimate for the absolute gain on axis was obtained from [22], Fig. 2, Careful examination reveals that the pattern of Fig. 3(f) of [22] has on-axis gain about 8.4 dB below that of a fully collimated horn, i.e., one that has zero phase deviation. Page 251 of [22] gives a figure of 84% for the effective area of a fully collimated conical horn relative to one with uniform amplitude, polarization, and phase across the aperture. This is equivalent to a gain of 84% of the uniform aperture, or -0.76 dB. The gain of a uniform aperture is known to be $4\pi A/\lambda^2$, where A is the area. Therefore, the gain of a uniform aperture 12.6λ in diameter is 1570, or 31.92 dB. Thus the fully collimated 12.6λ aperture would have a gain of 31.16 dB. The horn of Fig. 6.3 would have a gain of 31.16 - 8.4 dB = 22.76 dB on axis and a gain of 31.16 - 4 dB = 27.16 dB at the E-plane peaks. The losses in higher order modes must then be subtracted from the values of gain. These are estimated as from one to two dB.

These figures are of course approximations and in any event would vary over the frequency band. A clue to the performance over the band of the horn of Fig. 6.3 may be found in [21]. Figure 10(h) of [21] shows a pattern almost identical to Fig. 3(f) of [22]. The horns involved have the same aperture (4.1λ). The phase deviation for Fig. 10(h) of [21] is, however, 0.85λ, instead of 0.66λ. Thus the pattern may change little over a considerable range of phase deviation. It appears likely, therefore, that the present horn pattern will have the same general characteristics and approximately the same gain over the frequency band.

6.3 Double-Taper Horn

Double-taper horns were studied as a means of reducing the mode conversion produced at the throat of the developmental model horn. The mode conversion is reduced in this case by making L_1 of Fig. 6.4 one beat wavelength, and by adjusting the differential angles and cross sectional dimensions according to the relation

$$a_1\theta_1 = a_2\theta_2 \tag{6.5}$$

However, the results of calculations showed that the total length L (Fig. 6.4) required is of the order of 15 feet minimum. The overall length L is very long because of the requirement for making L_1 equal to one beat wavelength, which is long in the present case because both the desired and spurious modes are far above cutoff.

The 15 foot minimum value required for L is considered to be too large to be practical if the horn is to be used with a reflector (e.g., a folded-horn antenna). This can be understood by noting that the effective location of the phase center of the horn lies further than 15 feet back from the mouth. In this case a very long focal length reflector would be required.

7.0 Developmental Model Horn Radome

The radome selected as a result of this study is a sandwich-type construction in the form of a spherical segment that fastens to a flange at the mouth of the horn. Electrical and mechanical specifications on the radome result from consideration of the maximum VSWR consistent with the allowable pulse distortion and the waveguide pressurization required. Pattern distortion effects are small and will not be significant in this application.

The system pressurization has been specified as 2 atmospheres gauge of SF_6 or other insulating gas. Reduced pressure would be acceptable in expanded sections, as in the horn taper, to the extent that the peak power capacity is not reduced; however, it was determined that an electrically and mechanically adequate radome can be made at the mouth of the horn so that intermediate windows to reduce the pressure differential at the radome are not necessary.

The radome VSWR requirement is determined by the pulse response specification for the system. If the radome surface nearly coincides with the incident TE_{10} mode wave front, then a large fraction of the reflected energy will occur in the TE_{10} mode. This will travel down the horn and waveguide components and will be reflected again at the tube. If the distance from the tube to the radome is approximately 35 feet, the reflected energy will appear as a second transmitted pulse approximately 70 nanoseconds after the main pulse. If the radome surface does not coincide with the incident wave front, the reflected energy will be scattered backwards into several modes. Some of the modes will be relatively low order modes which can propagate in the 8" x 5.36" waveguide, and these will be reflected again at the tube and the combiner. The remaining modes will be relatively higher order modes which cannot propagate in the 8" x 5.36" waveguide, and these will be reflected within the horn or at the throat. Thus, if the radome surface is not nearly coincident with the wave

front of the incident TE_{10} mode in the horn, two spurious transmitted composite pulses each containing several modes will follow the main transmitted pulse, one corresponding to reflection of relatively higher order modes at the horn throat and the other corresponding to reflections of relatively lower order modes at the tube and combiner. The pulse heights of the two spurious pulses will be less than the height of the pulse reflection from the radome by a factor determined by the energy division between the two pulses. The larger of the two pulses will be reduced by a maximum of 3 dB. This assumes that the reflected pulses for the various modes overlap completely. Calculation of the relative travel times of the spurious modes containing the reflected energy showed that considerable overlap of the reflected pulses does occur for those modes reflected at the throat of the horn. For those modes reflected at the tube and combiner, although overlap is appreciable, it is far from complete. It appears to be advantageous to cause most of the reflected energy to occur in relatively low order modes which propagate in the waveguide and therefore experience incomplete pulse-overlap effects. The incomplete pulse overlap effects should cause a substantial reduction in the resultant height of the spurious transmitted pulse. In addition, the higher order spurious modes in traveling the round trip path from radome to tube experience considerable phase dispersion which tends to spread the spectral energy out in time, causing pulse broadening effects and reduction of the reflected pulse height.

The pulse response desired is at a -35 dB level at times where the relatively low order mode reflections appear. Assuming no losses in the system, this corresponds to an average radome VSWR of 1.036. With a normal VSWR characteristic, i.e., 1.0 at the midband frequency and a maximum value at the band edges, the maximum VSWR allowed would then be approximately 1.07. A radome design that satisfies this criteria would have to either use a minimum amount of radome material or comprise a relatively elaborate construction.

Calculations were made of the scattering from the principal mode to higher order modes by incidence on a radome surface which has a different radius of curvature than the phase front, to determine how much the allowable maximum VSWR can be increased. These calculations were made for a singly curved radome, i.e., a cylindrical shape on a rectangular output horn, with results as shown in Fig. 7.1. The expressions used are less accurate for small deviations of the phase front from the radome surface, and this is evident on the curve, since the reduction must approach zero with the deviation. It is expected that an additional 3 dB would be obtained for the case of a doubly curved surface. Fig. 7.2 shows the relationship between the maximum deviation of the phase front from the radome surface and the radii of curvature of the phase front and the radome.

Calculations were also made of the VSWR and mechanical stresses for several radome constructions. Curved shapes were considered, to minimize the stresses caused by bending moments. A cylindrical shape was considered for use on a rectangular horn and a spherical shape for a conical horn.

Use of the spherical segment for the radome leads to the minimum stresses in the radome. The tensile stress in a uniform isotropic material, in the absence of bending moments, is given by:

$$\sigma = \frac{Rp}{2t} \tag{7.1}$$

where R is the radius and t the thickness of the radome, and p is the pressure differential from the waveguide system to the atmosphere. This linear relationship is plotted in Fig. 7.3 for a 30 psi pressure differential. The glass cloth reinforced plastics useful for this application have tensile strengths in the order of 50,000 psi, however, a safety factor of 5 will be used to allow for aging, deterioration due to atmospheric exposure and flexing caused by application and release of the waveguide pressure.

Fastening the radome to the rigid flange on the horn results in bending near the flange. The bending stress imposed by this constraint adds to the tensile stress generated by the internal pressure. Computed results for the maximum bending stress in a spherical segment with a fixed edge, which occurs at the edge of the flange, are shown in Fig. 7.4. The values are only slightly lower than the tensile stress values shown in Fig. 7.3, indicating that the tensile stress used to establish the radome design should be approximately 5000 psi, to maintain the design safety factor of 5:1.

The simplest radome construction is a single dielectric layer. From Fig. 7.3, the thickness of this layer should be a minimum of 0.065 inch. The average VSWR over the frequency band of a typical glass-resin laminate of this thickness would be about 1.2, corresponding to a reflection coefficient of approximately 0.1, or -20 dB. It can be seen from Figs. 7.1 and 7.2 that it is not possible to obtain sufficient reduction of the reflection coefficient by scattering to other modes to meet the pulse response specification. The single-layer radome might also be made in the form of a half-wave layer, which would be about 7/8 inch thick. The VSWR for this construction would be 1.0 at the midband frequency, but would increase to about 1.4 at the band edges. Thus, the half-wave layer is also unsuitable for this application.

The VSWR at the band edges can be reduced by use of a two-layer, or sandwich construction. Normally, two thin skins and a core are bonded together to form a single composite structure. For this application, however, it appears that there are several advantages to a non-bonded construction. The inner skin can be sufficiently thick to contain the pressure itself, the outer skin then serving to provide a low VSWR and to protect the pressure cover from externally caused mechanical damage. The construction at the flanges can be simplified, and also made compatible for use with a continuing horn, as for a folded-horn

reflector construction, by replacement of the spacer between the two layers by a metal spacer ring. Choke grooves can then be put either into the flanges to provide an electrically smooth joint, as shown in Fig. 7.5.

Computations were made of the VSWR for sandwich structures with relatively thick skins, having air as the core material. Figure 7.6 shows the VSWR over one half of the 15% wide frequency band as a function of the thickness of one wall. This data, in conjunction with that shown in Figs. 7.1 to 7.4, establishes a radome design that satisfies the electrical and mechanical requirements on it. Thus, if we select a radome design matched to a VSWR of 1.2 at the band edges, 1.0 at the band center, the average reflection coefficient is -26 dB, and 9 dB additional reduction of the fundamental mode reflection is required to satisfy the pulse response specification. From Fig. 7.1, this can be obtained with a radome to phase front peak deviation of about 3.5 inches. With the phase front radius of about 8.5 feet, Fig. 7.2 shows that the radius of curvature of the spherical radome should be a maximum of 39 inches. Figure 7.3 shows that the inner wall thickness should be at least 0.118 inch to maintain the 5000 psi maximum stress, and Fig. 7.6 shows that this thickness will satisfy the VSWR requirement. The radome will therefore be a two-layer structure, each layer about 0.125-inch thick and separated by about 0.6 inch. A thin impermeable layer or coating on the inner surface will be used to insure against pressure leakage through the radome.

8.0 Breadboard-Model Duplexer

8.1 Introduction

Under item A003 of this contract, there is a requirement for the development of a breadboard-model duplexer. However, because of the very stringent requirements on peak-power-handling capability and on gas leakage rates with pressurization of 30 pounds gauge, it is not likely that a breadboard-model duplexer can be developed with the funds available under the present contract which would be fully operational in the actual system. Therefore, the breadboard models that would be built could only be employed to demonstrate operating principles and to obtain data for the development of a fully operational duplexer at a later time.

Several important results and findings were obtained during the study phase of this program. For example, under these studies the important problem of pre-triggering the duplexer was solved, and it was demonstrated experimentally that it is feasible to pre-trigger the duplexer to allow reflection of the short transmitted pulse without deterioration of the pulse rise time.

The cost of developing a future fully operational waveguide duplexer was reduced significantly when it was shown that essentially the same duplexer tube-mount design can be employed that was previously developed for 8.00" x 1.34" flat oversize waveguide under Contract F30602-67-C-0136. This is possible because it was shown experimentally that the metallic rods employed for pre-triggering do not cause appreciable detuning effects in the cold state. Therefore, by selecting a value of 5.36" for the height and a value of 8.00" for the width of the full-oversize waveguide, one can employ almost identically the same coupling slot design as previously developed for flat oversize waveguides having a height of 1.34". The value of 5.36" for the height was chosen to be four times the 1.34" value in order to allow the use of eight slot-coupled gas tubes with

the same dimensions and periodic spacing as used with the previous two tubes and 1.34" spacing.

Under these studies it was also shown that a balanced branch-guide coupler is the optimum configuration for the balanced duplexer that is proposed. This coupler is made even more feasible by the use of 8" x 5.36" oversize waveguide which, as stated previously, is optimum from the point of view of the duplexer tube-mount design. With a 5.36" waveguide height, the spurious LSE_{12} mode can be well suppressed with a coupling length of only 42", thereby decreasing the cost of fabricating the coupler.

Figure 1.1 is an overall system layout showing the placement of the developmental model components to be delivered under the present contract and the placement of a future operational duplexer. This layout also shows the configuration of the interim system that contains no duplexer. In this case the duplexer is replaced by a section of straight waveguide (shown dotted). Two holes are provided in the roof of the building, one for the interim system and one for the future system with duplexer.

A fully operational duplexer must comprise the following components and component assemblies:

1. 180° H-plane bend assembly
2. Oversize-waveguide balanced top-wall 3-dB coupler
3. Pre-triggered duplexer tube mount
4. Low-power receiver output section
5. High-power-combiner output section

Each of these components and component assemblies represents a costly fabrication, and this demonstrates the fact that it is not possible to develop a fully operational duplexer with the funds available under the present contract.

8.2 Description of Overall Duplexer

The duplexer employs an array of slot-coupled gas tubes mounted between 3-dB directional couplers. The 3-dB coupler on the high-power side is a balanced top-wall configuration comprising an 8.00" x 5.36" oversize waveguide coupled by means of branch guides to a pair of balanced 8.00" x 2.68" waveguides. An output combiner is employed to combine the reflected high power carried by the pair of 8.00" x 2.68" waveguides into an 8.00" x 5.36" waveguide which leads to the antenna. The receiver section employs WR284 waveguide couplers to combine the receive signal transmitted past the duplexer tubes into four tapers from 8.00" x 2.68" to 2.84" x 1.34" waveguides.

The number of flanges employed in the system has been minimized, based on convenience of fabrication and assembly of the system; all the flanges employed are shown in Fig. 1.1. All the flanges are stainless steel with crushable soft copper gaskets, except for the components on the low-power side of the duplexer tube mount.

It is seen from Fig. 1.1 that the total insertion length of the duplexer assembly in the elevation direction (i.e., the vertical distance from the load switch output flange to the output flange of the duplexer output combiner), will be approximately 6.5 feet. This insertion length is minimized by the use of the 180° H-plane bend assembly. The total horizontal offset of the vertical system axis introduced by inserting the duplexer into the system will be approximately 8.5 feet. This value of horizontal offset does not include the effects of the approximately 12-inch straight sections of waveguide that may be inserted between the four 45° H-plane bends comprising the 180° H-plane bend in order to increase the bandwidth of the 180° bend. Insertion of the 12-inch straight sections would increase the horizontal offset

by approximately 2.4 feet. The elevation of the uppermost part of the 180° H-plane bend will be increased by approximately 8.4 inches if the 12-inch straight sections are inserted. For the configuration shown in Fig. 1.1 the clearance between the 180° bend and the ceiling beam is approximately 16 inches. Therefore, there will be ample ceiling clearance even with the 12-inch straight sections inserted.

Figure 1.1 shows the output flange of the duplexer power combiner in the space between beams. This elevation position is based on the minimum possible length of the combiner (see Fig. 8.9). Figure 1.1 also shows a connecting straight section between the duplexer combiner output and the 90° H-plane bend input. It will be attempted to eliminate this straight section by incorporating an appropriate length of straight waveguide into the duplexer combiner. This can be part of the electroformed component thereby eliminating two flanges.

8.3 180° H-Plane Bend Assembly

Figure 8.1 shows the H-plane bend assembly employed to connect the duplexer into the system between the load switch and the high-power-combiner output section (see Figures 1.1 and 8.9). The flange at A-A in Figure 8.1 connects to ports 1 and 2 of the 3-dB coupler shown in Figure 8.2; the flange at B-B connects to the output of the load switch (Figure 1.1); and the flanges at C-C connect to the pair of 8" x 2.68" waveguides shown in Figure 8.9.

Four 50"-radius 45° H-plane bends are employed to obtain a total bend angle of 180° for the 8.00" x 5.36" waveguide. All flanges are stainless steel; and all except the flange at A-A are affixed by a grow-on process during electroforming. The flange at A-A will be assembled to the two ≈40"-long straight sections of 8.00" x 2.68" waveguides and to a single 45° bend after these components have been electroformed. Inserts must be employed in order to obtain the 0.88" separation between the waveguides.

The dimensions of the H-plane bends were accurately determined from the design data presented in Figure 1 of reference [9]. Thus, for a value of $a/\lambda = 2.27$, for the center of the operating frequency band, a value of R/a equal to 6.25 is required for low mode conversion at band center. For a = 8.00", this results in R = 50", as shown in Figure 8.1. These values of a/λ and R/a apply for one-cycle 45° bends, two-cycle 90° bends, and for four-cycle 180° bends. Thus, in a 180° bend four cycles of mode conversion and reconversion occur along the length of the bend.

The mode conversion characteristics for a pair of 45° bends having R/a = 6.25 and connected directly together without any intermediate straight section to form a 90° bend should be similar to the characteristics shown in Figure 9 of [9]. These data are for a bend having R/a = 5.95, and show that the center frequency for low mode conversion corresponds to a value of a/λ of approximately 2.15. With R/a = 6.25, as in the present case, the frequency for low mode conversion is higher and corresponds to a value of $a/\lambda = 2.27$.

The data in Figure 9 of [9] for a 90° bend show that the mode conversion from the TE_{10} to the TE_{20} mode is below -15 dB at the ends of a 15 percent operating band. The average mode conversion over the -15 percent band is, therefore approximately -21 dB.

Analysis shows that a 180° bend made up of four 45° bends connected directly together as shown in Figure 8.1 would have considerably higher mode conversion because of in-phase additions of the TE_{20} mode amplitudes generated in the four 45° bends. However, a 180° bend with reduced mode conversion can be obtained by inserting straight waveguide sections of length L between the four 45° bends. Analysis shows that L should be one quarter beat wavelength $(\lambda_B)_{20}$ between the TE_{10} and TE_{20} modes. For 8" waveguide operating at a frequency corresponding to $a/\lambda = 2.27$, $(\lambda_B)_{20}$ is equal to 45.40", and L is therefore 11.35".

The straight sections required to optimize the 180° bend can be built into the individual 45° bends. One convenient way that this can be accomplished is by the addition of 5.675-inch straight sections on each end of the two inner 45° bends shown in Figure 8.1 and on the inner ends of the two outer 45° bends. Each 45° bend with optimizing straight sections can be electroformed as one part, thereby eliminating the necessity of any additional flanges.

8.4 Oversize-Waveguide Balanced Top-Wall 3-dB Coupler

Figure 8.2 shows the configuration proposed for the oversize waveguide coupler required for the duplexer. This is a balanced configuration which provides 3-dB coupling between a main 8.00" x 5.36" oversize waveguide and a pair of 8.00" x 2.68" waveguides. High power from the transmitter flows into port 1. The duplexer tube mount described in Section 8.5 is attached to ports 3 and 4. The high power reflected from the duplexer tubes flows to balanced ports 2 which are combined by means of the combiner described in Section 8.7.

The coupling is through branch waveguides of length approximately equal to $\lambda/4$ (i.e., 0.88"), width = 8", and height b' which varies from approximately 0.280" at the center of the pair of symmetrical 30-branch-guide coupling arrays to approximately 0.030" at the ends. Since 30 branch-guide pairs are employed, the spacing can be made nearly $\lambda/2$ without incurring high VSWR. In this case, the spacing is 1.4" or $\approx 0.4\lambda$.

In order to minimize the total length of the coupler ($\approx$ 42"), the outer edges of the branch-guide coupling elements on the ends of the coupler are located precisely at the faces of the input and output flanges. This also eliminates the necessity of providing electrical contact at these edges. The edges of all branch-guides are radiused or chamfered in order to maximize the peak-power-handling capability.

The 42-inch coupling length that is employed corresponds to approximately three beat wavelengths between the desired TE_{10} and the spurious LSE_{12} mode. With a coupling length of three beat wavelengths, the amplitude of the LSE_{12} mode generated by the coupler is expected to be less than -30 dB relative to that of the incident TE_{10} mode.

The fact that the LSE_{12} mode is the lowest order spurious mode for the balanced configuration of Figure 8.2 represents its principal advantage. Alternate coupler configurations could consist of a pair of 8" x 5.36" waveguides coupled along common top walls or side walls. In the top wall case, the lowest order spurious mode would be the LSE_{11} mode with a beat wavelength of approximately 60". The coupling length for three beat wavelengths would therefore be 180". In the side wall case, the TE_{20} mode would be the principal spurious mode with beat wavelength of 45"; and the required coupling length would be 135". Both of these alternate configurations appear to be impractical.

The stainless steel flange at ports 1 and 2 mates with the H-plane bend assembly described in Section 8.3. This flange employs a crushable copper gasket. The brass flange at ports 3 and 4 mates with the duplexer tube mount described in Section 8.5. The duplexer tube mount will be designed so that the short-circuit plane for the duplexer tube mount in the fired state will be a distance $\lambda/4$ from the face of the coupler flange. In this way, the currents at the flange contact will be greatly reduced, thereby allowing a brass flange to be used.

The coupler can be fabricated by the electroform method by employing three polished 42-inch long aluminum mandrels, one 8" x 5.36" and two 8" x 2.68". Approximately 60 copper branch-guide elements having dimensions 0.88" x (1.4-b')" would be sandwiched between the three aluminum mandrels. The copper parts would be separated by aluminum spacers having dimensions 8" x 0.88" x (b')". After

the assembly is bolted together, approximately 0.200" copper would be grown on the top, bottom and side surfaces. The flanges would be affixed by a grow-on process during this same operation. Following this, the aluminum parts would be dissolved out chemically.

8.5 Pre-triggered Duplexer Tube Mount

Figure 8.3 shows the configuration of the duplexer tube mount that would be employed. This can be machined from brass, and would attach to the brass flange (right end) of the oversize-waveguide balanced top-wall 3-dB coupler of Figure 8.2. A one-quarter wavelength section of waveguide would be included as part of the duplexer tube mount, as shown, in order that the equivalent short-circuit plane in the fired state will be located one-quarter wavelength from the flange contact. In this way the flange contact would be at a current minimum, and therefore a crush-type high-power seal would not be required at this flange contact. However, in order to obtain a pressure seal, O-ring grooves (not shown) for neoprene or Teflon gaskets would be provided in either the duplexer tube mount or the flanges which mate with the mount.

The main waveguide dimensions (i.e., 8.00" x 5.36") were selected, as discussed in Section 8.1, in order to be able to use as nearly as possible the same slot dimensions and spacings as were determined for a flat-oversize waveguide duplexer tube mount developed under Contract F30602-67-C-0136.

The interspace between the two quartz tubes will be filled with an inert gas such as argon at a pressure of approximately 15 mmHg. In order to obtain a short recovery time the radial spacing between the two quartz tubes will be made small (i.e., ≈ 0.030").

Pre-triggering will be accomplished by means of high-voltage dc pulses applied to the 0.125-inch diameter offset trigger rods extending through the entire length of the gas tubes. These are shown in greater detail in Figure 8.4.

The trigger rods are offset so as to come into close contact with the wall of the gas tube. It is estimated that it will only be necessary to reduce the coupling slot length, ℓ, by about 2% in order to compensate for the detuning effect of the trigger rods on the band-pass characteristics of the duplexer in the untriggered state.

Pre-triggering experiments were performed with the flat-oversize-waveguide duplexer developed under Contract F30602-67-C-0136. The flat oversize waveguides have a width of 8.00 inches and a standard S-band height of 1.34 inches. The duplexer tube mount in this case consisted of four gas tubes identical to those shown in Figure 8.3. Figure 8.4 shows a sketch of the flat-oversize-waveguide duplexer with port designations, and cross-sectional dimensions of the gas tubes. Offset trigger rods as shown in Figure 8.5 were employed for these tests. Figure 8.6 shows the circuit for the dc pulse generator employed to trigger the four gas tubes.

Some measured data for the pre-triggered duplexer are shown in Figure 8.7. The effect of applying the dc trigger pulse on the transmission coefficient T_{14} from the transmitter (port 1) to the antenna (port 4) is shown in Figure 8.7a. Before the trigger is applied T_{14} is very small (typically -30 dB). When the trigger is applied, T_{14} increases rapidly to a value of approximately -1.2 dB. For these tests the dc supply voltage applied to the trigger generator (Figure 8.6) was 20 kV. The trigger repetition rate was 60 pps. Under these conditions the value of T_{14} measured with approximately 40 mW CW power at 3.3 GHz remained approximately -1.2 dB for a period of approximately 15 μsec before observable plasma decay effects occurred. Following this period during which T_{14} was essentially -1.2 dB, plasma decay caused T_{14} to decrease to -6 dB at a time approximately 40 μsec after the pulse was applied. The transmission coefficient T_{42} from the antenna (port 4) to the receiver

(port 2) was also measured during the period that the trigger pulse was applied. The recovery time from the start of the trigger pulse to the time at which T_{42} had a value of -3 dB was approximately 50 μsec. Previous measurements [3] of the same flat-oversize-waveguide duplexer operated untriggered with 880 kW peak, 1.8 μ sec pulses at 3.35 GHz indicated a recovery time of 95 μsec. This shows that the recovery time is a function of the excitation level. Reduced recovery time can be obtained by employing lower gas pressure (5 mmHg rather than 15 mmHg) and/or smaller gap dimension in the gas tubes (0.020 inches rather than 0.030 inches).

The isolation between transmitter (port 1) and receiver (port 2) during the hot state (i.e., the time during which T_{14} was essentially -1.2 dB) is -28 dB. The transmission from port 1 to port 3 in the hot state was approximately -14 dB.

Figure 8.7b shows the transmission coefficient T_{42} in the cold state between antenna (port 4) and receiver (port 2). By comparison with previous measurements [3] of T_{42} without the trigger rods present, it is concluded that the trigger rods cause only a small detuning effect (center frequency decreases from 3.35 GHz to 3.30 GHz) and the effect on the bandwidth is negligible.

8.6 Low-Power Receiver-Output Section

Figure 8.8 shows the configuration proposed for the receiver-output section. This comprises four tapers from 8.00" x 2.68" to 2.84" x 1.34" waveguide connected through WR284 E-plane offsets to a WR284 combining network employing a pair of WR284, short-slot couplers and a single WR284 magic tee. The large flange containing the 8.00" x 2.68" ends of the four tapers connects to the low-power side of the duplexer-tube mount (Figure 8.3), while the coaxial-line output of the WR284 magic tee connects to the receiver.

All items except the flanges and tapers can be purchased as stock items from outside vendors. Since the length of the signal paths in the WR284 waveguide components will be relatively short, no appreciable deterioration of the pulse build-up time is expected. An alternate configuration employing a coaxial-line combining network offers lower dispersion, and will also be considered; however, the required coaxial-line components having adequate power-handling capability may not be available as stock items, and may therefore be much more costly.

8.7 High-Power-Combiner Output Section

Figure 8.9 shows the configuration that will be employed to combine the two balanced 8" x 2.68" waveguides from port 2 of the oversize waveguide 3-dB coupler shown in Figure 8.2. The output of the combiner will be a single 8" x 5.36" waveguide.

A pair of E-plane bends each of bend angle approximately 14.5°, average bend radius of approximately 55", and arc length of approximately 13.83" will be employed to obtain a total E-plane offset of 3.51". The arc length is made one beat wavelength for the LSE_{11} mode in the 8" x 2.68" waveguide, in order to minimize the amplitude of this mode at the bend output. With two bends in cascade, as shown, the mode conversion from the two bends cancels over the operating frequency band. For the dimensions shown, the mode conversion from the E-plane offset is expected to be negligible.

The pair of 8" x 2.68" waveguides are combined at the output of the E-plane offset by means of a tapered E-plane bifurcation. The tapered bifurcating plate is employed for two reasons. The first is to reduce the tendency for breakdown to occur at the edge of the bifurcating plate in the event that the amplitudes of the TE_{10} modes incident in the two 8" x 2.68" waveguides are not equal. The edges are radiused or chamfered.

The second reason for employing a tapered bifurcating plate is to reduce the VSWR that would result due to the 0.100" plate thickness. Because of the high degree of symmetry that is employed, only the LSE_{1n} modes having n equal to or greater than 4 will be excited by the bifurcating plate. The TE_{30} mode will also be generated by the tapered plate, but the amplitude of this mode is expected to be negligible.

A 3.5-inch long E-plane taper is employed to transform from the 8" x 5.56" cross section at the output end of the bifurcating plate to the 8" x 5.36" cross section. The 3.5-inch length was established as the length required for -30 dB mode conversion from the TE_{10} mode to the LSE_{12} mode at the 8" x 5.56" cross section. The mode conversion at the 8" x 5.36" cross section is nearly equal and opposite to that at the 8" x 5.56" cross section. Therefore, low net mode conversion is expected over the operating frequency band with a taper length of 3.5 inches, since this is only a small fraction of the geometric-mean beat wavelength ($\approx$ 14 inches) between these two cross sections.

As can be seen from Figure 8.9, the overall length of this component is expected to be less than 4 feet. Therefore, it may be possible to electroform this component as one piece.

9.0 Breadboard Model Rotary Joint

Rotary joints in the waveguide runs were considered for the breadboard model. Two different concepts were investigated - one utilizing a circularly polarized TE_{11}^{o} mode and one utilizing the TE_{01}^{o} mode.

9.1 The Use of the Circularly Polarized TE_{11}^{o} Mode

The use of the circularly polarized TE_{11}^{o} mode to obtain a rotary joint is discussed in [24]. One method that has been considered for obtaining circular polarization employs modified square waveguide as shown in Fig. 9.1. Starting with a square waveguide cross section at the input (Section A-A), the cross section is transformed gradually to that shown in Section B-B by cutting off two diagonally opposite corners. Beyond Section B-B, the other pair of diagonally opposite corners are also cut until a symmetrical octagonal cross section is obtained as shown by Section C-C. The symmetrical octagonal cross section is then gradually transformed to a circular cross section which contains the motional joint. By adjusting the lengths of the modified square waveguide sections, a circularly-polarized TE_{11}^{o} mode can be obtained in the circular waveguide. The remaining sections beyond the motional joint are the same as those preceding, except that they are in reverse order.

The operation of the modified-square-waveguide circular polarizer can be understood by noting that a pair of characteristic modes of propagation of the modified square waveguide can be defined which are polarized along the two diagonal directions. The propagation constants of the two modes differ depending on the relative amounts of the corners that have been removed along the two diagonals. A TE_{10} mode incident in the square waveguide with electric field E_{in} as shown, results in equal power in the two diagonal modes. If the transitions are gradual, reflection will be small and the equality of power in the two modes will be maintained all along the length of the rotary joint. The

propagation constants of the two modes being different, however, will cause a phase shift between the two diagonal modes, and for a 90° differential phase shift, circular polarization will result in the circular waveguide section.

If the modified square waveguide is analyzed in terms of coupled modes rather than characteristic modes, it can be seen that the removal of the corners causes coupling between an incident TE_{10} mode and the cross-polarized TE_{01} mode. Coupling also occurs from the incident TE_{10} mode to the TE_{30} and LSE_{12} modes, but not to the TE_{20} mode. From this, one can deduce that the spurious mode amplitudes will have low values at the output of the polarizer if the length L_1 (Fig. 9.1) of the transducer from square to octagonal cross section is of the order of 2.5 beat wavelengths between the TE_{10} and LSE_{12} modes. For 8" square waveguide and $a/\lambda = 2.27$ at mid band this would require L_1 approximately 3'. The transition from octagonal to circular cross section would probably require an additional length of approximately 1.5'. The overall length of an S-band rotary joint would therefore be approximately 10'.

Elliptical waveguide can also be employed to obtain circular polarization. This has an advantage in that the propagation constants of the characteristic modes are known [25]. With elliptical waveguide, the major axis of the ellipse would be oriented at 45° to the incident polarization E_{in}. The modified square waveguide polarizer appears to be much easier to fabricate, however, Furthermore, one could also rather simply determine the propagation constants of the characteristic modes in the modified square waveguide either by approximate analytical methods or experimentally.

Some consideration was given to the design of the motional joint for the configuration shown in Fig. 9.1. This joint can employ conventional reactive chokes [25] which are lossless and ordinarily introduce very low insertion loss.

In the case of oversize waveguides such a choke may suffer from spurious resonances (Ref. 2, pp. 291-294). It may be possible to minimize the effects of these resonances by employing a modified choke design as shown in Fig. 9.2. This employs a circumferential choke groove in the usual way, and in addition employs radial grooves to force the current flow in the choke region to conform to that of the current flowing from the main waveguide. The radial grooves accomplish this by inhibiting propagation in the circumferential direction. In Fig. 9.2 the dimensions of the circumferential groove have the usual values; i.e., ℓ_1 and ℓ_2 are approximately $\lambda/4$ and D_3 is large compared to D_2. The gap g is made as small as possible depending on the mechanical alignment that can be maintained. The depth ℓ_3 and the spacing S of the radial grooves are adjusted to obtain a cutoff-filter effect in the circumferential direction; i.e., ℓ_3 and S are approximately $\lambda/4$. The width W can be approximately $\lambda/10$.

An alternate approach* to the motional joint problem is to eliminate all the grooves, both circumferential and radial, in Fig. 9.2, and to allow the energy entering the region between the flanges to radiate into a dissipative medium. This approach minimizes the spurious resonance problem, but introduces a small power loss P_L given by

$$\frac{P_L}{P_{in}} = \frac{2g}{D_1}$$

where P_{in} is the power incident in the waveguide. The insertion loss associated with this power loss is given by 8.686 g/D. For example, if g is 0.100" and D is 8.00", the insertion loss is 8.686/80 = 0.109 dB.

9.2 Rotary Joint with TE^{o}_{01} Mode

Another configuration considered for the rotary joints employs two axial transducers from the TE_{10} mode in oversize rectangular waveguide to the circular electric TE^{o}_{01} mode in circular waveguide. The two transducers are connected

* This motional joint can be employed with a large diameter folded-horn antenna as discussed in Section 9.3.

back-to-back with the motional joint in the circular section. Since the TE_{01}° mode has zero longitudinal current flow, leakage and breakdown problems at the motional joint in the circular waveguide are minimized.

Figure 9.3 shows a proposed configuration for a transducer from oversize rectangular waveguide carrying the TE_{10} mode to circular waveguide carrying the TE_{01}° mode. The oversize rectangular waveguide, having a width $a = 2.27\lambda (a_1 = 8")$ and a height $b = 5.36"$, is transformed by means of an H-plane taper to a waveguide having a width, a_2, less than 1.5λ (in order to prevent the $TE_{30}^{\square}$ mode from propagating) and a height $b = 6.92"$. The taper is followed by a short straight section and E- and H-plane bifurcations which divide the power equally and in phase among eight standard, single-mode, WR284 waveguides ($a_4 = 2.84$ inches). The eight single-mode waveguides are twisted in order to obtain the relative phases and polarizations shown in Section B-B. The individual rectangular waveguide cross sections are then transformed into circular sector cross sections as shown at Section C-C. From cross section C-C, the TE_{01}° mode is launched into the circular waveguide with minimum reflection and minimum electric field enhancement.

The type of H-plane bifurcation junction shown in Fig. 9.3 has been demonstrated experimentally ([4] and [3]). The measured VSWR was less than 1.06 over a 12 percent bandwidth and was less than 1.1 over a 15 percent bandwidth.

The total peak power-handling capability of the eight WR284 waveguides is about 50 percent of the capability of 8 inch by 5.36 inch oversize waveguide or about 70 percent of the total capability of four WR430 waveguides. The power-handling capability of the straight waveguide section having a width $a_2 = 4.3"$ and a height $b_2 = 6.92"$ is the same as that of eight WR284 waveguides.

It may be feasible to use standard WR284 waveguides between Sections A-A and B-B which have been twisted by established waveguide bending and twisting

techniques. Special care would be taken to insure that the electrical path lengths of the eight sections of waveguide are identical and shimming techniques would be used if necessary. The path length between Sections A-A and B-B is estimated to be about 18". Thus, each rotary joint will contain about three feet of standard width waveguide. Transient measurements [3] have shown that the dispersion of three feet of WR284 waveguide will increase the rise time of a zero rise time pulse to about three radio frequency cycles.

9.3 Rotary Joints for Folded-Horn Antennas

An alternate concept offers to eliminate the need for rotary joints in the 8.00 x 5.36-inch oversize-rectangular-waveguide part of the system. This concept would be employed in conjunction with a folded-horn antenna [26,27]. Azimuth and elevation motion would be accomplished by means of large-diameter motional joints beyond the radome in the vertical and horizontal conical sections of the folded-horn reflector antenna. The choked motional joint configuration shown in Fig. 9.2 or the alternate dissipative configuration described in Section 9.1 can be employed. The use of motional joints as part of the folded-horn antenna system would result in a shorter overall system and lower dispersion.

10.0 Developmental-Model Signal-Sampling Coupler

Sampling couplers will be placed at the output of the developmental-model combiner and at the input to the developmental-model horn in order to monitor the waveform and power of the desired mode and selected spurious modes. Coupling values in the range -40 to -60 dB are desirable. However, it may be difficult to achieve this high a coupling through one or two small holes on the side walls as proposed below. With looser coupling, greater shielding precautions must be taken against interfering signals entering the sampling coupler detectors through other than the desired path.

Table 10.1 lists all the propagating TE_{mn}, TM_{mn} modes in the 8.00" x 5.36" waveguide along with the waveguide wavelengths and the beat wavelengths relative to the desired TE_{10} mode. As a result of the symmetry of the developmental-model combiner, however, only the TE_{10}, LSE_{11}, LSE_{12}, and LSE_{13} propagating modes will be excited appreciably over the operating frequency band in the 8.00" x 5.36" oversize waveguide by an arbitrary phase and magnitude distribution among the four output waveguides from the tube. It will be recalled that the LSE_{mn} modes are linear combinations of the TE_{mn} and TM_{mn} modes having the electro-field vector lying in a longitudinal section parallel to the E plane of the desired TE_{10} mode. By proper design the spurious mode conversion of the combiner can be below -30 dB, and for purposes of discussion, this will be defined as an ideal combiner. Thus, with an ideal combiner, the four output waveguides from the tube represent four degrees of freedom for exciting the oversize waveguide system in the four characteristic TE_{10}, LSE_{11}, LSE_{12} and LSE_{13} propagating modes.

A study of the tube output configuration shows that if mechanical symmetry is maintained in the output waveguides, and if the electron beam couples equally to each of the two waveguides leaving each output cavity, then a further

simplification is possible. In this connection, it is convenient to define an ideal tube output system as one in which the wave amplitudes a_1 and a_3 (referenced at the combiner input) from one of the tube cavities are equal to each other in magnitude and phase, and furthermore the amplitudes a_2 and a_4 from the other tube cavity are equal to each other in magnitude and phase. In this definition, the amplitudes a_1 and a_3 can differ from the amplitudes a_2 and a_4 in magnitude and phase. A study of the combiner shows that with an ideal tube output system only the LSE_{12} spurious mode is excited in the oversize waveguide if the symmetrical method of interleaving is employed in the combiner, and only the LSE_{13} spurious mode is excited if the anti-symmetrical method is employed.

Since it appears somewhat simpler to measure the combination of the desired TE_{10} mode and the spurious LSE_{12} mode, than the combination of the desired TE_{10} mode and the spurious LSE_{13} mode, the decision was made to employ the symmetrical method of interleaving in the combiner.

Figure 10.1 shows a method for measuring the TE_{10} and LSE_{12} mode amplitudes in the main oversize waveguide. In this method, the y component of the magnetic field of the LSE_{12} mode and the z component of the TE_{10} mode are measured by means of two small round holes located on one of the side walls of the oversize waveguide of width a and height b. These holes couple the oversize waveguide to either round or square sampling waveguides of cross-sectional dimension b'. The sampling waveguides are loosely coupled by means of electric-field probes to coaxial lines which are combined by hybrid combiners not shown in Figure 10.1. The outputs from the probes marked 10 and 10' result from the y component of magnetic field of the TE_{10} mode, and the outputs from the probes marked 12 and 12' result from the z component of the magnetic field of the LSE_{12} mode. The hybrid combiners add the outputs of probes 10 and

10' to obtain the TE_{10}-mode output signal, and add the output of probes 12 and 12' to obtain the TE_{12}-mode output signal. The power not coupled to the coaxial lines is absorbed in the matched loads. The electric-field probes are only loosely coupled in order to maintain low reflections from these probes and thereby prevent a high standing wave between the probes and the coupling holes. By placing the probes close to the coupling holes the transient response time of the sampling system will be short.

The y component $(H_y)_{LSE}$ of the magnetic field of the LSE_{mn} mode is given by

$$(H_y)_{LSE} = \frac{2\sqrt{\frac{\lambda}{z_o ab \lambda_{mn}}} \left(\frac{na}{mb}\right) \left[\frac{\left(\frac{m\lambda}{2a}\right)^2 + \left(\frac{n\lambda}{2b}\right)^2}{1 - \left(\frac{m\lambda}{2a}\right)^2 - \left(\frac{n\lambda}{2b}\right)^2} \right] \cos\frac{m\pi x}{a} \sin\frac{n\pi y}{b}}{\left\{ \left[1 + \left(\frac{na}{mb}\right)^2\right] \left[1 + \left(\frac{na}{mb}\right)^2 \left(\frac{\lambda_{mn}}{\lambda}\right)^2\right] \right\}^{1/2}} \qquad (10.1)$$

The z component $(H_z)_{10}$ of the magnetic field of the TE_{10} mode is given by

$$(H_z)_{10} = \left(\frac{\lambda}{a}\right) \frac{1}{\sqrt{2abz_o}} \left(\frac{\lambda_{10}}{\lambda}\right)^{1/2} \cos\frac{\pi x}{a} \qquad (10.2)$$

In Eqs. (10.1) and (10.2) unit power is assumed in the LSE_{mn} and TE_{10} modes; z_o and λ are the wave impedance and wavelength, respectively, of a free-space uniform plane wave; λ_{mn} is the wavelength of the m,n th mode.

The system calibration factor is the ratio R_c between the amplitudes V_{12} and V_{10} of the output voltages of the LSE_{12}-mode hybrid and the TE_{10}-mode hybrid for equal power in the two modes. R_c is given by

$$R_c = \frac{\frac{a}{\lambda}\,4\sqrt{2}\;\frac{a}{b}\sqrt{\frac{\lambda^2}{\lambda_{10}\lambda_{12}}}\left[\frac{\left(\frac{\lambda}{2a}\right)^2+\left(\frac{\lambda}{b}\right)^2}{1-\left(\frac{\lambda}{2a}\right)^2-\left(\frac{\lambda}{b}\right)^2}\right]}{\left\{\left[1+\left(\frac{2a}{b}\right)^2\right]\left[1+\left(\frac{2a}{b}\right)^2\left(\frac{\lambda_{12}}{\lambda}\right)^2\right]\right\}^{1/2}} \qquad (10.3)$$

Equation 10.3 was obtained by dividing the right-hand side of Eq.(10.1) by the right-hand side of Eq.(10.2) after setting m = 1, n = 2, x = a/2 and b = y/4. As a typical example, let a = b $\approx 2\lambda$; in this case, $\lambda_{mn}/\lambda \approx 1$ and

$$R_c \approx \frac{8\sqrt{2}\left[\frac{1}{16}+\frac{1}{4}\right]}{5} = 1/\sqrt{2}$$

Thus, the normalized amplitude A_{12} of the LSE_{12} mode in the oversize waveguide relative to the normalized amplitude A_{10} of the TE_{10} mode is ≈ 3 dB greater than the measured value of (V_{12}/V_{10}) in the above typical example. In general

$$A_{12}/A_{10} = (V_{12}/V_{10})/R_c \qquad (10.4)$$

where (V_{12}/V_{10}) is the measured ratio of the output voltages of the LSE_{12} and TE_{10}-mode hybrids. For equal power in the TE_{10} and LSE_{12} modes V_{12}/V_{10} is equal to R_c by definition.

Consideration was also given to the effect of the cross-polarized TE_{01} mode. This mode has a strong component of H_y along the side wall as shown in Fig.(10.1), and can cause significant errors in the measurement of the amplitude of the LSE_{12} mode if the hybrid employed to combine the outputs of probes 12 and 12' does not have high isolation and directivity. In this connection, the ratio R between the y components of the magnetic fields of the LSE_{12} and TE_{01} modes is important. R is given by

$$R = \frac{\frac{4a}{b}\sqrt{\frac{\lambda_{01}}{2\lambda_{12}}}\left[\frac{\left(\frac{\lambda}{2a}\right)^2 + \left(\frac{\lambda}{b}\right)^2}{1 - \left(\frac{\lambda\lambda}{2a}\right)^2 - \left(\frac{\lambda}{b}\right)^2}\right]}{\left\{\left[1 + \left(\frac{2a}{b}\right)^2\right]\left[1 + \left(\frac{2a}{b}\right)^2\left(\frac{\lambda_{12}}{\lambda}\right)^2\right]\right\}^{1/2}} \qquad (10.5)$$

In the case of the typical example given previously ($a = b = 2\lambda$).

$$R \approx \frac{4/\sqrt{2}\left[\frac{1}{16} + \frac{1}{4}\right]}{5} = 1/4\sqrt{2} = -15 \text{ dB}$$

Thus, for equal power in the two modes, the y component of the TE_{01} mode is 15 dB greater than that of the LSE_{12} mode. Since it is conceivable that the spurious TE_{01} mode can have approximately the same power as the LSE_{12} spurious mode, it is seen that accurate measurement of the amplitude of the LSE_{12} mode requires an overall system electrical balance (including the phase length of connecting coaxial lines and combining hybrids) of the order of 20 to 30 dB.

The diameter of the coupling holes required for the configuration shown in Fig. 10.1 has not been determined during the study phase. However, based on previous experience with coupling holes between a pair of full-oversize waveguides it appears that hole diameters D less than 0.4λ can produce coupling values considerably greater than -60 dB. Since λ is 3.522" at mid band, D in this case would be approximately 1.4". Since b is 5.36", a considerably larger hole can actually be accommodated. The electric-field probes should be decoupled by -10 to -20 dB to prevent dispersive effects due to multiple reflections between hole and probe. It appears, therefore, that an overall coupling value of -60 dB may be attainable.

In the event that it is not permissible to assume an ideal tube output system, as defined previously, provision must be made for measuring all four of the possible propagating modes (i.e., the TE_{10}, LSE_{11}, LSE_{12} and LSE_{13} modes) beyond the combiner in the oversize waveguide. Figure 10.2 shows one

possible method for measuring the normalized amplitudes of the LSE_{11} and LSE_{13} modes relative to the normalized amplitude of the TE_{10} mode. In this method, the side wall of the oversize waveguide of height b is divided into six equal sections as shown, and coupling to sampling waveguides of height $b' \approx b/6$ (or smaller) is accomplished through slots of transverse width equal to w/2 and longitudinal length equal to ℓ. The longitudinal slots have w considerably less than ℓ, and therefore respond primarily to the longitudinal magnetic field H_z related to the y component I_y of the current flowing on the side wall. The variation of H_z along the side wall is also shown in Figure 10.2 for the LSE_{11} and LSE_{13} modes; H_z for the TE_{10} mode is constant along the side wall.

It is seen that V_o, the voltage generated in the sampling waveguide at the center of the side wall, is proportional to the normalized amplitude A_{10} of the TE_{10} mode, since H_z is zero at the center for both the LSE_{11} and LSE_{13} modes. Furthermore, the difference between V_2 and V_2' is proportional to the normalized amplitude A_{11} of the LSE_{11} mode, since H_z is zero for the LSE_{13}, while H_z for the TE_{10} mode is equal and in phase at these holes.

The normalized amplitude A_{13} of the LSE_{13} mode can be determined by subtracting the outputs of waveguides at 1 and 1' and subtracting this difference from the difference between the outputs of the two half-height waveguides 3 and 3'. Thus,

$$V_1 - V_1' = 2k_{11}A_{11}/2 + 2k_{13}A_{13}$$

$$\frac{V_3 - V_3'}{2} = k_{11}A_{11} + k_{13}A_{13}$$

$$(V_1 - V_1') - \left(\frac{V_3 - V_3'}{2}\right) = k_{13}A_{13}$$

where k_{11} and k_{13} are proportionality factors.

The developmental-model sampling coupler delivered under the present contract will have the capability of measuring only the desired TE_{10} mode and the LSE_{12} spurious mode; i.e., only the configuration shown in Fig. 10.1 will be built. However, experience with the tube in actual operation may show that all four modes (i.e., the TE_{10}, LSE_{11}, LSE_{12} and LSE_{13}) excited by an arbitrary phase and magnitude distribution of the four tube outputs should be measured. In this case, the sampling method shown in Fig. 10.2 can be employed, and the necessary coupling holes can be incorporated at a later time in the side wall directly opposite to that containing the coupling holes for the configuration of Fig. 10.1.

Table 10.1

Waveguide Wavelengths and Beat Wavelengths for TE_{mn} and TM_{mn} Propagating Modes in 8.00" x 5.36" Rectangular Waveguide

Lower Band Edge

f = 3.09874 GHz, λ = 3.80892", a/λ = 2.10033

m	n	λ_{mn}	$(\lambda_B)_{mn}$
0	0	3.80892	-132.489
0	1	4.07481	104.347
0	2	5.41365	14.2297
1	0	3.92166	0
1	1	4.21375	56.5757
1	2	5.75297	12.3197
2	0	4.33135	41.4608
2	1	4.73507	22.8291
2	2	7.35298	8.40375
3	0	5.44155	14.0405
3	1	6.31571	10.3457
4	0	12.4726	5.72023

Band Center

f = 3.34998 GHz, λ = 3.52326", a/λ = 2.27062

m	n	λ_{mn}	$(\lambda_B)_{mn}$
0	0	3.52326	-143.536
0	1	3.7305	113.63
0	2	4.67519	15.8815
0	3	21.1198	4.35707
1	0	3.61192	0
1	1	3.83623	61.7725
1	2	4.88854	13.831
2	0	3.92433	45.3702
2	1	4.21706	25.1704
2	2	5.76141	9.68124
3	0	4.69312	15.678
3	1	5.21994	11.725
3	2	9.71524	5.74944
4	0	7.4415	7.01854
4	1	10.3381	5.55149

Table 10.1 (cont.)

Upper Band Edge

f = 3.60122 GHz, λ = 3.27746", a/λ = 2.44092

m	n	λ_{mn}	$(\lambda_B)_{mn}$
0	0	3.27746	-154.562
0	1	3.44228	122.853
0	2	4.14202	17.4775
0	3	8.22596	5.64722
1	0	3.34846	0
1	1	3.52483	66.9223
1	2	4.2882	15.2796
1	3	9.59053	5.14469
2	0	3.59281	49.2355
2	1	3.81335	27.4665
2	2	4.84146	10.8583
3	0	4.15447	17.2592
3	1	4.50667	13.0291
3	2	6.57507	6.82338
4	0	5.7171	8.08206
4	1	6.75845	6.6365

11.0 Conclusions and Recommendations

The following conclusions and recommendations are made as a result of the work carried out during the study phase of this program. Conclusions and recommendations pertaining to each of the required system components will be given.

1. Developmental-Model Combiner - The approach for this component is to employ an E-plane bifurcation for combining waveguide outputs into a single oversize waveguide. The results of the study show that a reduction in overall system length would result if the twists required for the combiner were included as part of the tube output section. However, this may not be feasible from other considerations. In any case, it is concluded that the use of waveguide twists for orienting the tube outputs is superior to the other methods considered including the use of phase shifting sections. It should also be noted that the high-power output-waveguide configuration shown in Fig. 2.1c leads to the simplest twist configuration for the combiner. It is also concluded that flexible waveguide sections should be placed between the combiner and tube output for stress relief. These flexible sections will not be supplied under the present contract.

2. Developmental-Model Load Switch - The results of the studies show that a load switch employing a motional choke joint can be designed for oversize waveguide. It is concluded that the configuration employing translational motion has important advantages over the configuration employing rotational motion.

3. Developmental-Model Straight Lengths of Waveguide - It is concluded that 8.00 x 5.36-inch cross-sectional dimensions are optimum. These can be electroformed in up to 4-foot lengths.

4. Developmental-Model Bends - It is concluded that a cost saving can result through the use of a pair of 45° H-plane bends instead of the originally specified 60° and 90° bends. The 45° bends will have 50-inch average radius.

5. Developmental-Model Horn Radiator - It is concluded that an optimum configuration for the horn consists of a gradual transition from the 8.00 x 5.36-inch rectangular waveguide input to the 44.4-inch diameter round radiating aperture. This configuration reduces the overall system length and can be fabricated economically. This horn will be fully compatible with a future folded-horn reflector antenna.

6. Developmental-Model Radome - A spherically shaped two-layer glass-resin structure is recommended for this radome. Each layer is approximately 0.125-inch thick.and the layers are separated by air interspace 0.600-inch thick with the inner layer supporting the pressure. The radome flange will be adaptable to a future folded-horn reflector antenna.

7. Breadboard-Model Duplexer - A successful method was demonstrated for pre-triggering the duplexer. This method employs dc pulse excited trigger rods extending the full length of each gas tube. It was also shown that a balanced 3-dB branch-guide coupler is optimum for the balanced duplexer application. The choice of 8.00-inch x 5.36-inch oversize waveguide allows an existing duplexer tube mount design to be employed and results in a shorter 3-dB coupler.

The design of the several components and component assemblies required for the duplexer are described in Section 8 of this report. Each of these represents a costly fabrication, and this demonstrates the fact that it is not possible to develop a fully operational duplexer with the funds available under the present contract.

8. Developmental-Model Rotary Joint - Two configurations for rotary joints for oversize rectangular waveguides are described in this proposal. One of these configurations (Fig. 9.1) appears to have the advantages of simplicity, high-power handling and low dispersion.

Design approaches are also described in Section 9.3 for large-diameter rotary joints to be used in a folded-horn antenna beyond the 44-inch diameter cross section. Since a folded-horn antenna is being proposed for use with the nanosecond radar system, it is recommended that further work be confined to motional joints for this type of antenna.

9. Developmental-Model Sampling Coupler - Analysis of the tube output system reveals that if symmetry is maintained, the problem of spurious mode measurements can be greatly simplified. In this case, only the LSE_{12} mode is generated in the oversize waveguide system if a symmetrical method of interleaving is employed in the combiner.

It is therefore recommended that a sampling coupler for measuring only the desired TE_{10} mode and the spurious LSE_{12} mode be developed. Couplers of this type will be placed at the input to the load switch and at the input to the horn radiator.

12.0 List of References

[1] J. P. Quine, C. Younger, J. W. Maurer, "Ultra high power transmission line techniques," RADC-TR-65-164, Final Report, Contract AF30(602)-2990, September 1965.

[2] J. P. Quine and C. Younger, "High power microwave components in oversized waveguide," RADC-TR-67-117, Final Report, Contract AF30(602)-3682, May 1967.

[3] J. P. Quine, C. Younger, "Low-dispersion high-power waveguide systems," Technical Report No. RADC-TR-68-154, Final Report Contract F30602-67-C-0136, June 1968.

[4] J. P. Quine and C. Younger, "Low-dispersion high-power waveguide systems, RADC-TR-67-534, Contract F30602-67-C-0136, Rome Air Development Center, November 1967.

[5] H. A. Wheeler and H. Schwiebert, "Step-twist waveguide components," IRE Transactions - Microwave Theory and Techniques, Vol. MTT-3, pg. 48, October 1955.

[6] T. Moreno, Microwave Transmission Design Data, New York: McGraw-Hill, 1948, pg. 164.

[7] L. Lewin, "Propagation in curved and twisted waveguides of rectangular cross-section," Proc. IEE, Vol. 102, pt. III, pp. 75-80, January 1955.

[8] R. C. Johnson, "Design of linear double tapers in rectangular waveguides," IRE Transactions on Microwave Theory and Techniques, Vol. MTT-7, No. 3, pg. 376, July 1959.

[9] J. P. Quine, "E- and H-plane bends for high-power oversized rectangular waveguide," IEEE Transactions on Microwave Theory and Techniques, Vol. MTT-13, No. 1, pp. 54-63, January 1965.

[10] G. L. Ragan, Microwave Transmission Circuits, MIT Radiation Laboratory Series, Vol. 9, Boston Technical Publishers, Inc., Lexington, Mass., 1964, pp. 208-209.

[11] ibid, pp. 100-114, 193-203, 291-294.

[12] J. J. Jarek, H. W. Moore, J. P. Quine, C. Younger, "High power waveguide components in oversized waveguides," Technical Report No. RADC-TR-65-485, April 1966, Contract AF30(602)-3682.

[13] R. D. Lending, "New criteria for microwave components," Proc. N. E. C., Vol. 11, 1955, pp. 391-401.

[14] L. G. Virgile, "Deflection of waveguide subjected to internal pressure," IRE Trans., Vol. MTT-5, pp. 247-250, October 1957.

[15] J. P. Quine, "Oversize tubular metallic waveguides," in Microwave Power Engineering, (E. C. Okress, ed.) New York: Academic Press, 1968, Vol. 1, pg. 191.

List of References (cont'd)

[16] K. Tomiyasu et al, Super Power CW Transmission Line Techniques, Technical Report No. RADC-TR-67-609, pg. 83, December 1967.

[17] G. Piefke, "Reflection at incidence of an H_{mn}-wave at junction of circular waveguide and conical horn," in Electromagnetic Theory and Antennas (E. C. Jordan, ed.). New York: MacMillan, 1963, part 1, pp. 225-226.

[18] H. E. M. Barlow, "The relative power-carrying capacity of high-frequency waveguides," Proc. IEE (London), Vol. 99, part III, pp. 21-27, January 1952.

[19] M. G. Schorr and F. J. Beck, "Electromagnetic field of the conical horn," Jour. of Appl. Physics, Vol. 21, pp. 795-801.

[20] T. Li and R. H. Turrin, "Near-zone field of the conical horn," IEEE Trans. on AP, Vol. 12, pp. 800-802, November 1964.

[21] G. C. Southworth and A. P. King, "Metal horns as directive receivers of ultra-short waves," Proc. IRE, Vol. 27, pp. 95-102, February 1939.

[22] A. P. King, "The radiation characteristics of conical horn antennas," Proc. IRE, Vol. 38, pp. 249-251, March 1950.

[23] H. Jasik, Antenna Engineering Handbook. New York: McGraw-Hill, 1961, pp. 10-12.

[24] G. L. Ragan, Microwave Transmission Circuits, M. I. T. Radiation Laboratory Series, Vol. 9, Boston Technical Publishers, Inc., Lexington, Mass., 1964, pp. 428-432.

[25] L. O. Chu, "Electromagnetic waves in elliptic hollow pipes of metal," Jour. of Appl. Physics, Vol. 9, pp. 583-591, September 1938.

[26] A. J. Giger and R. H. Turrin, "The triply-folded horn reflector: a compact ground station antenna for satellite communication," Bell System Technical Journal, Vol. 44, pp. 1229-1253, September 1965.

[27] J. N. Hines, Tingye Li and R. H. Turrin, "The electrical characteristics of the conical horn-reflector antenna," Bell System Technical Journal, Vol. 42, pp. 1187-1211, July 1963.

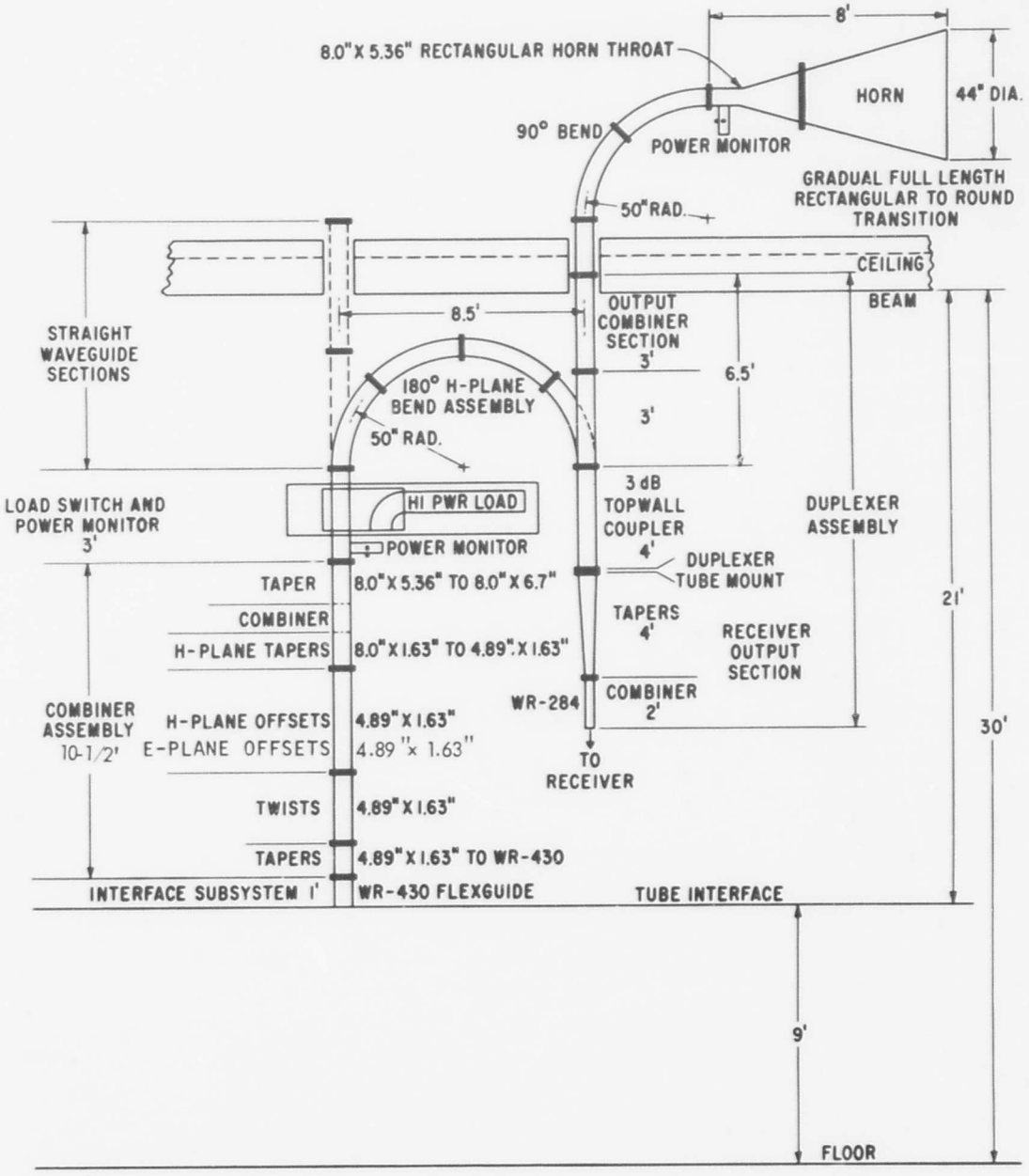

Figure 1.1. Overall Layout of Oversize Waveguide System

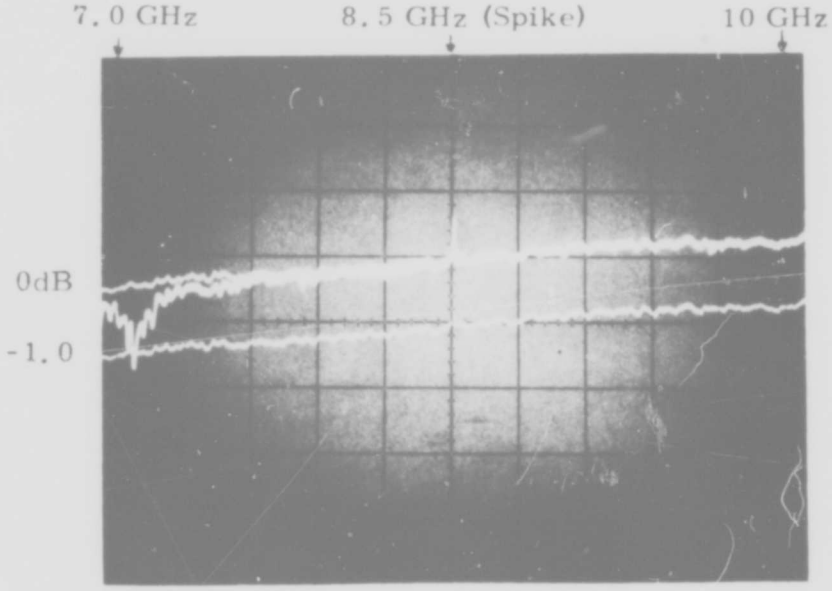

a) Transmission Coefficient

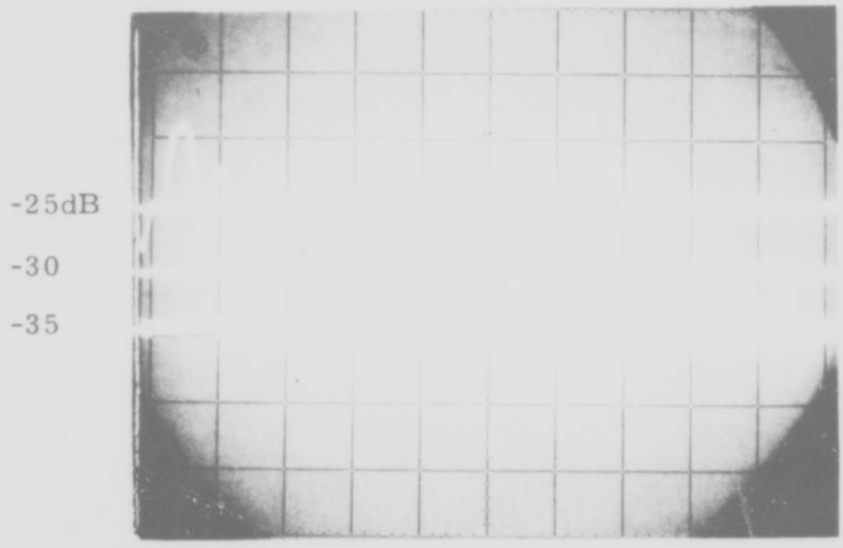

b) Reflection Coefficient

Figure 3.4 Transmission and Reflection Coefficients of Double-Groove X-Band Choke Joint with 0.050 inch gap.

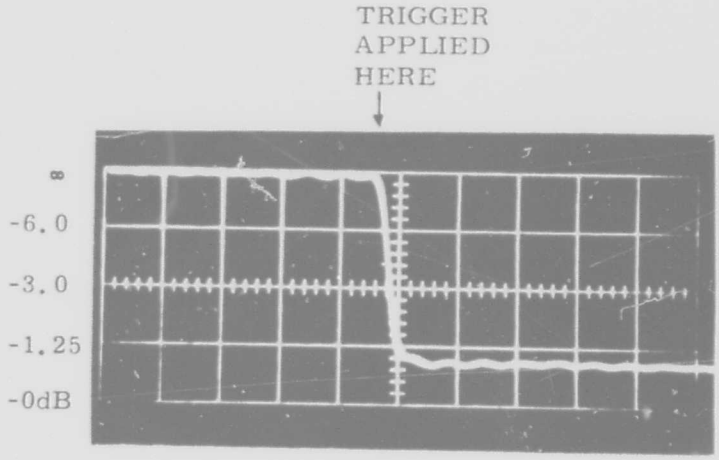

a) Transmission Coefficient from Transmitter to Antenna f=3.3 GHz. Horizontal Scale: 0.1 μsec/cm

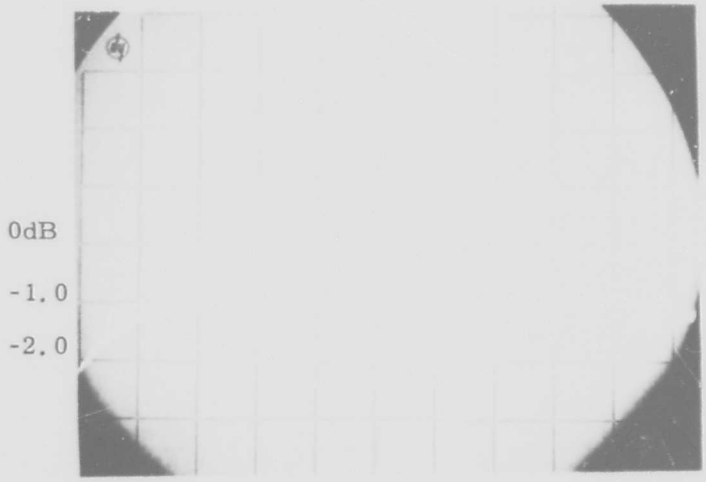

b) Cold State Transmission Coefficient From Antenna to Receiver. Horizontal Scale: 0.1 GHz/cm with 3.35 at center. Vertical Scale: 1 dB/cm

Figure 8.7 Pre-Triggered Duplexer Characteristics.

(a) Original Concept of Tube Output Configuration

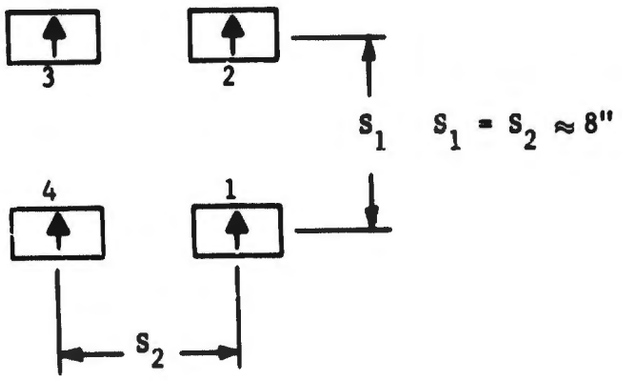

(b) Output Configuration of First Tube

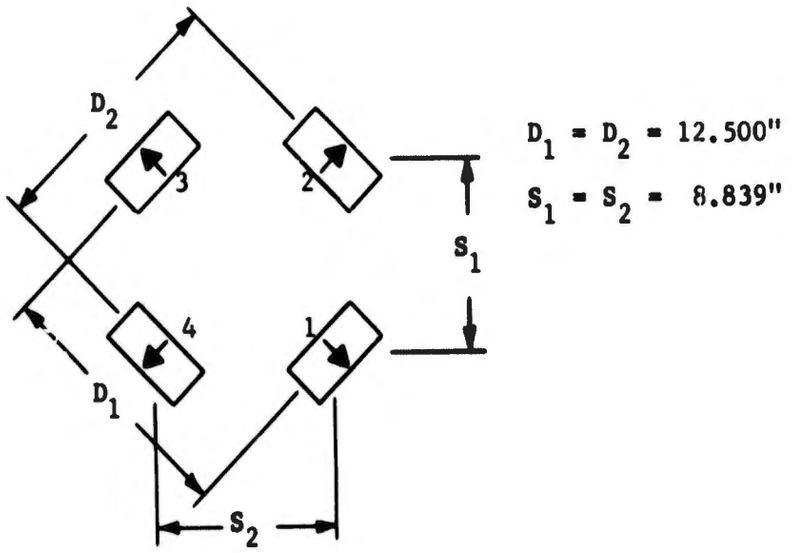

(c) Proposed Alternate Output Configuration

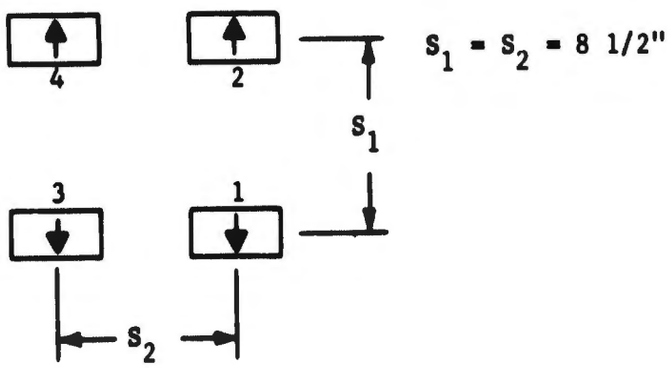

Figure 2.1 High-Power Klystron Output-Waveguide Configurations

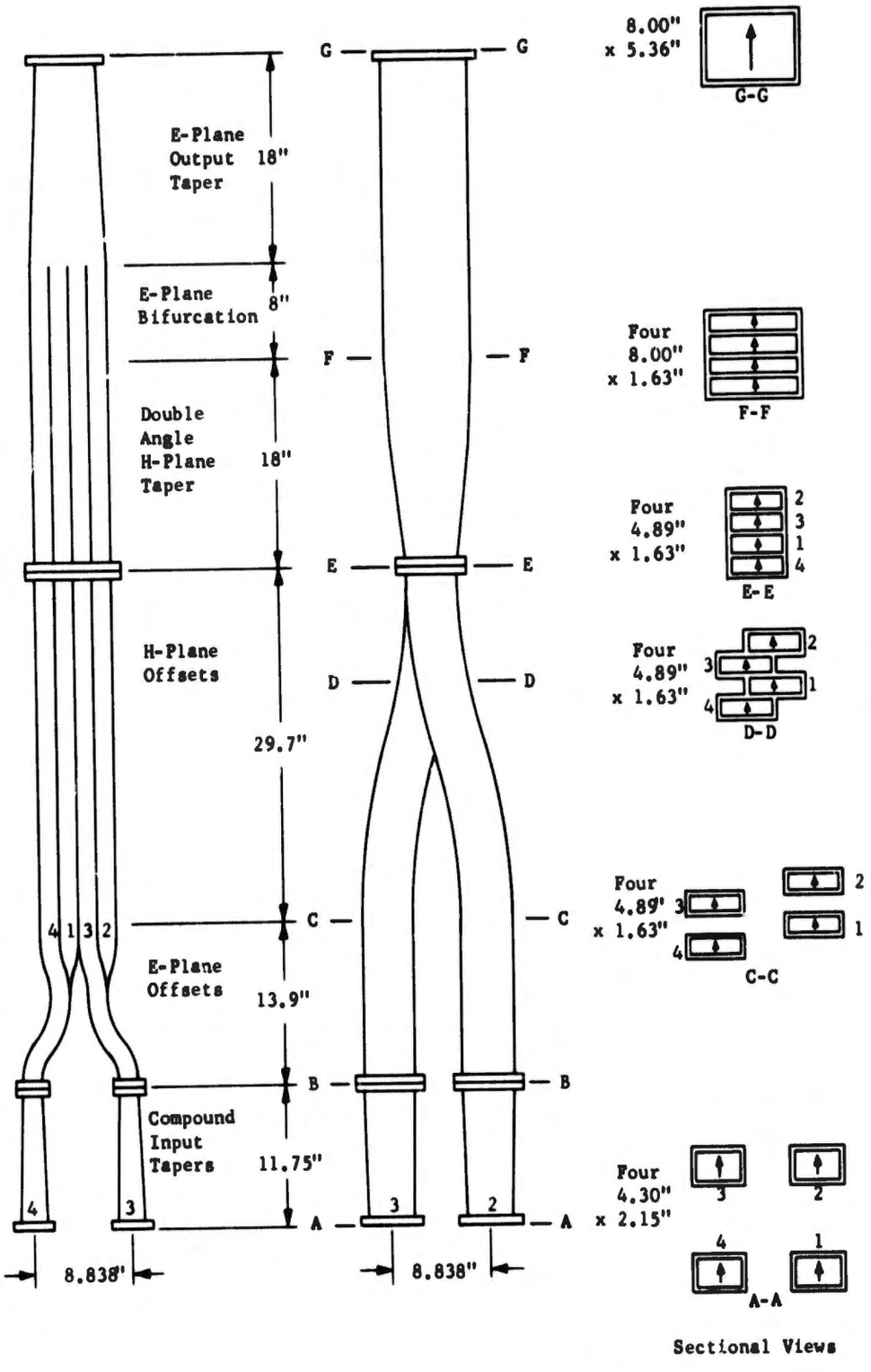

Figure 2.2 Power Combiner without Twists.

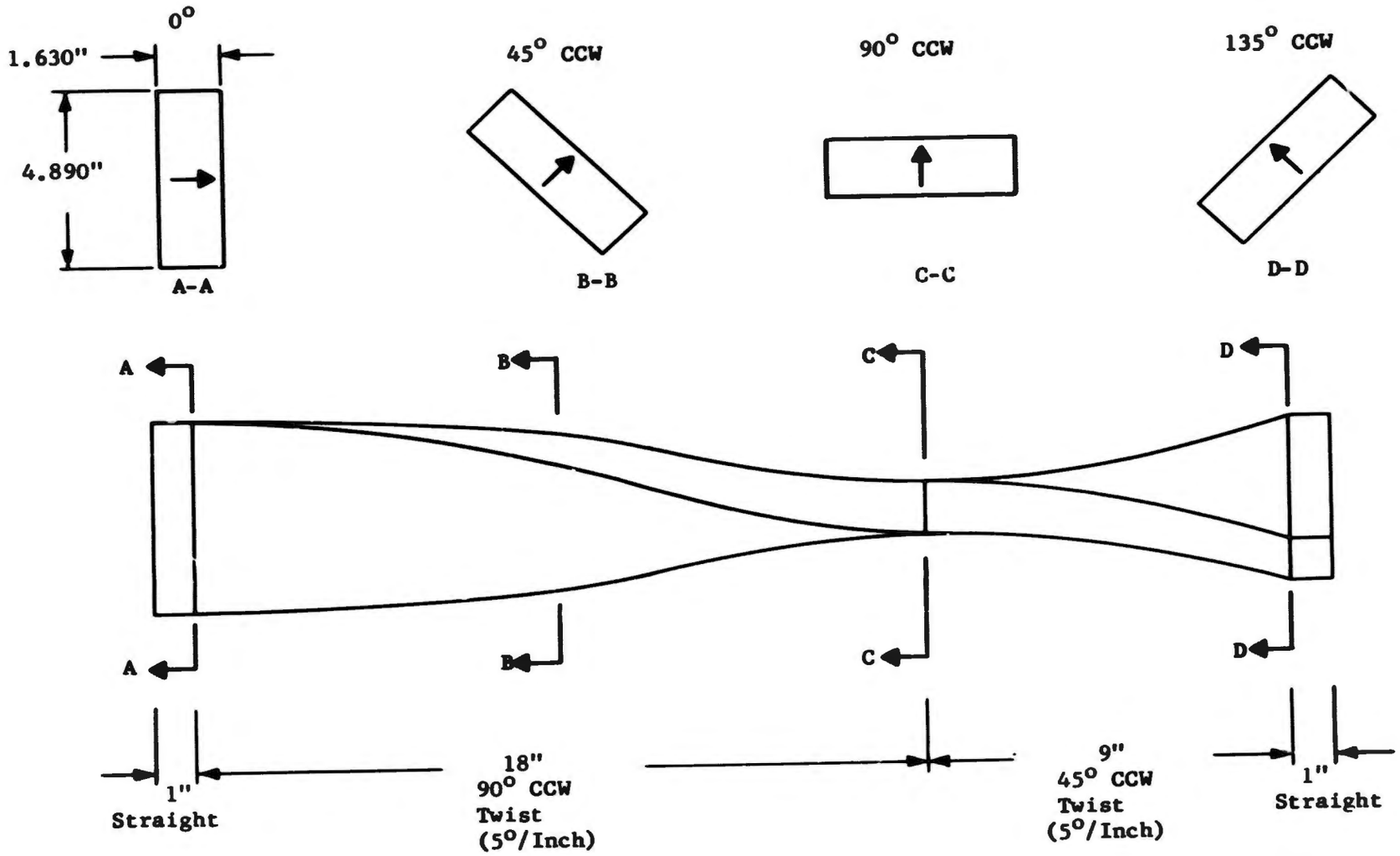

Figure 2.3a Twist Mandrel Assembly #1 (135° CCW Net Twist).

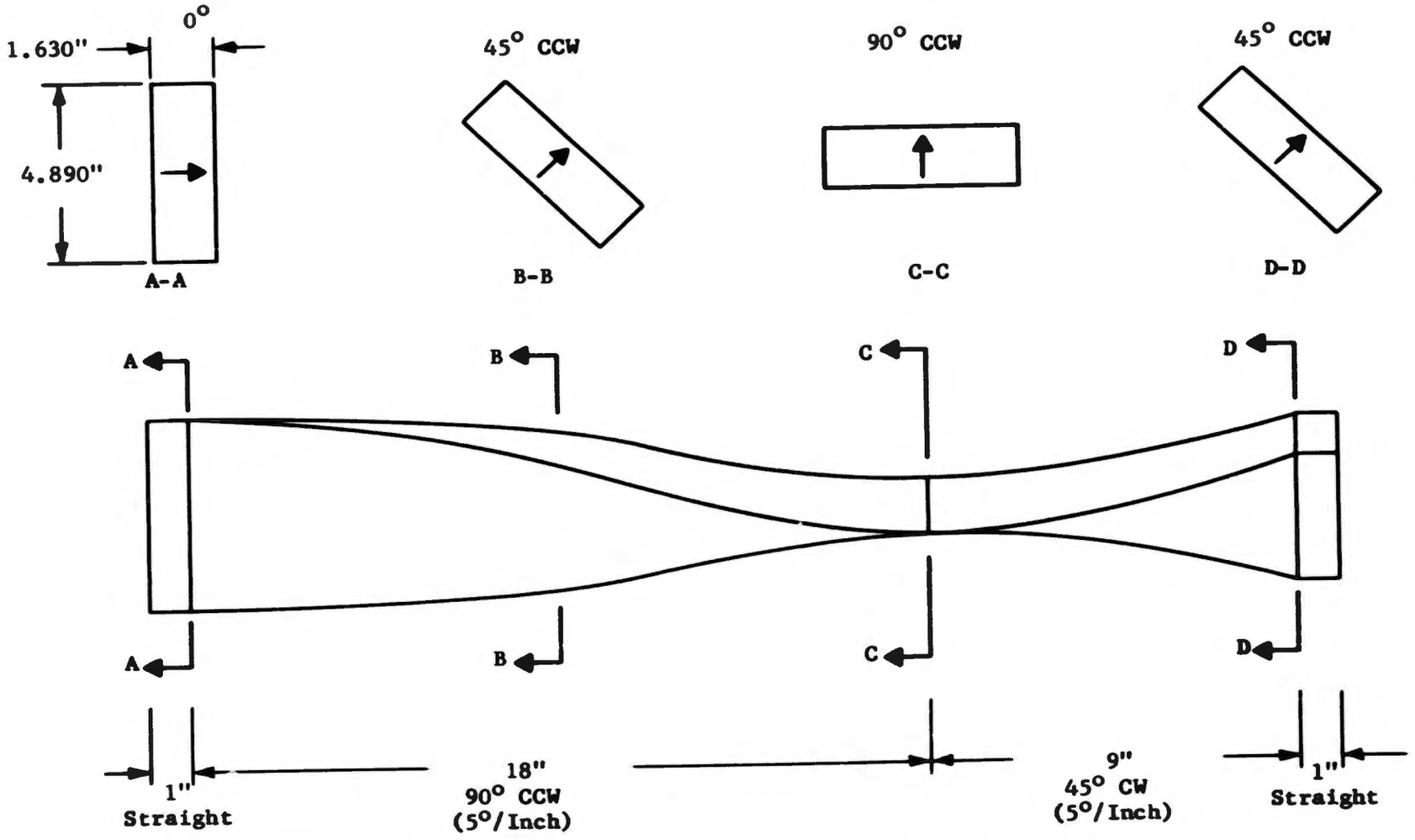

Figure 2.3b Twist Mandrel Assembly #2 (45° CCW Net Twist).

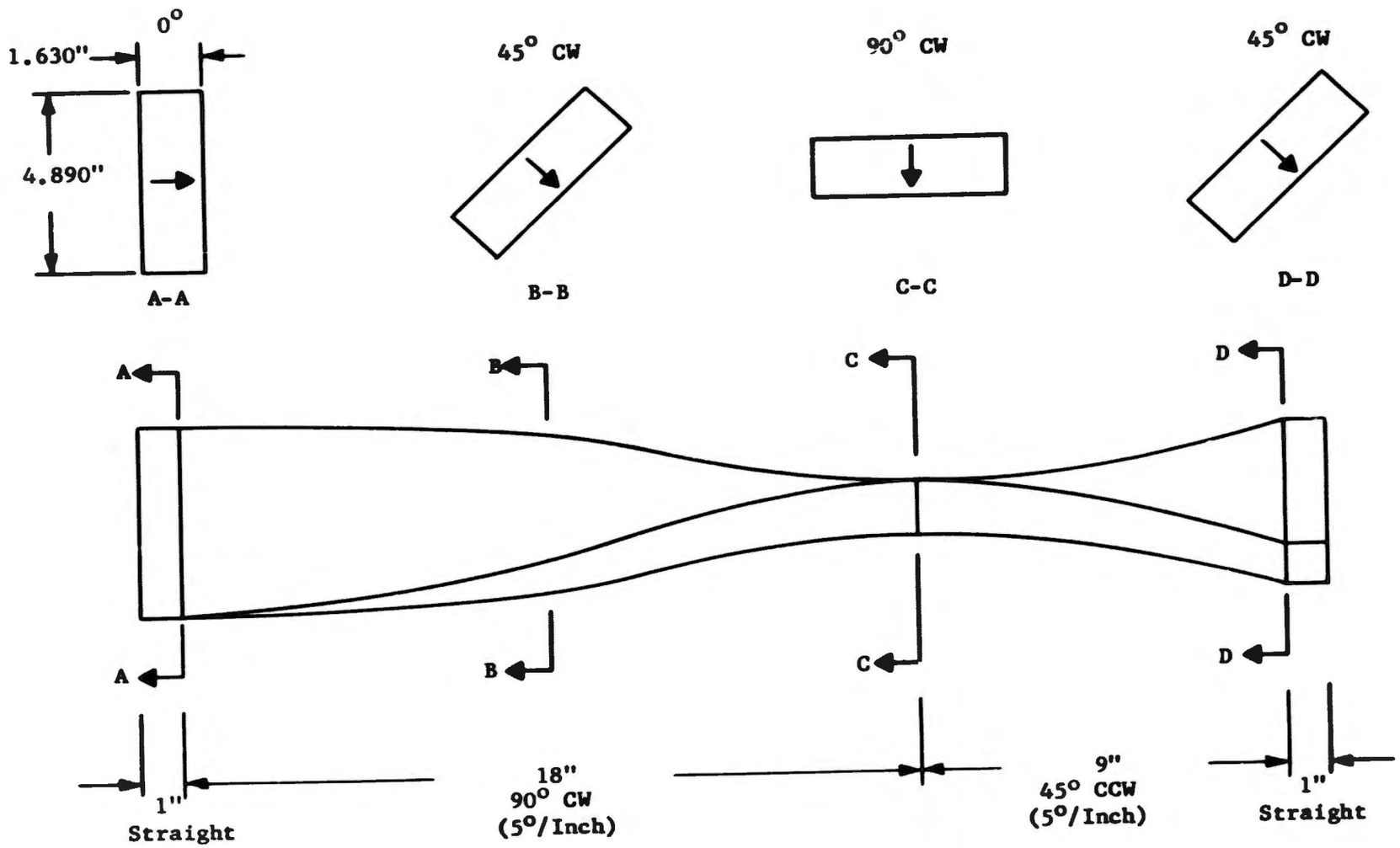

Figure 2.3c Twist Mandrel Assembly #3 (45° CW Net Twist).

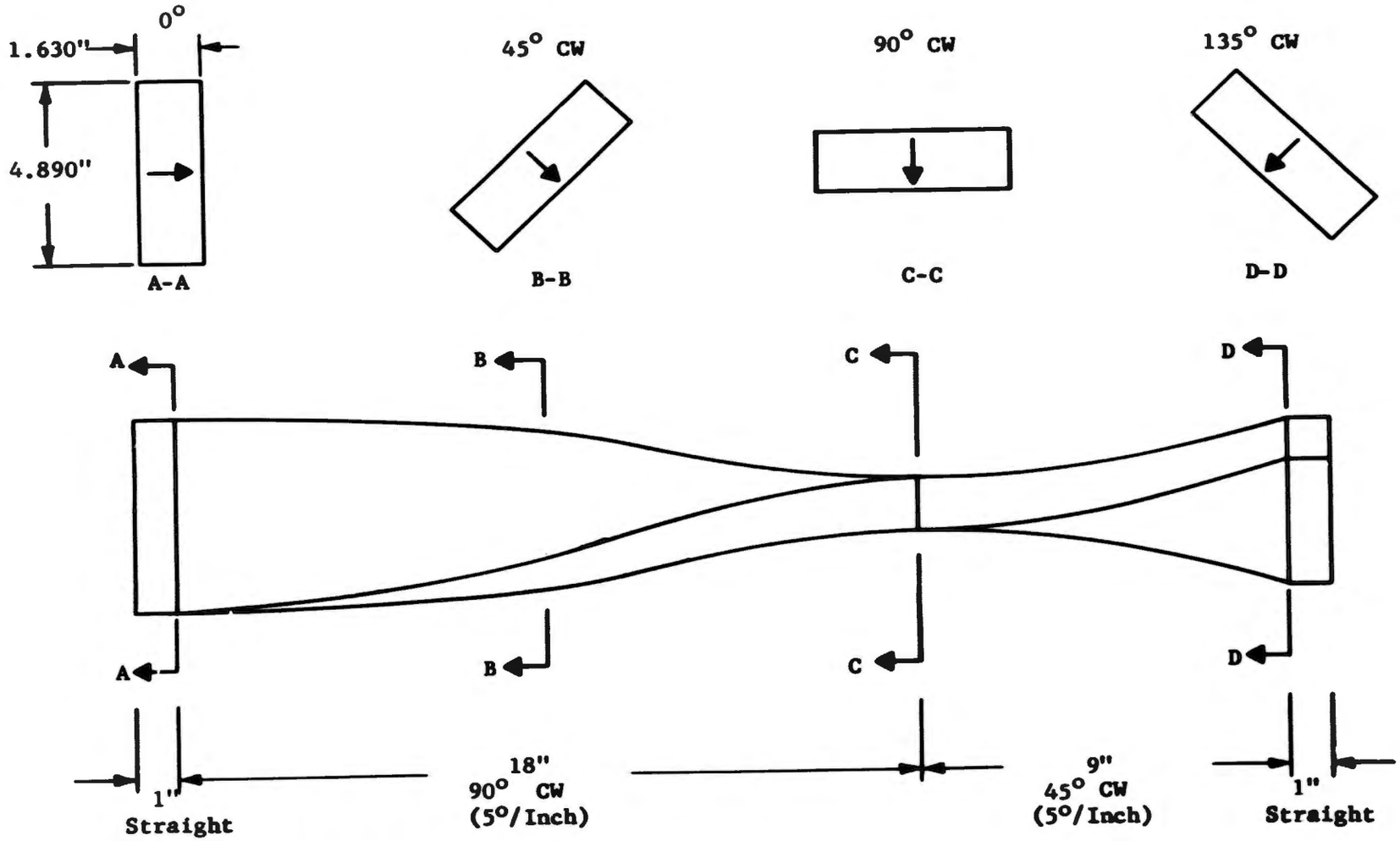

Figure 2.3d Twist Mandrel Assembly #4 (135° CW Net Twist).

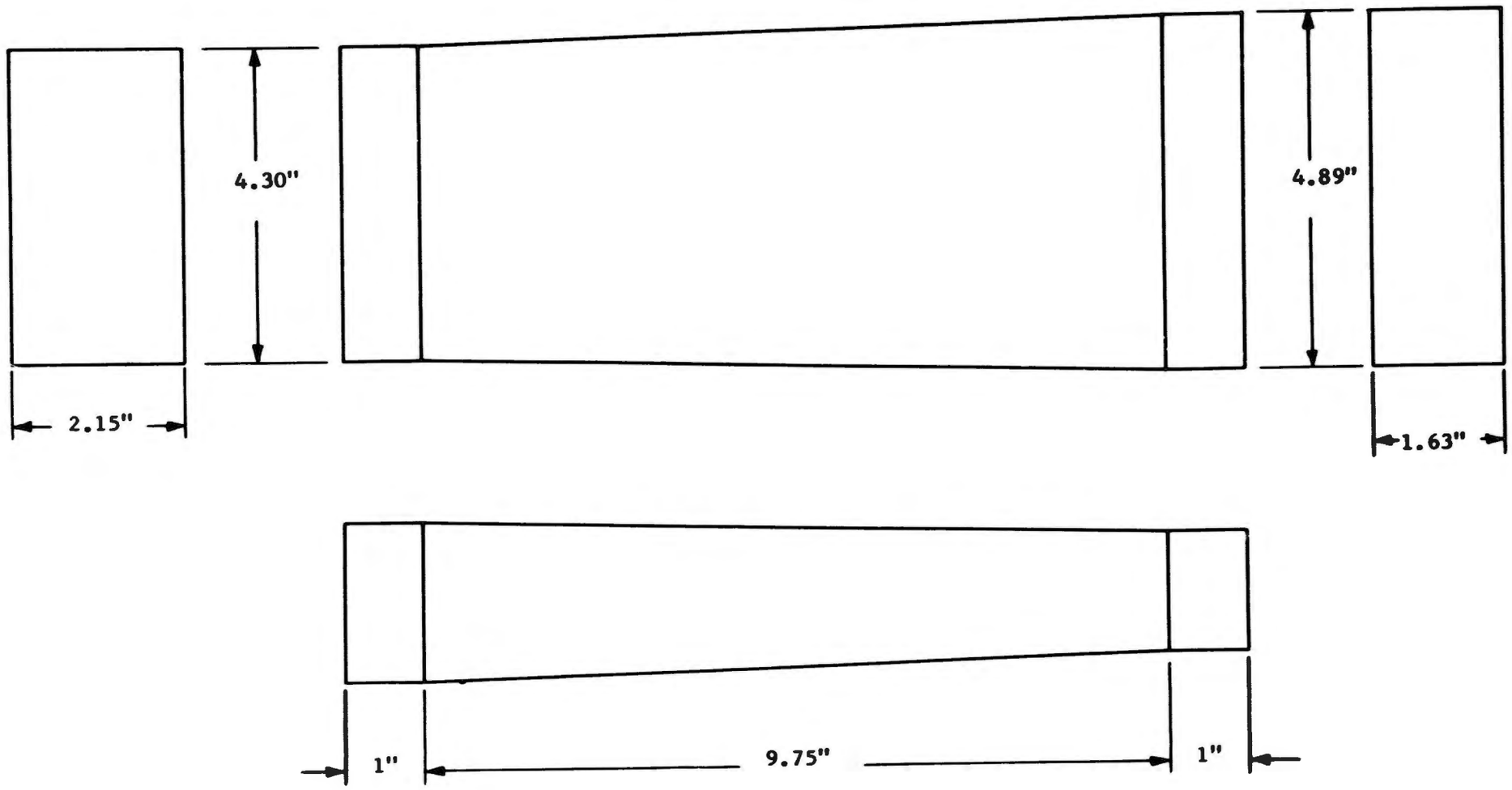

Figure 2.4 Compound Input Taper for Combiner.

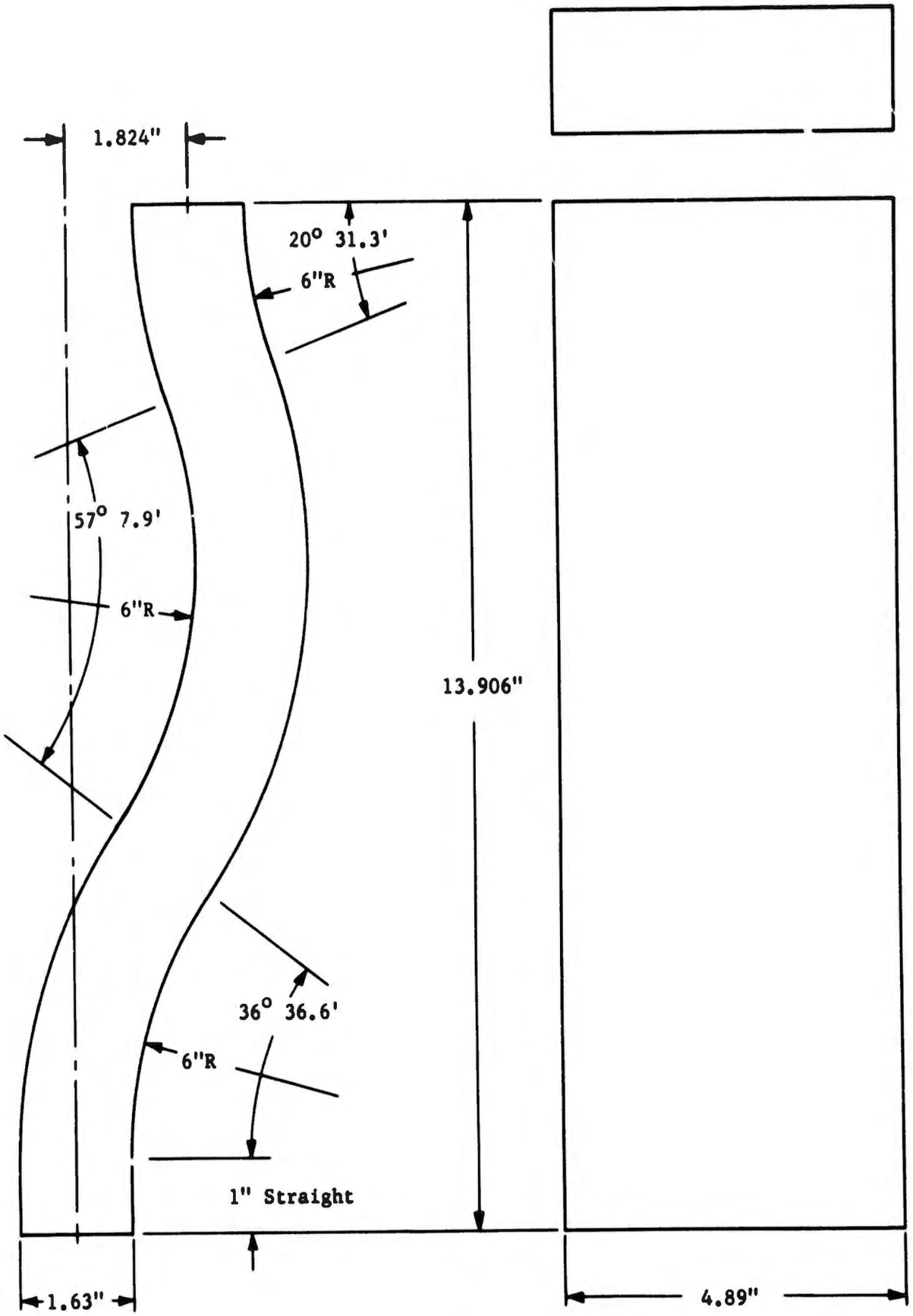
1.824"
20° 31.3'
6"R
57° 7.9'
6"R
13.906"
36° 36.6'
6"R
1" Straight
1.63"
4.89"

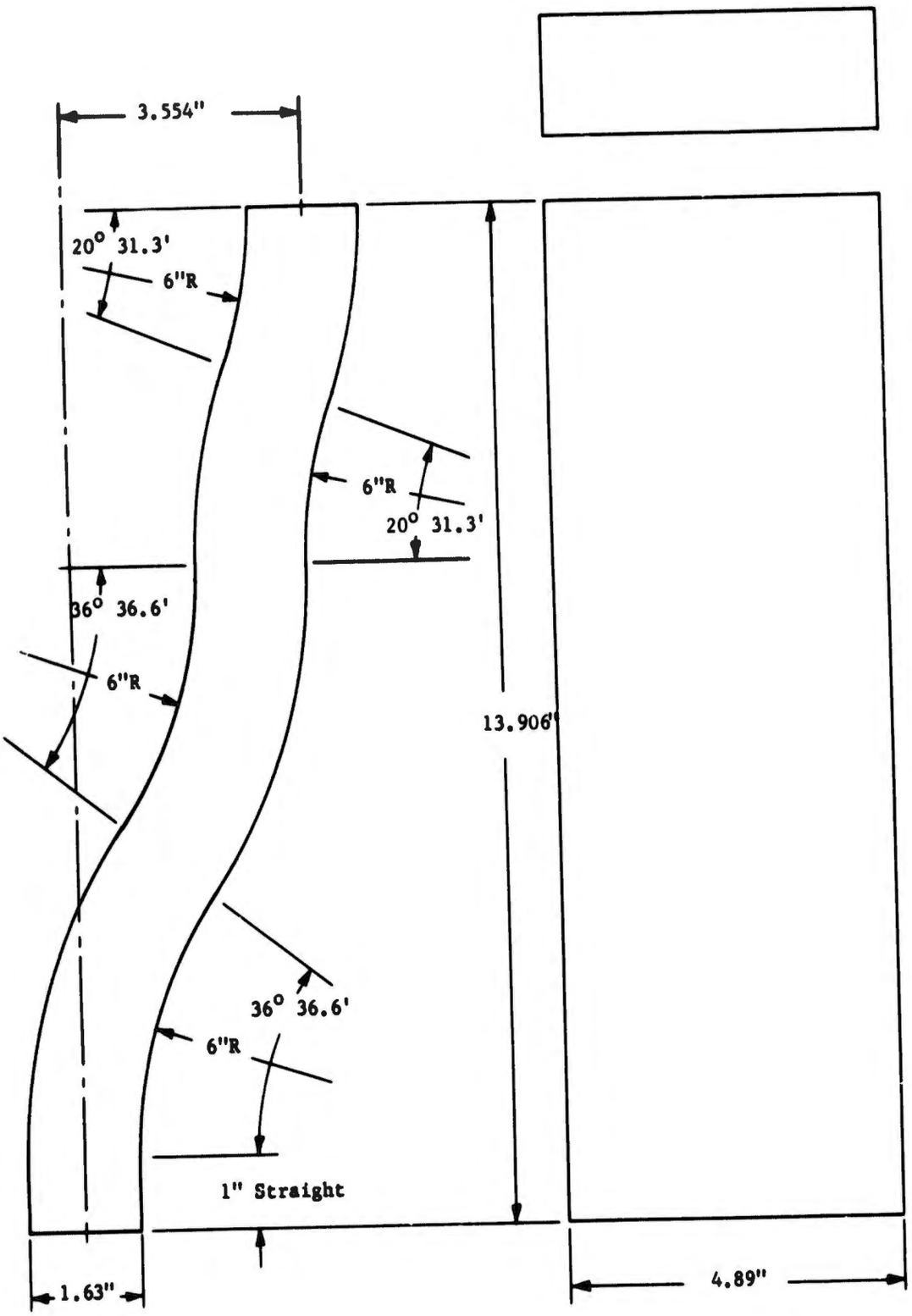

Figure 2.5b E-Plane Offset Mandrel for Waveguide Runs 1 and 3.

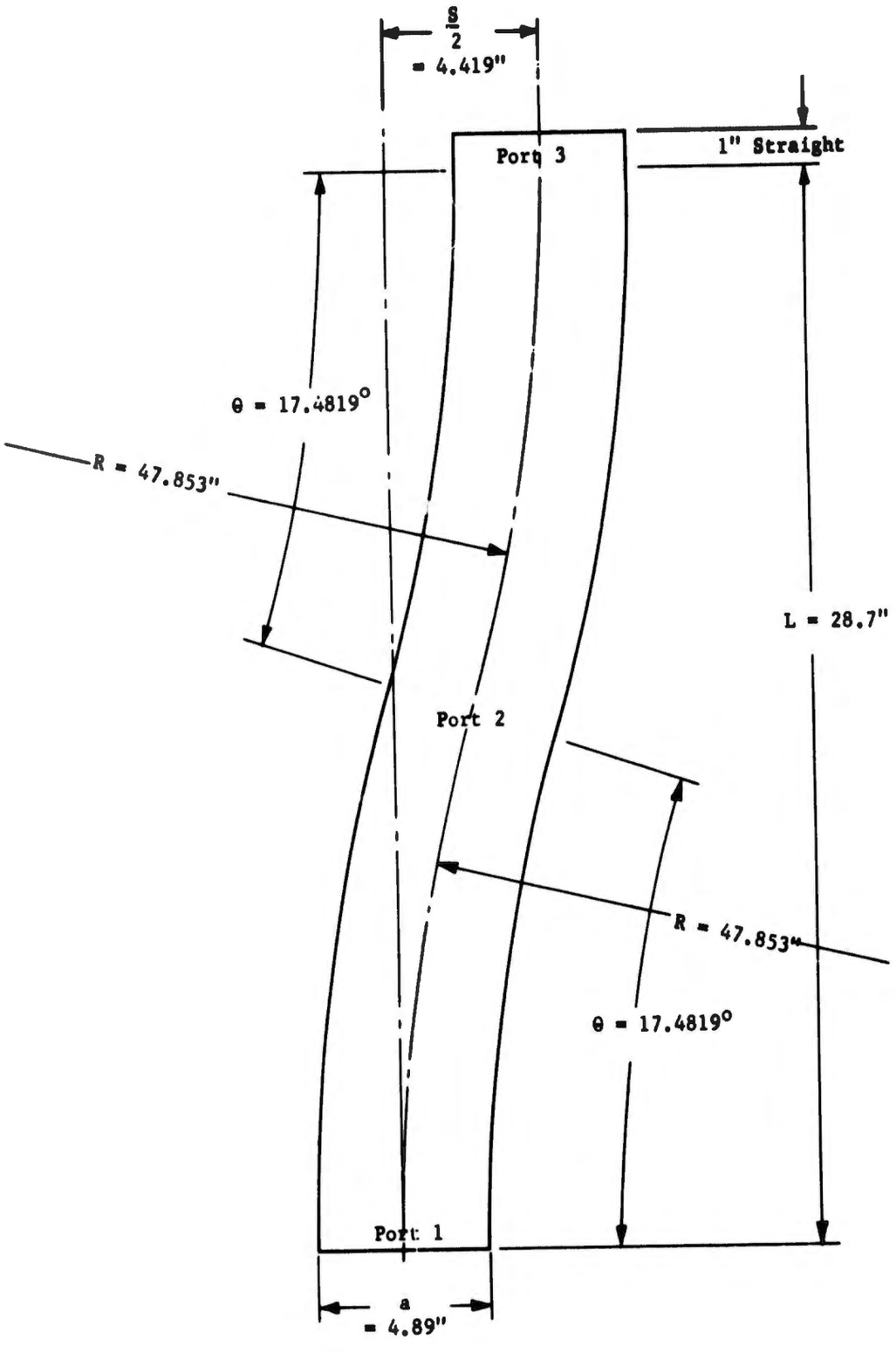

Figure 2.6a H-Plane Offset

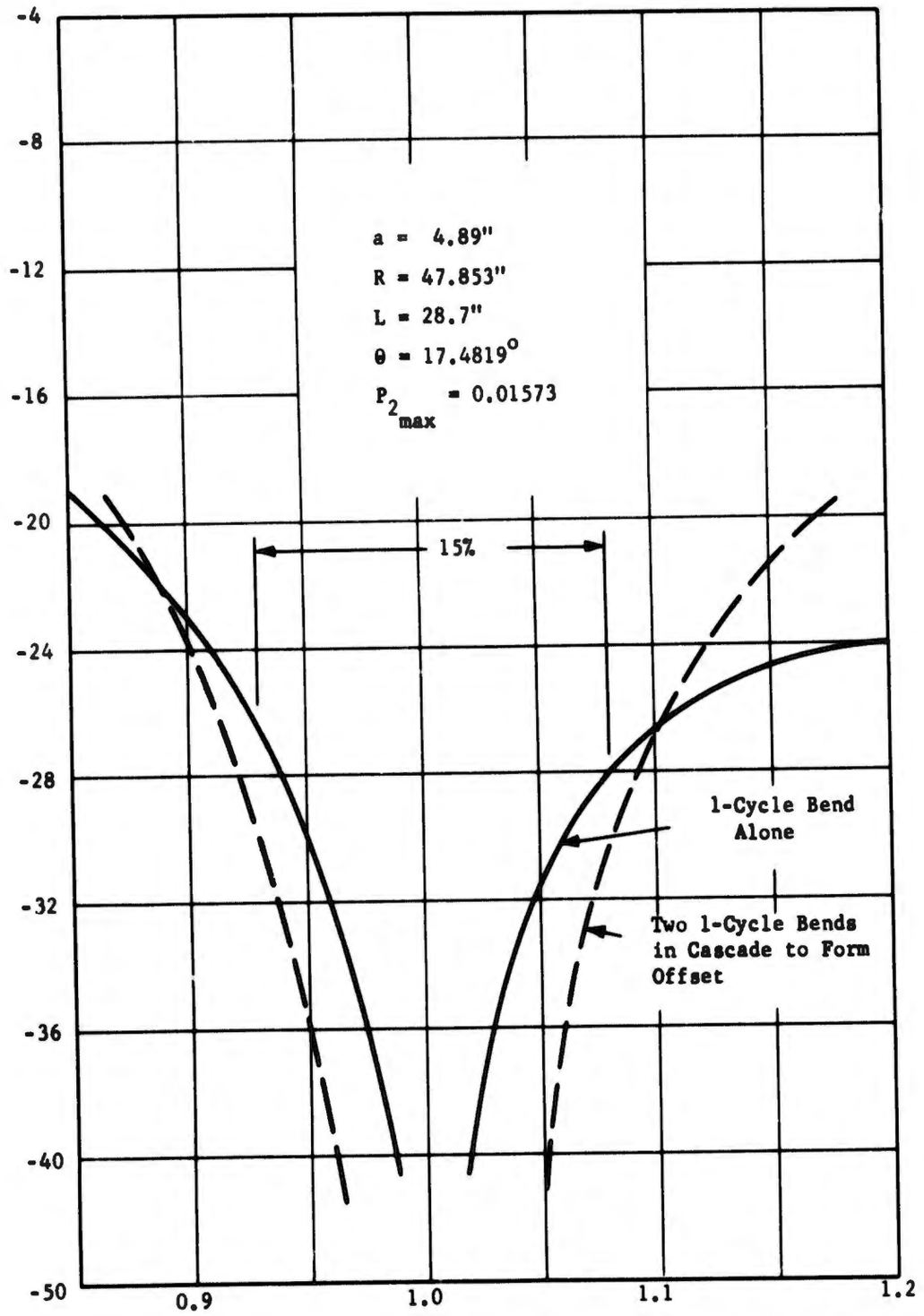

Figure 2.6b Calculated Spurious Mode Amplitudes for a Single 1-Cycle Bend and for Two Bends Forming H-Plane Offset of Fig. 2.6a.

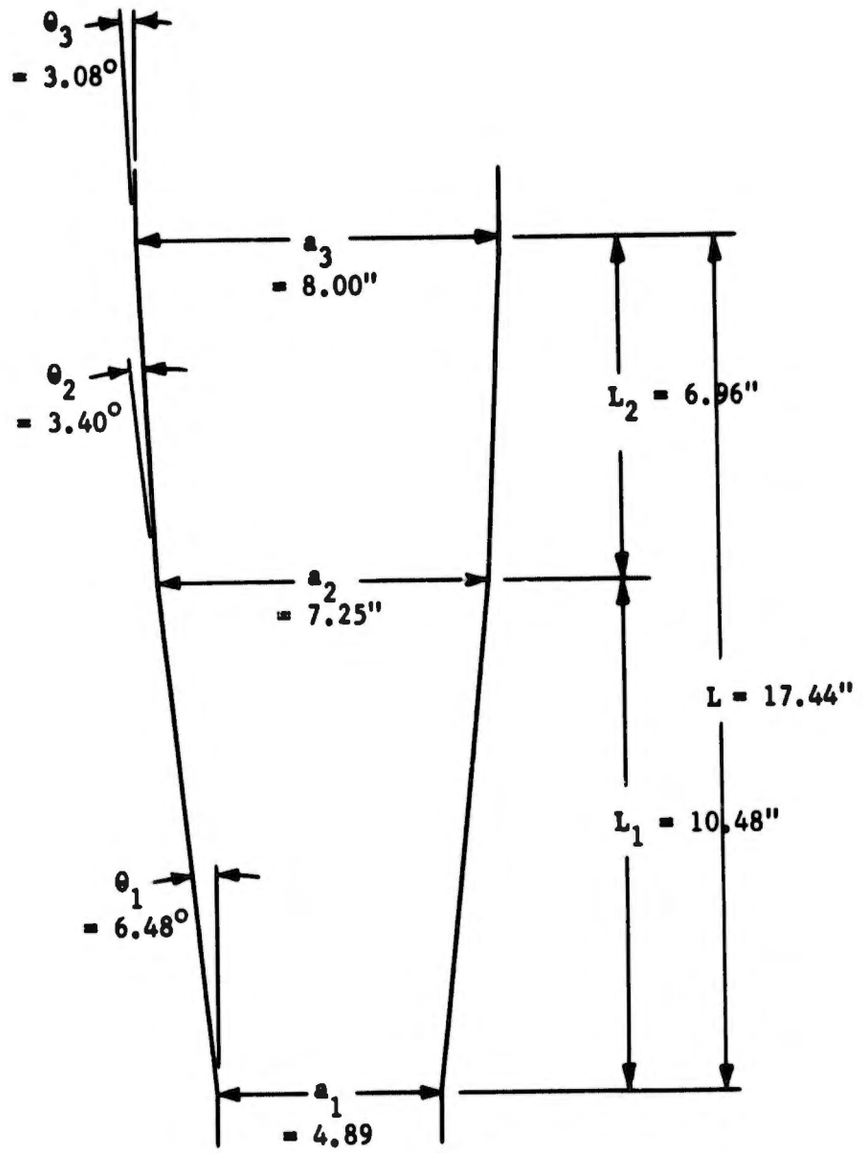

Figure 2.7a Double Angle H-Plane Taper.

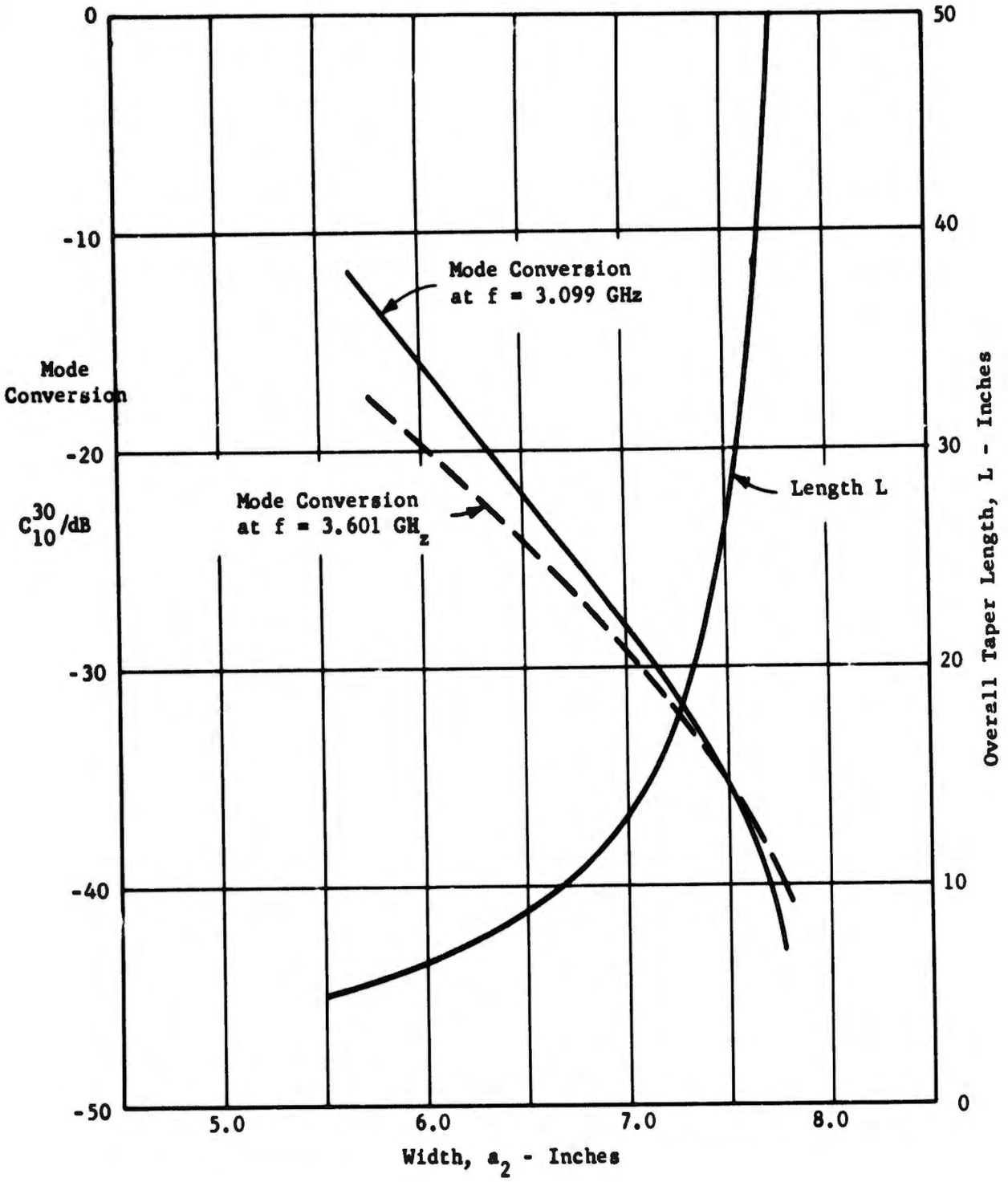

Figure 2.7b Double Angle Taper Length and Mode Conversion at Band Edges vs Width a_2.

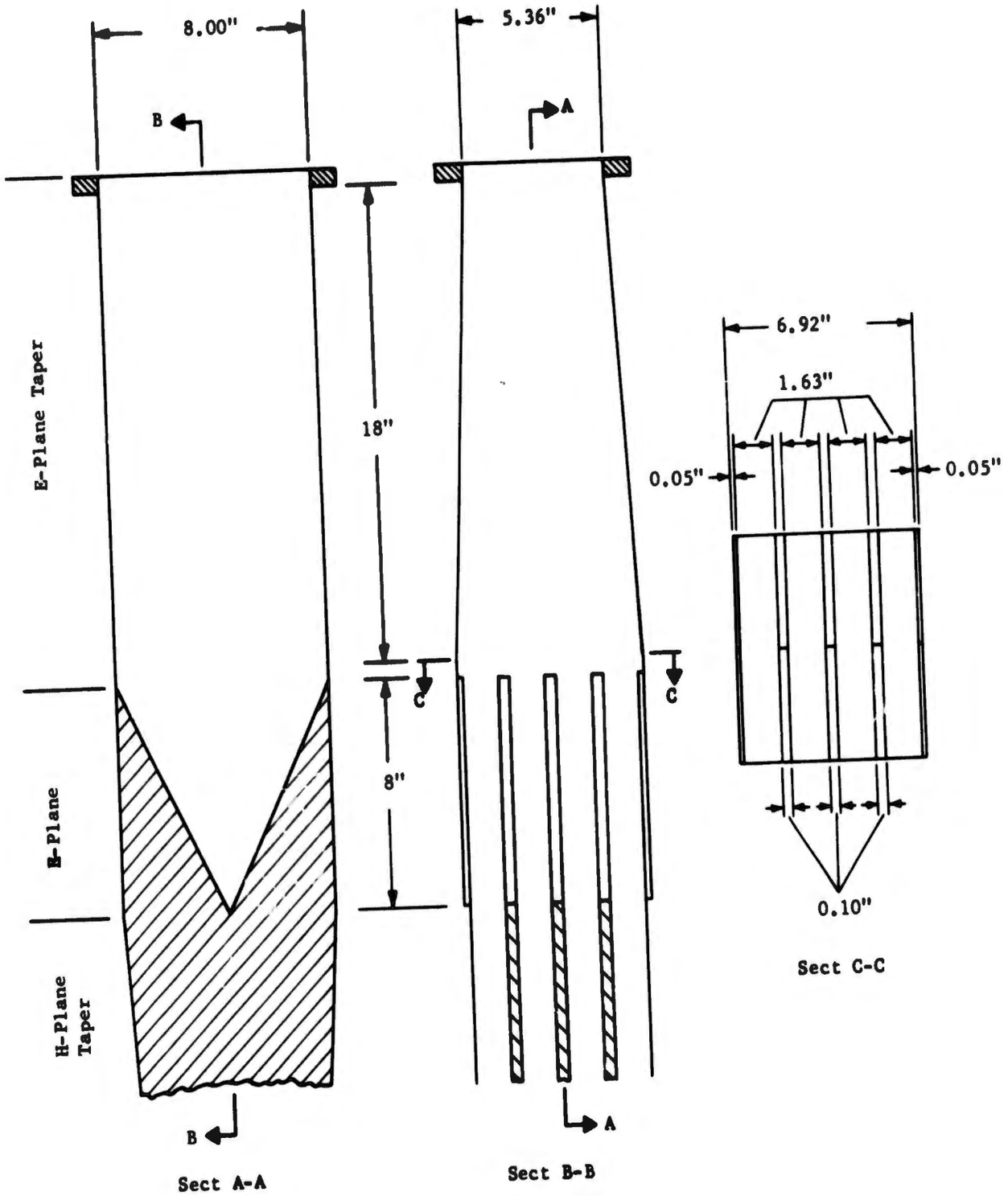

Figure 2.8 E-Plane Bifurcation & E-Plane Taper.

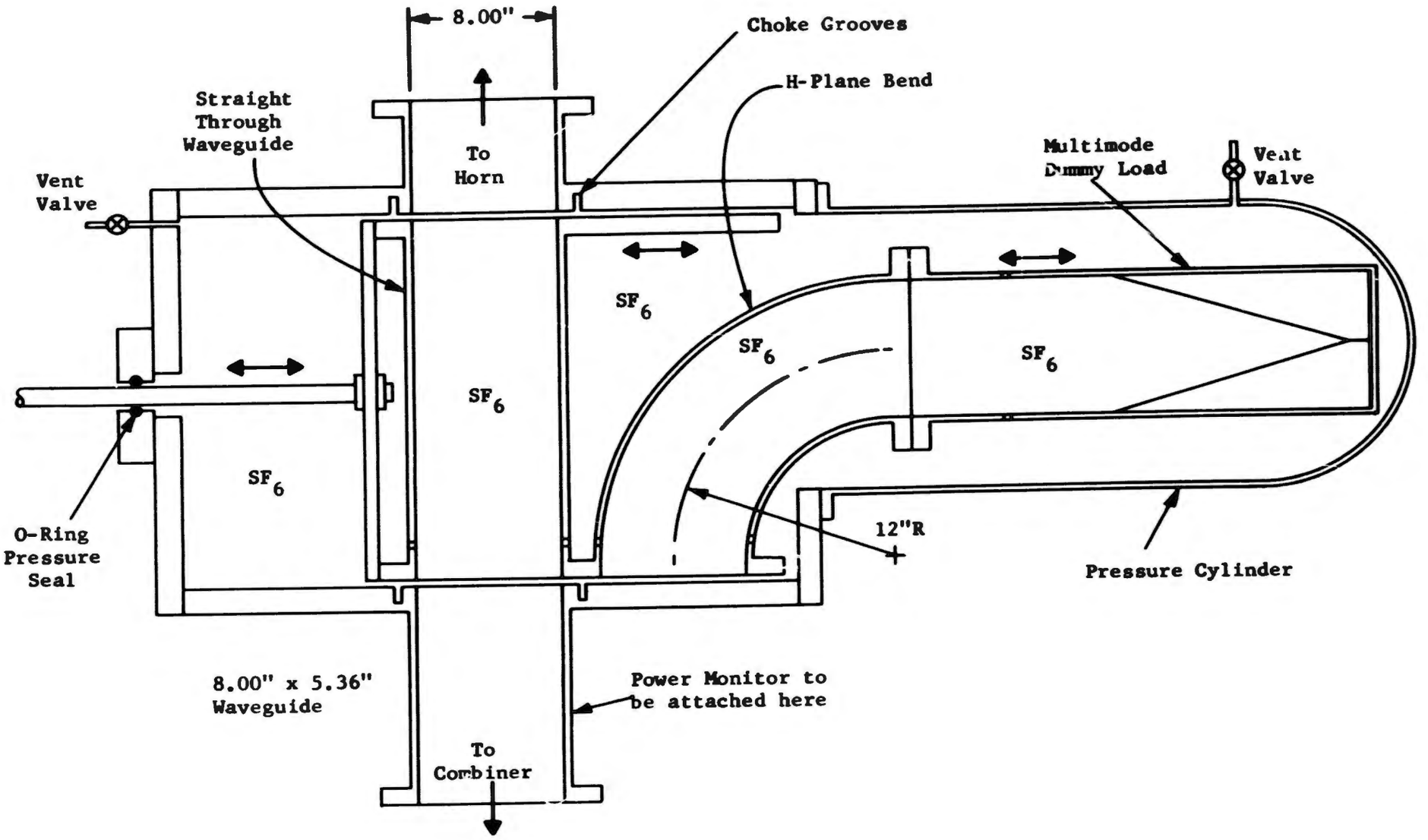

Figure 3.1 Sectional View of Load Switch.

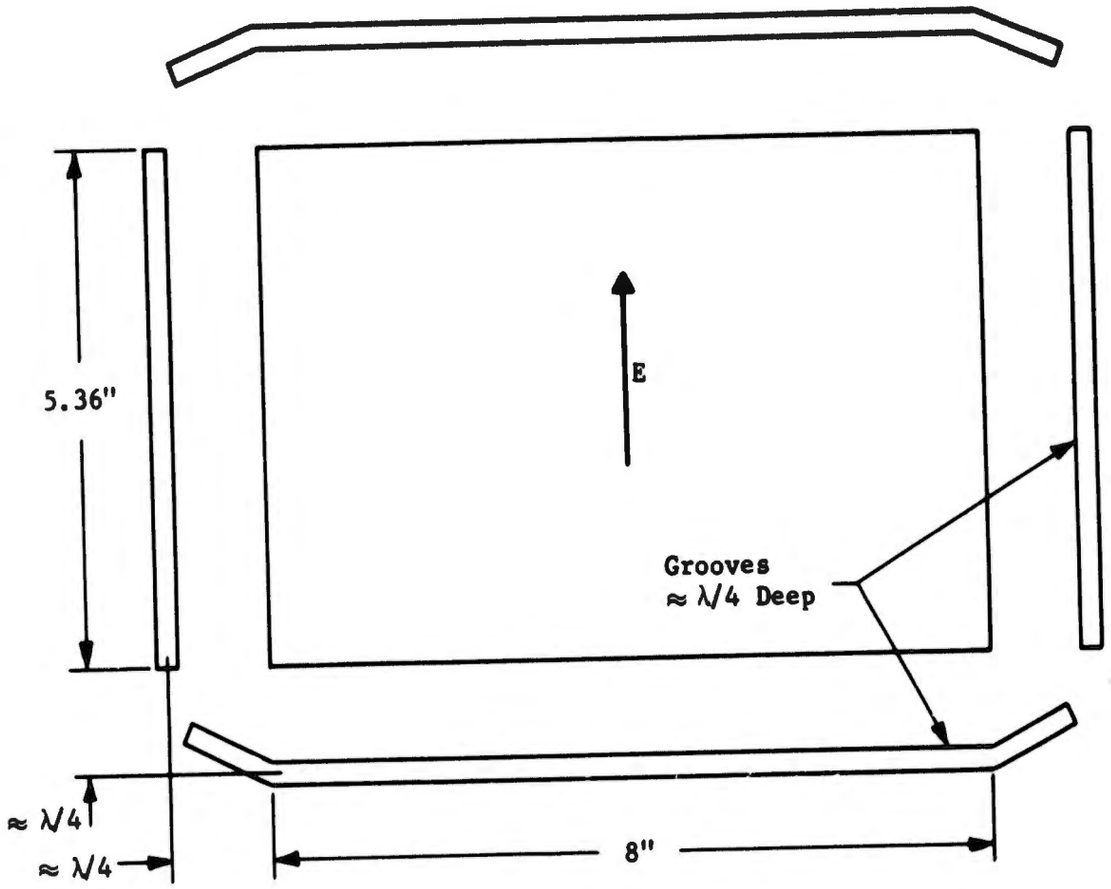

Figure 3.2 Proposed Choke Configuration Employing Top-Wall and Side-Wall Grooves.

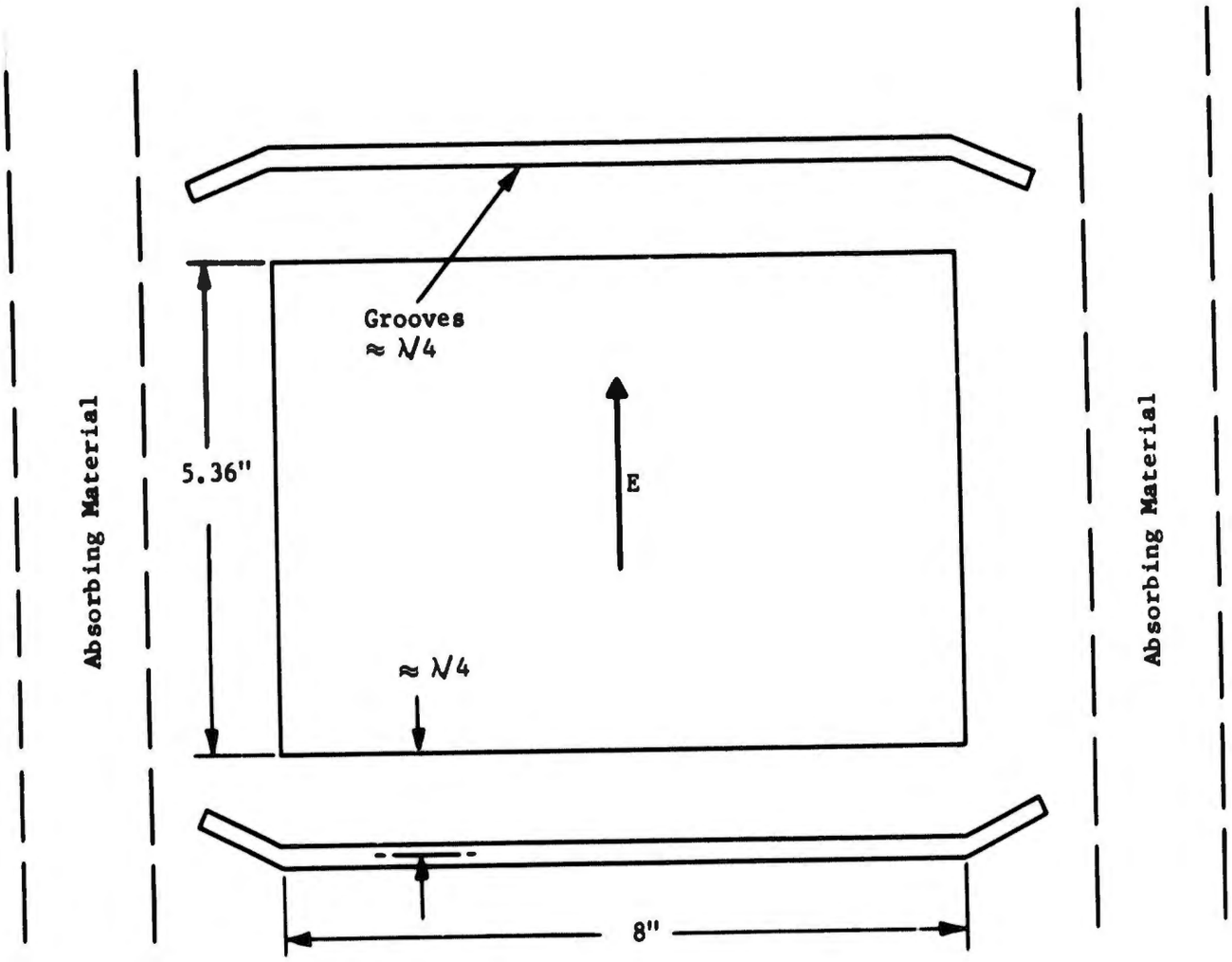

Figure 3.3 Proposed Choke Configuration
Employing Absorbing Material.

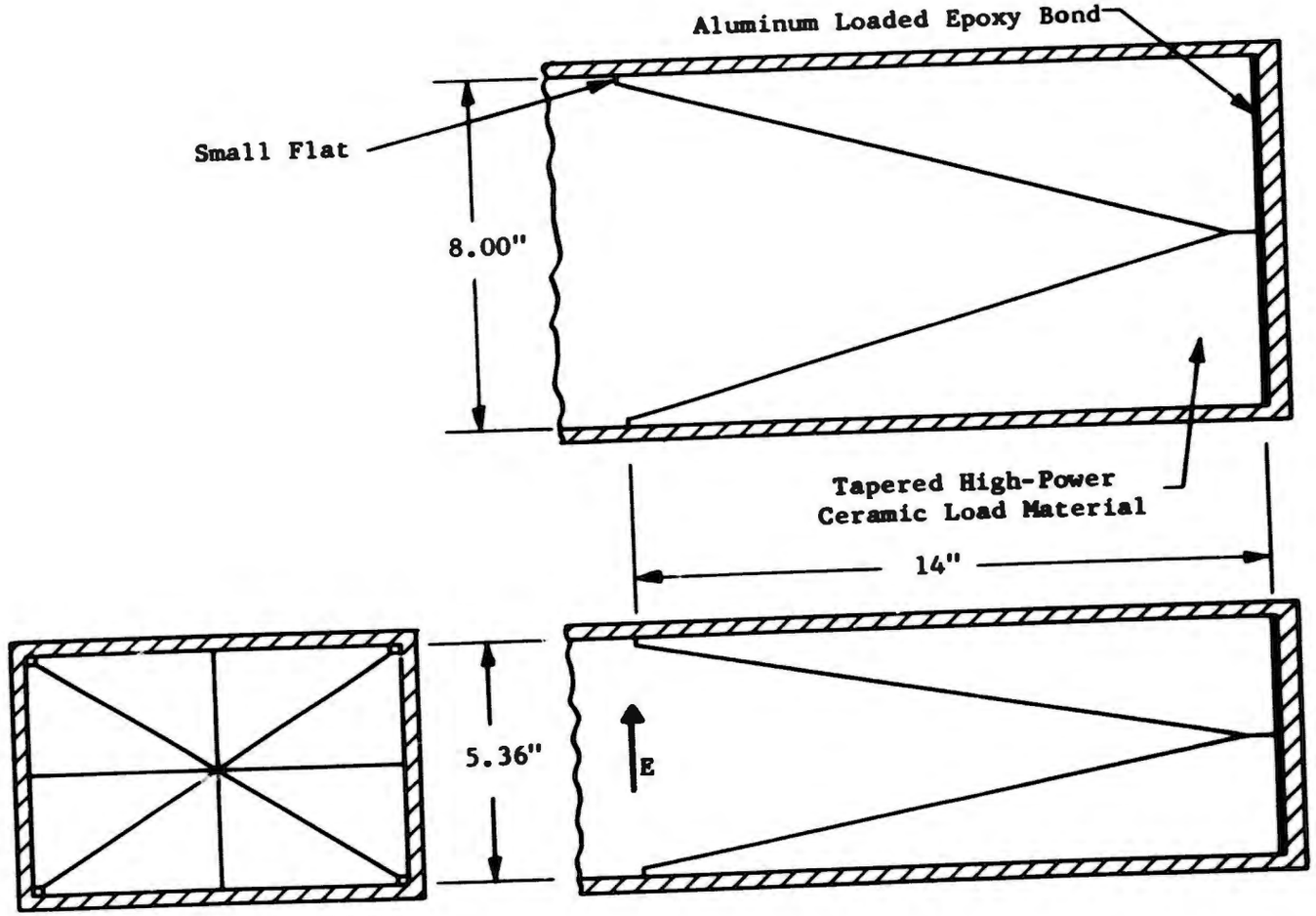

Figure 3.5 Outline of Load.

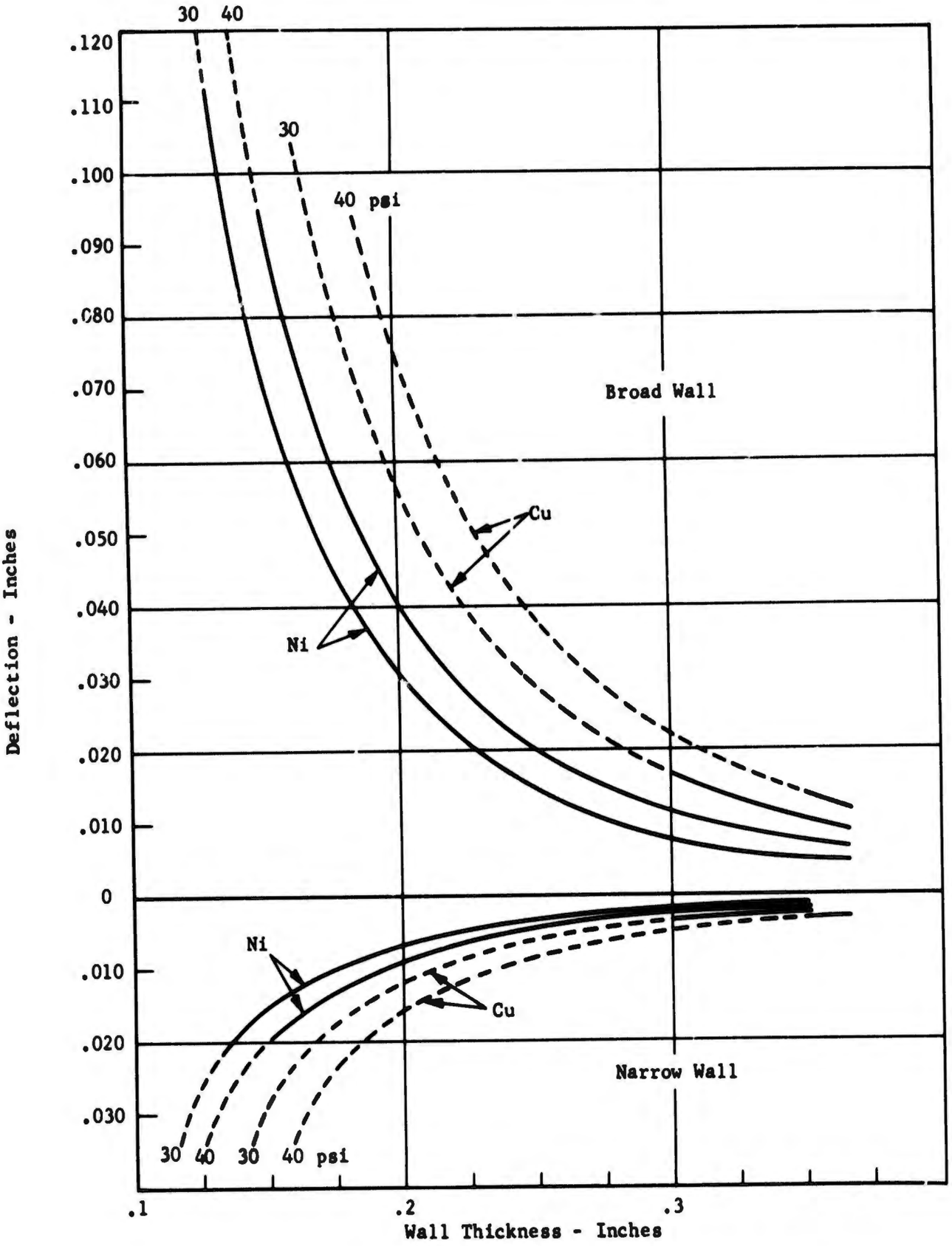

Figure 4.1 Computed Wall Deflections
8" x 5.36" ID Waveguide.

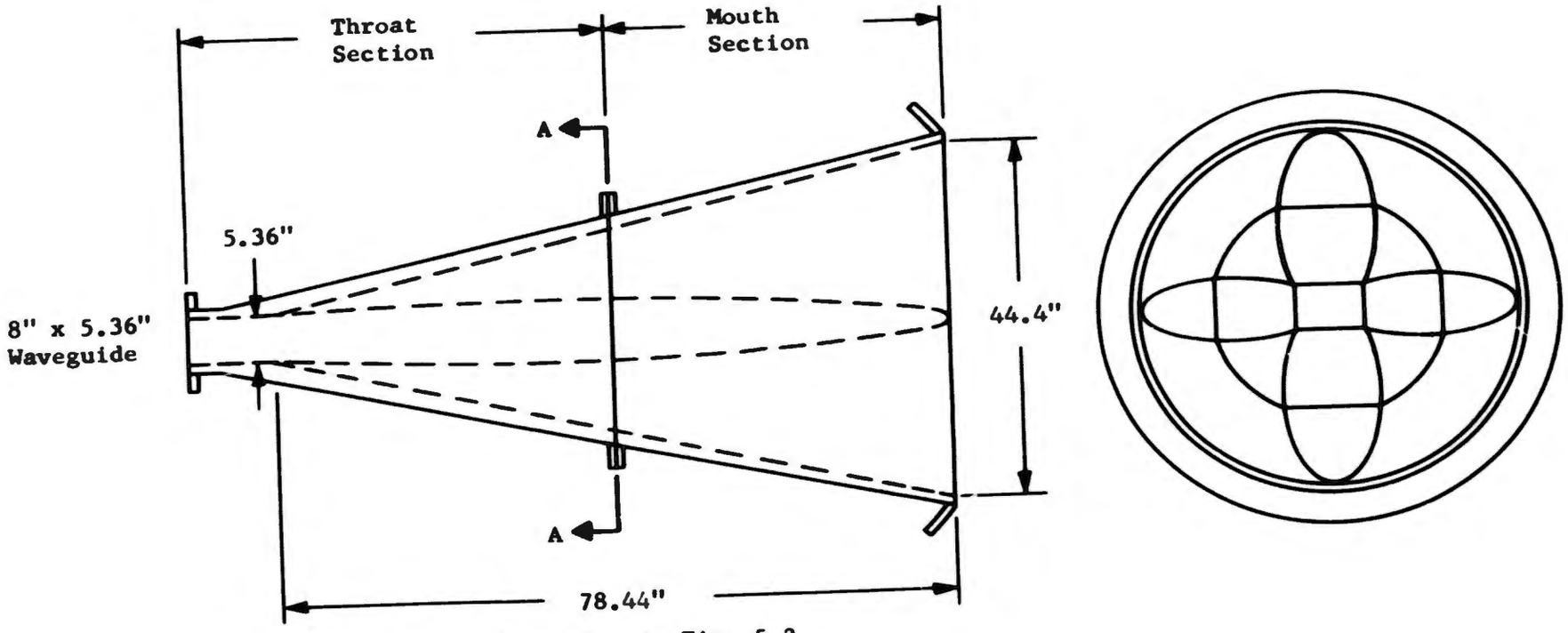

Figure 6.1 Conical Horn
Rectangular Throat, Full Length
Transition to Circular Mouth

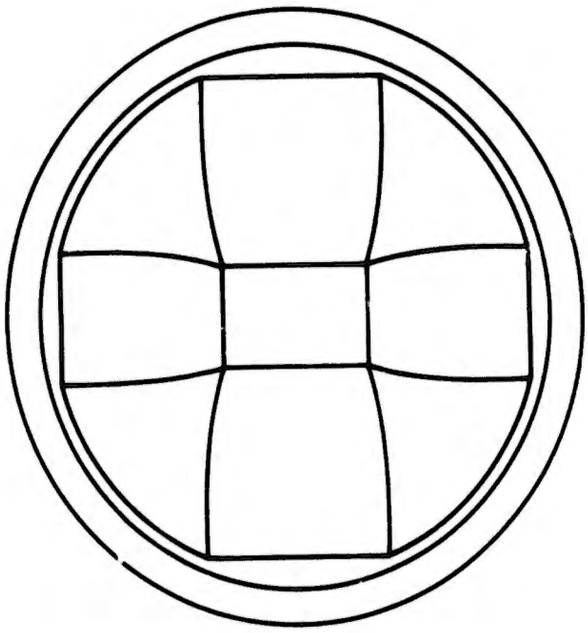

Section A-A
(see Fig. 6.1)

Figure 6.2 End View of Throat Section

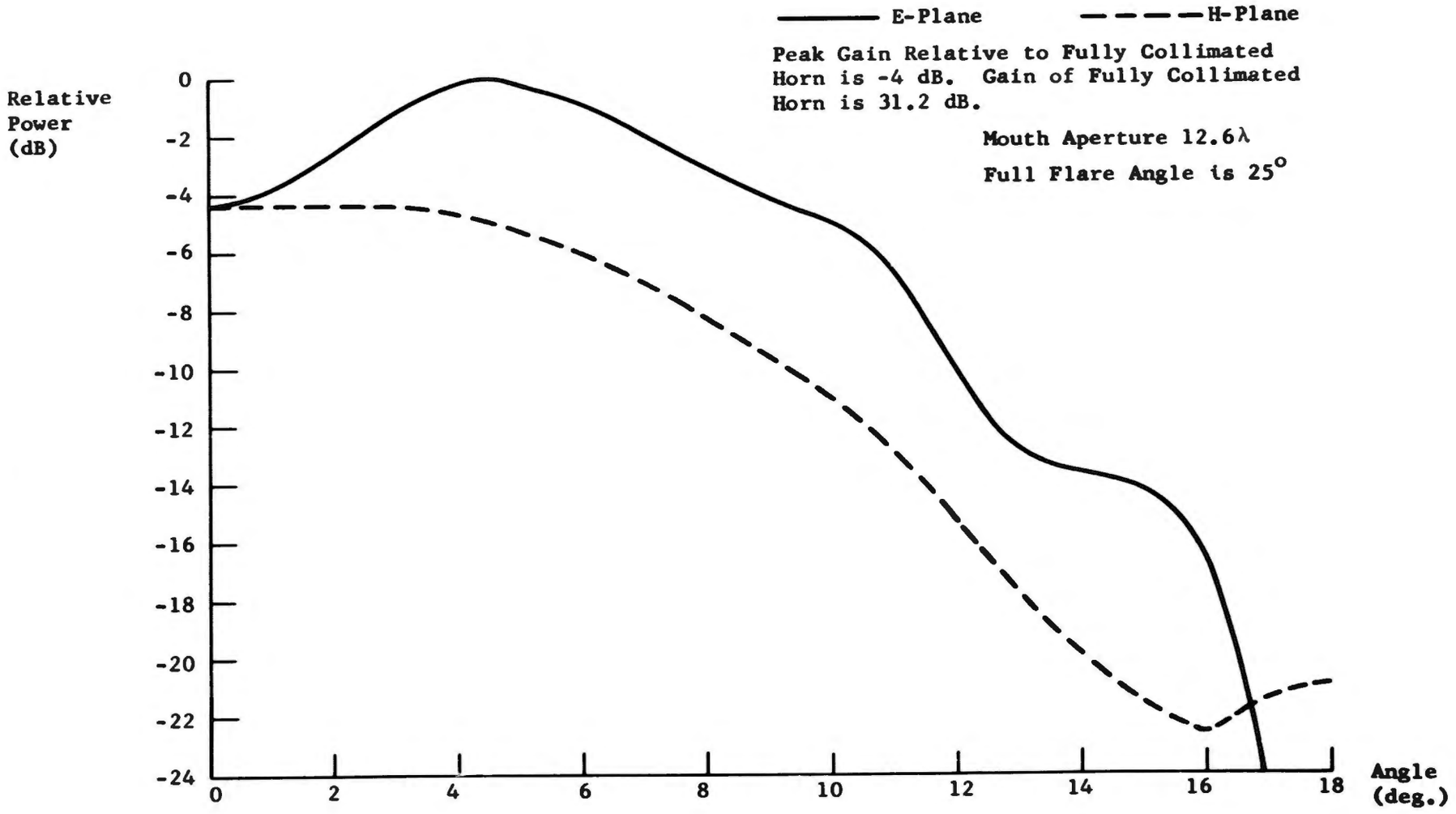

Figure 6.3 Conical Horn Patterns

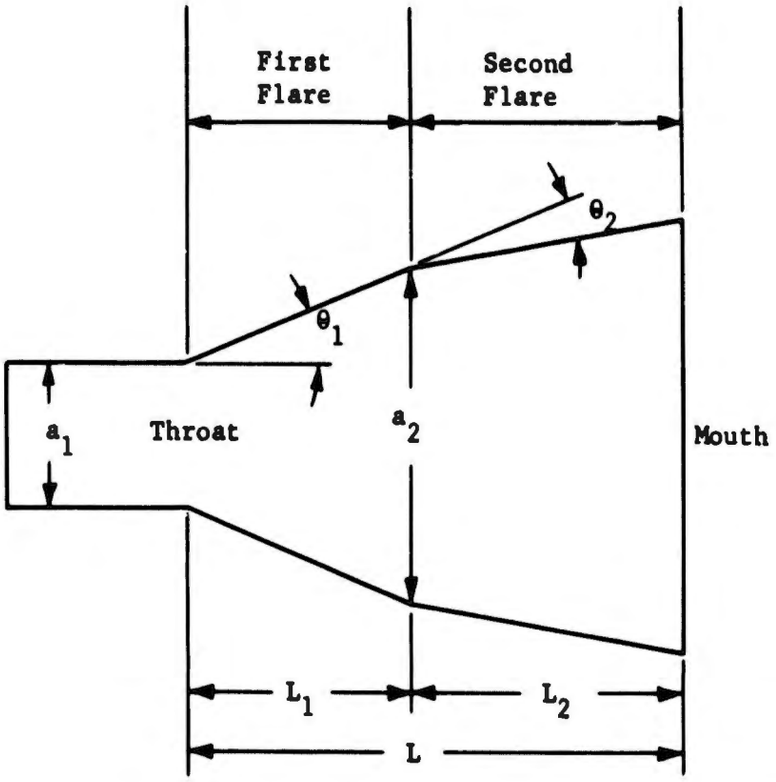

Figure 6.4 Double Taper Horn

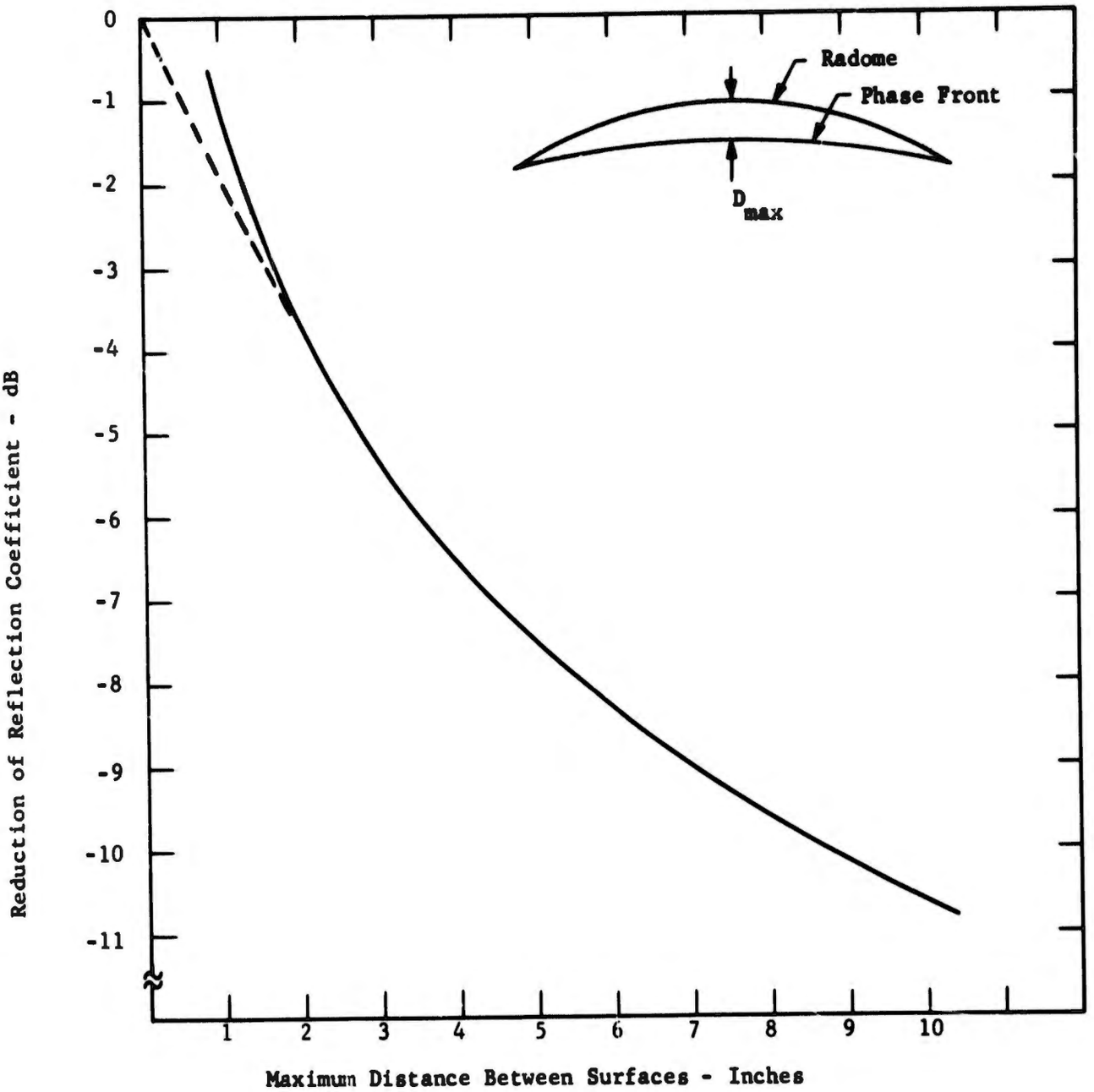

Figure 7.1 Reduction of Reflection Coefficient for the TE_{10} Principal Mode Caused by Deviation of the Reflecting Surface from the Wave Front. Singly Curved Case. Frequency = 3.35 GHz.

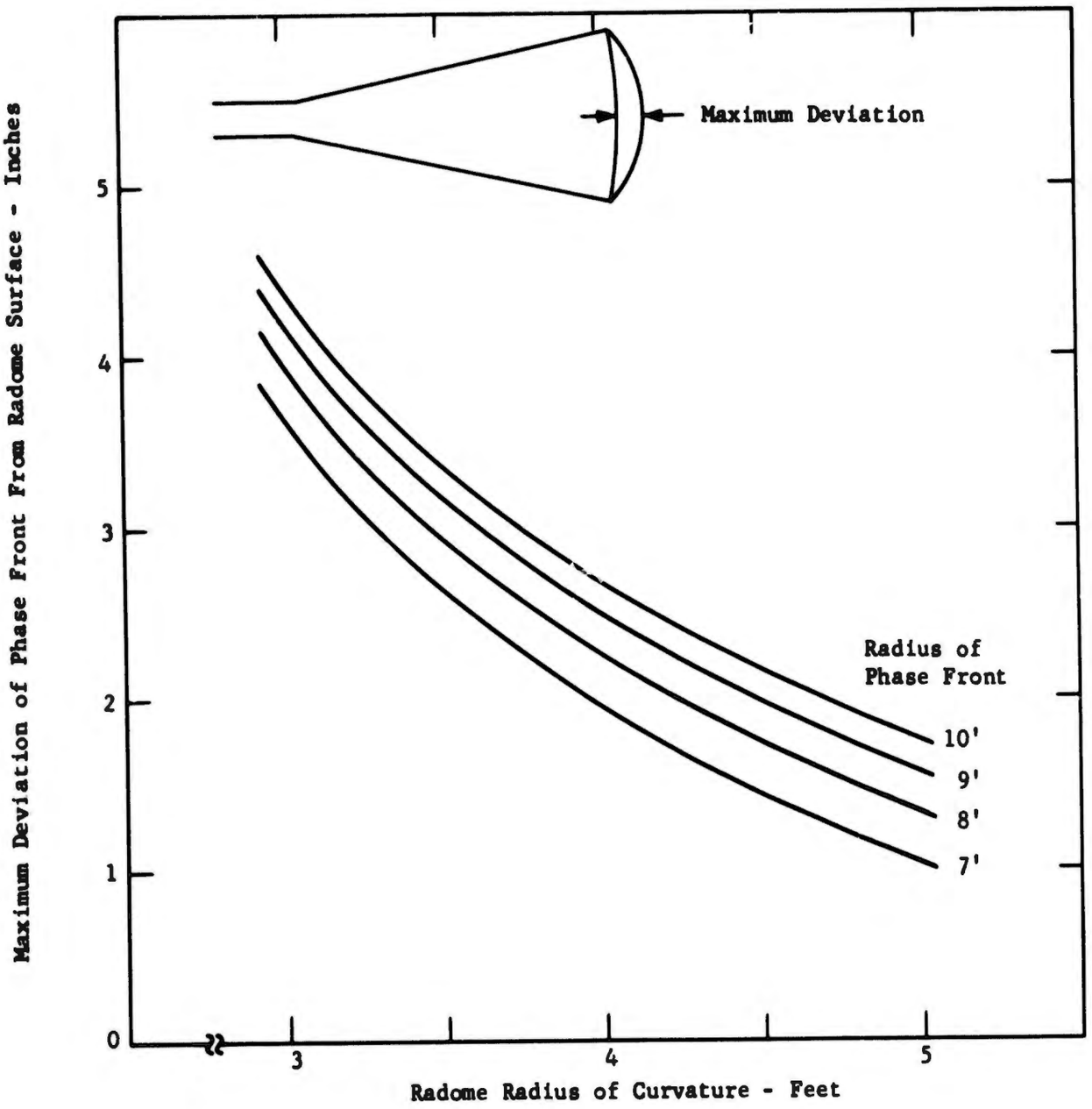

Figure 7.2 Maximum Deviation Between Phase Front and Radome Surface.

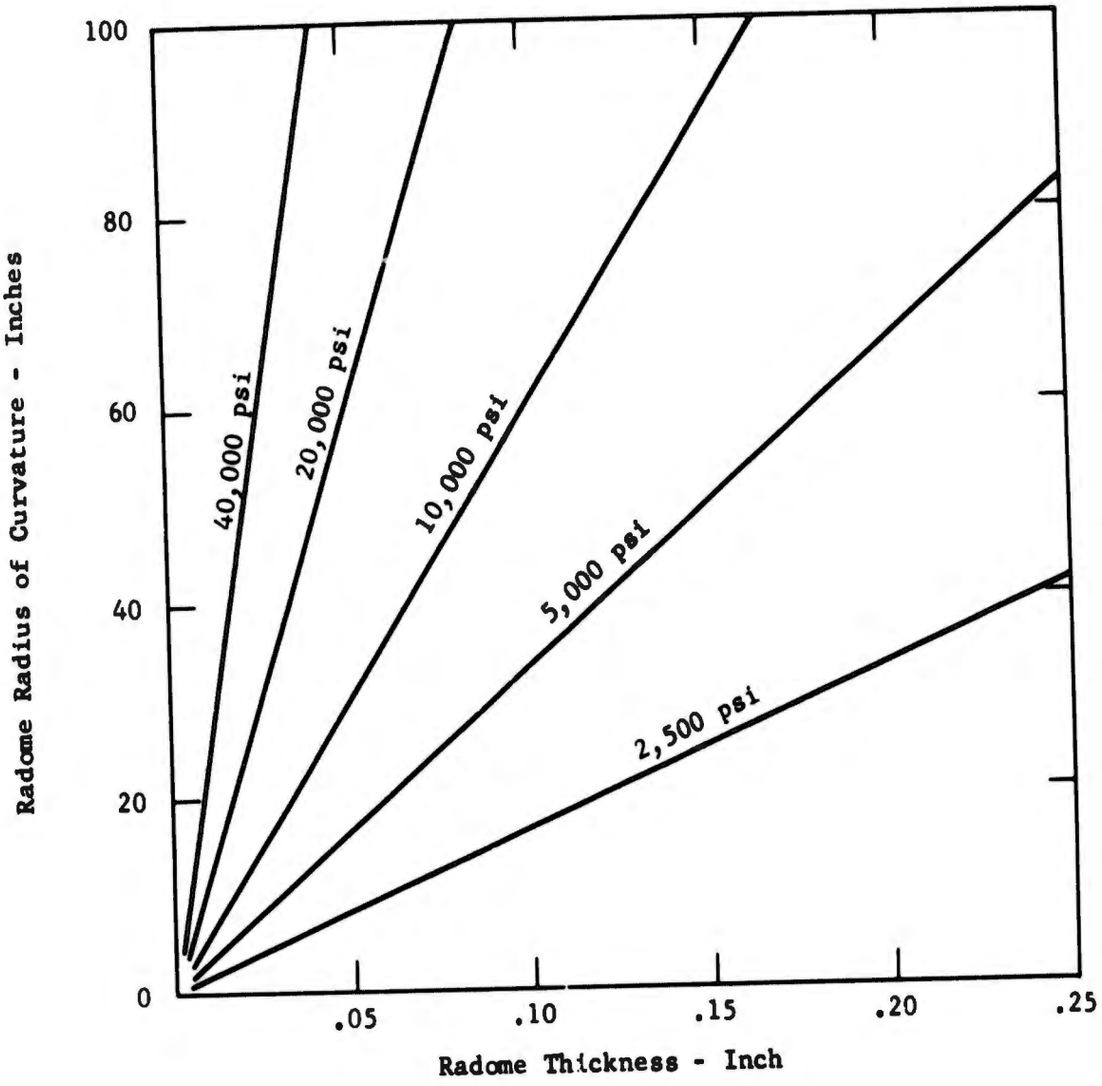

Figure 7.3 Tensile Stress in a Spherical Radome at 2 Atmospheres (Gauge) Internal Pressure.

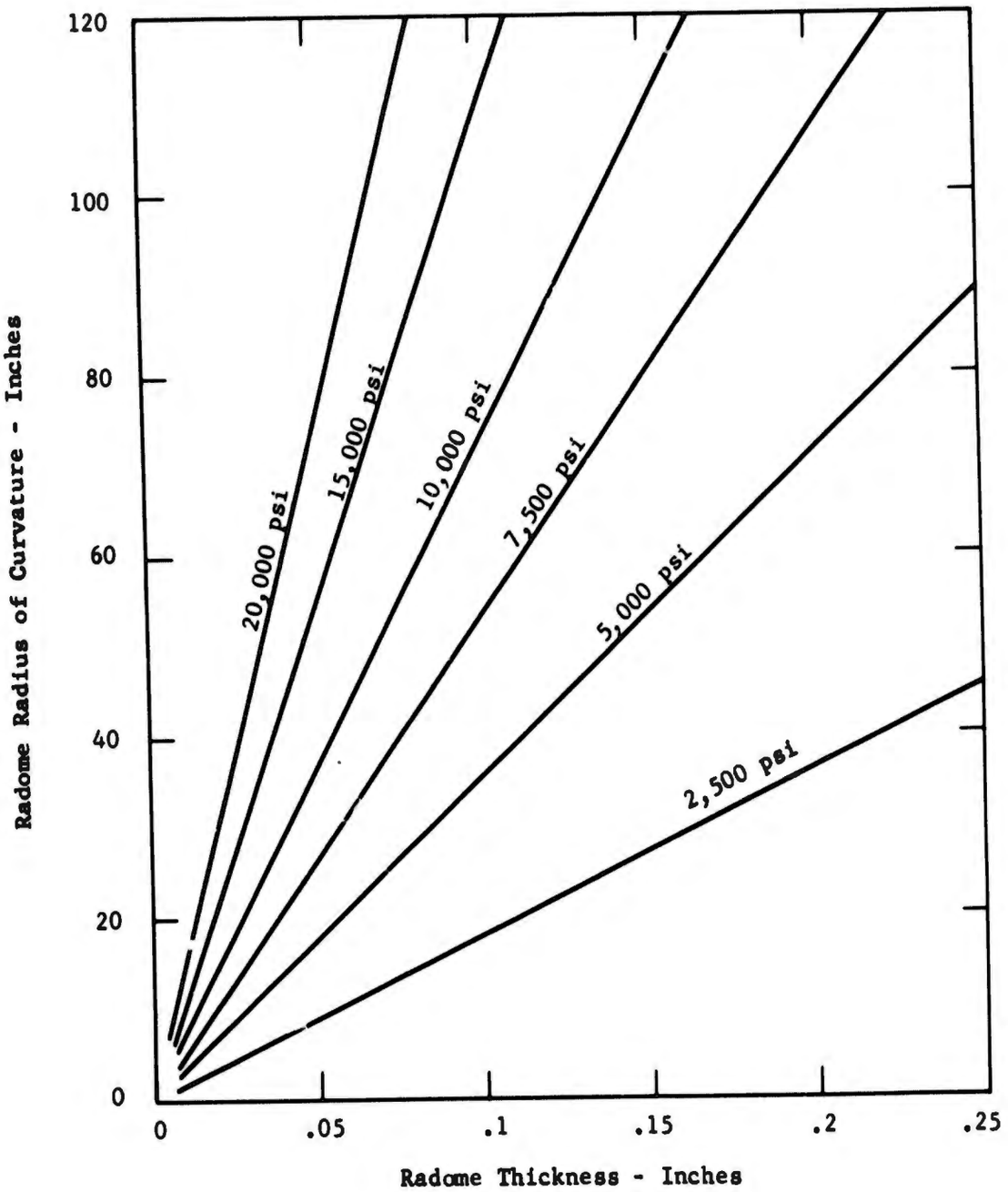

Figure 7.4 Bending Stress in a Spherical Radome Due to Rigid Attachment. 40" Circular Diameter Aperture, 2 Atmospheres (Gauge) Internal Pressure.

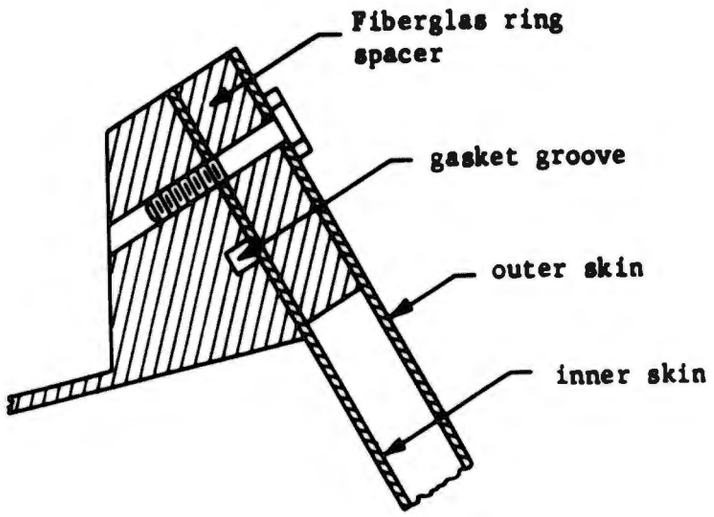

Horn Flange Detail

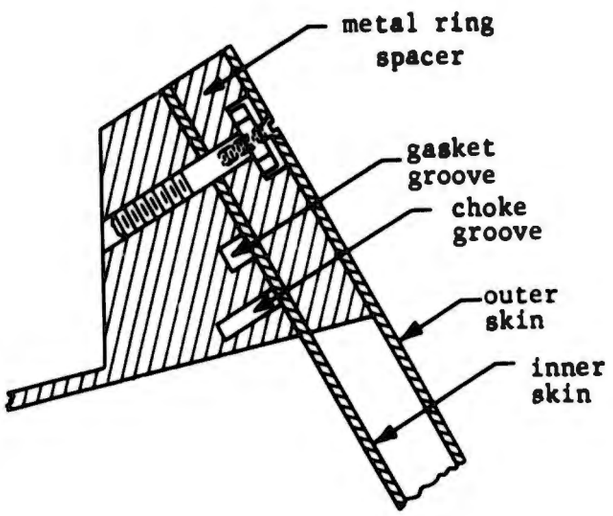

Horn Flange Modified for
Horn Continuation

Figure 7.5 Detail of Horn Flange.

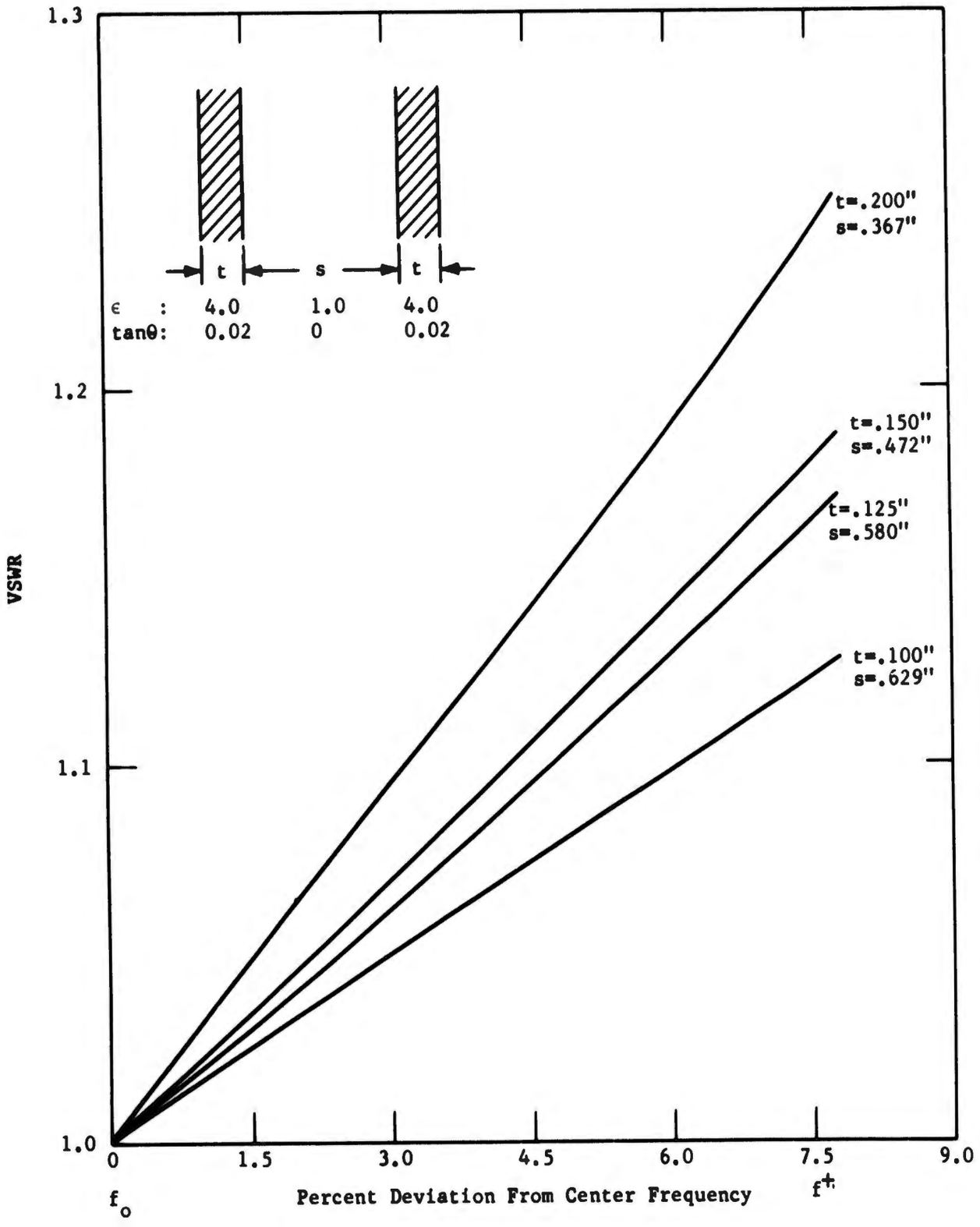

Figure 7.6 Calculated VSWR of Two Layer Radomes.

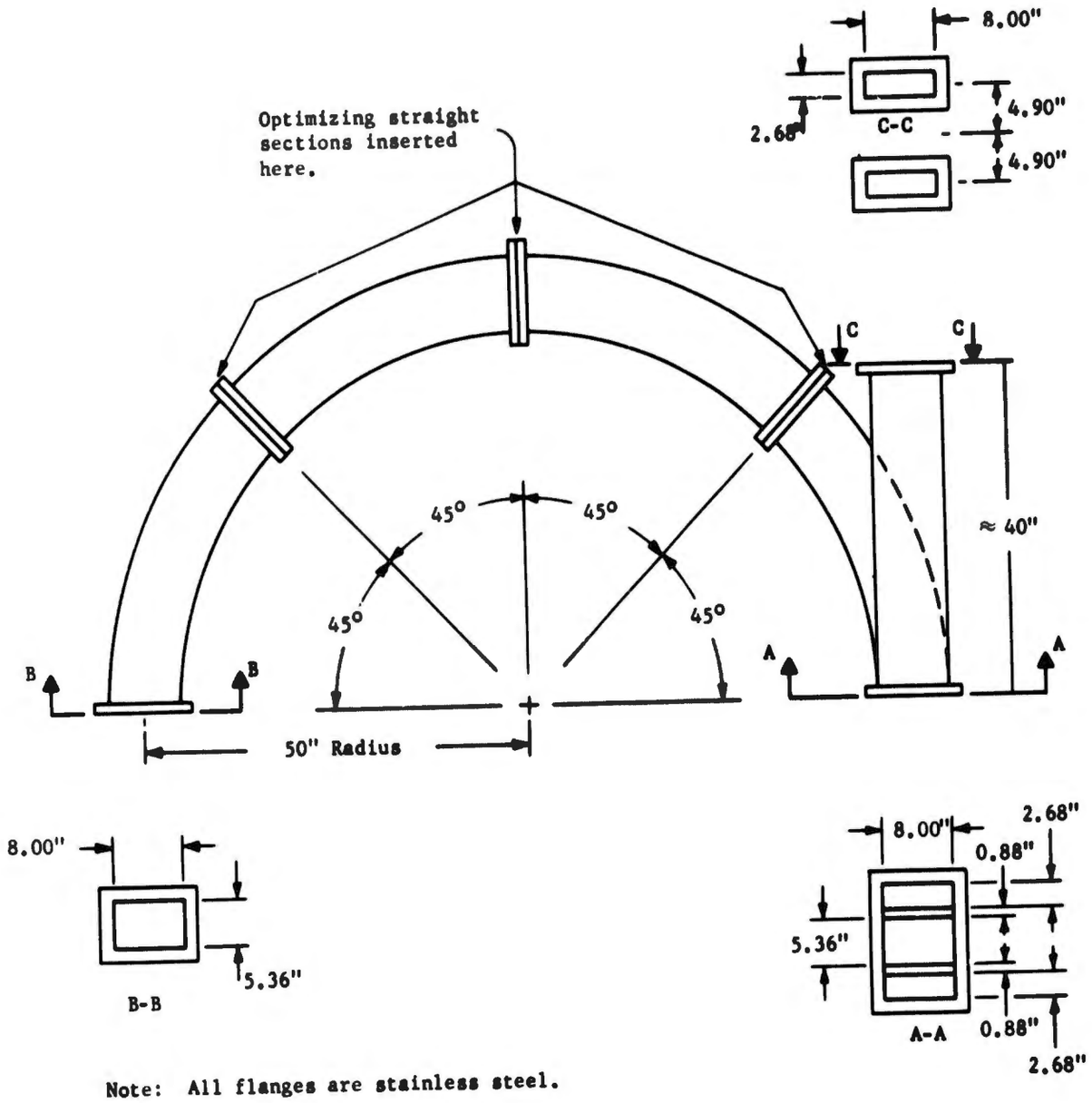

Note: All flanges are stainless steel.

Figure 8.1 H-Plane-Bend Assembly

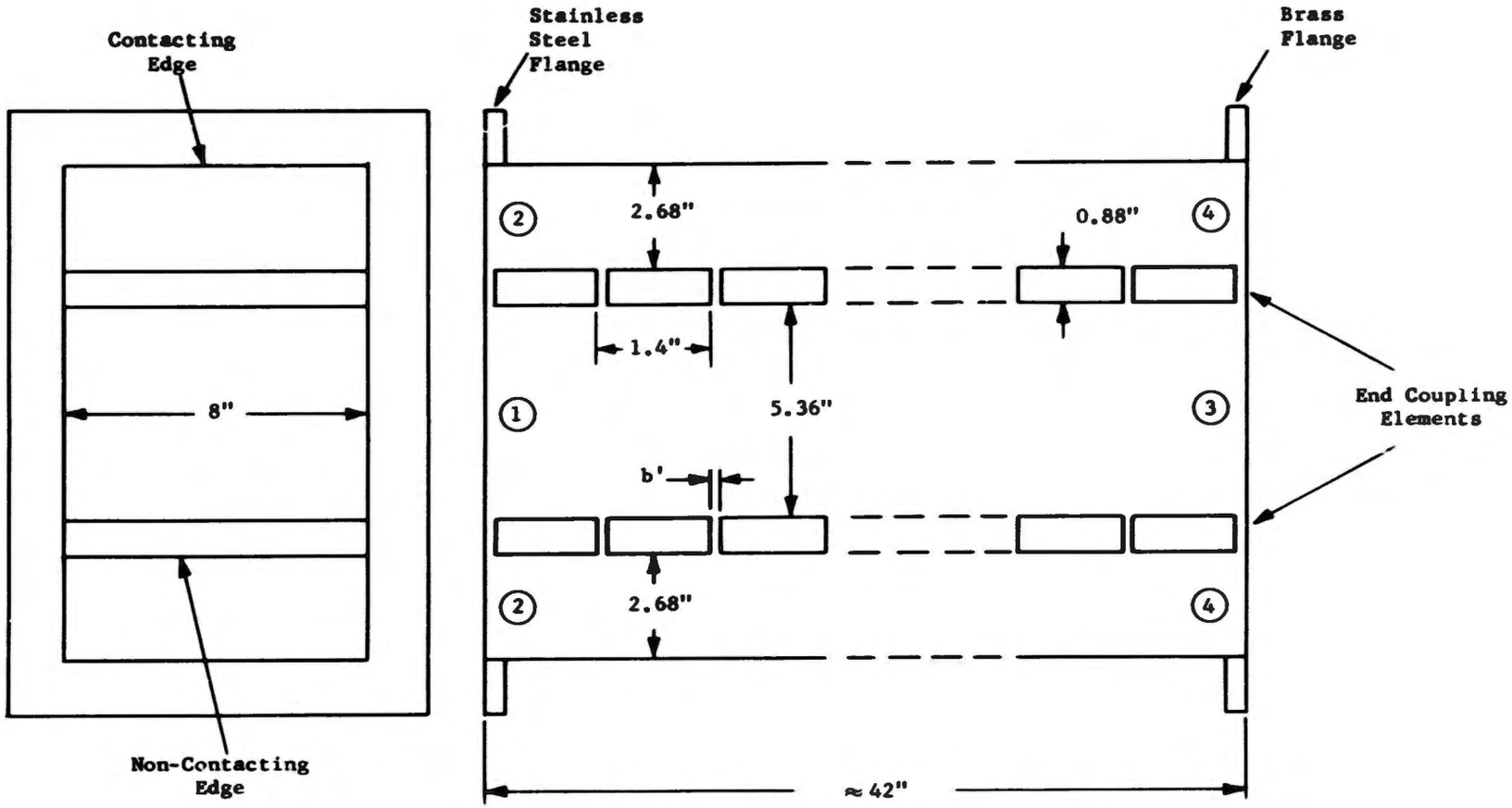

Figure 8.2 Balanced Top-Wall 3-dB Coupler
For 8.00" x 5.36" Oversize Waveguide.

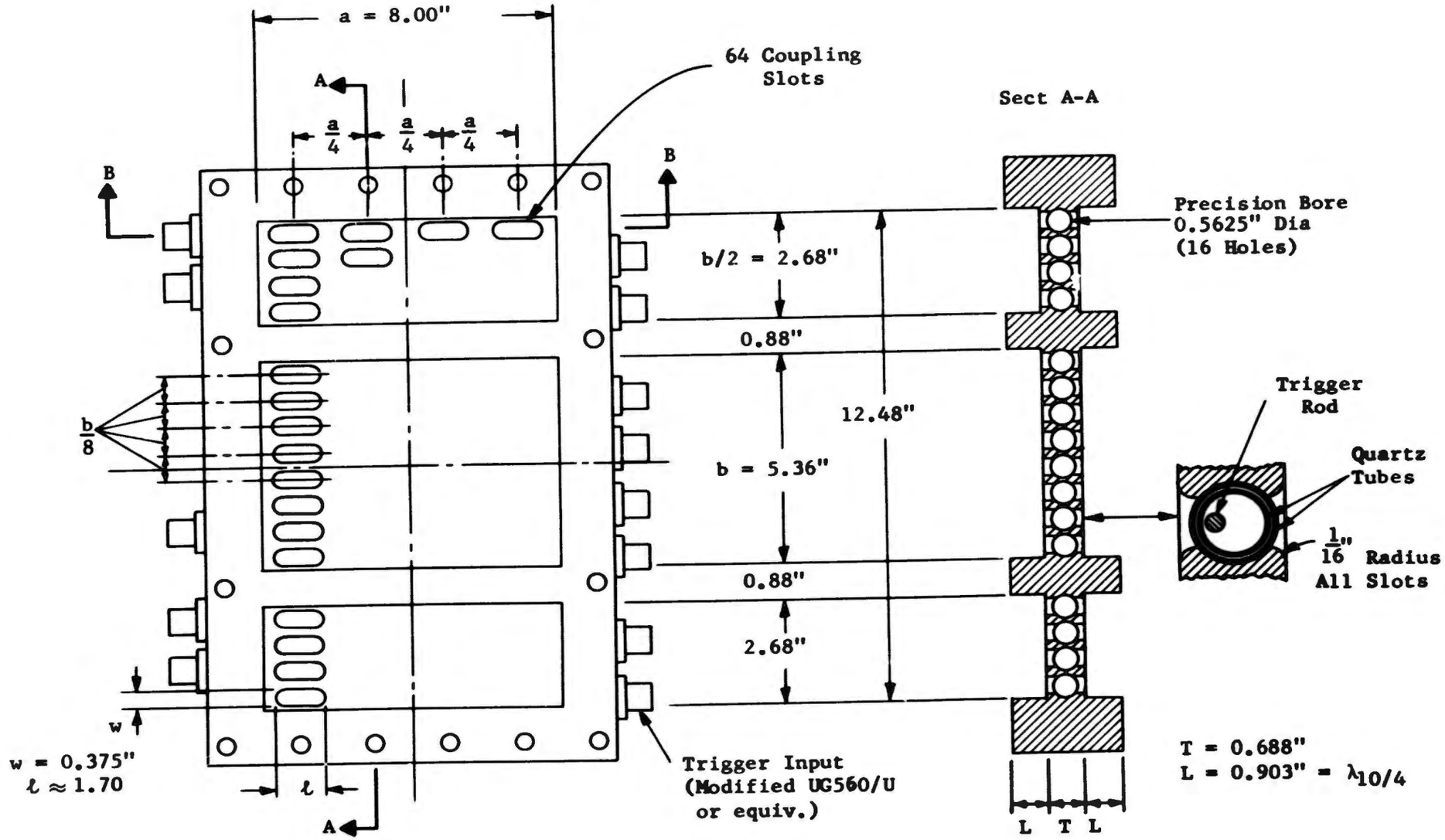

Figure 8.3 Duplexer Tube Mount.

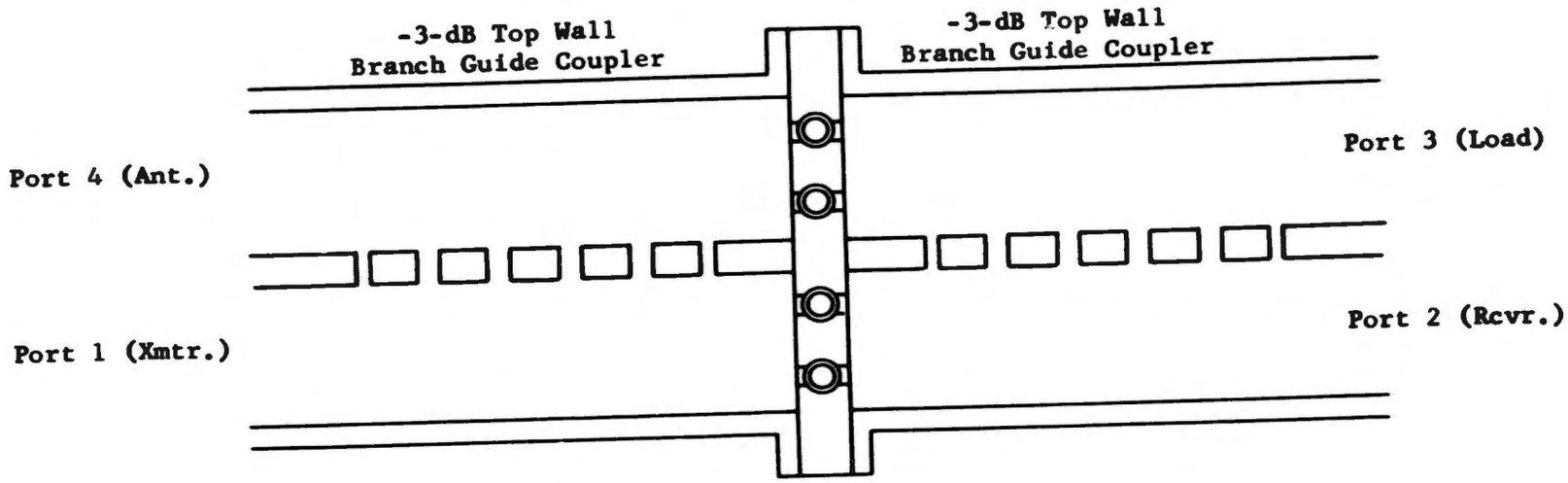

Figure 8.4 Flat-Waveguide Duplexer Configurations Showing Port Designations.

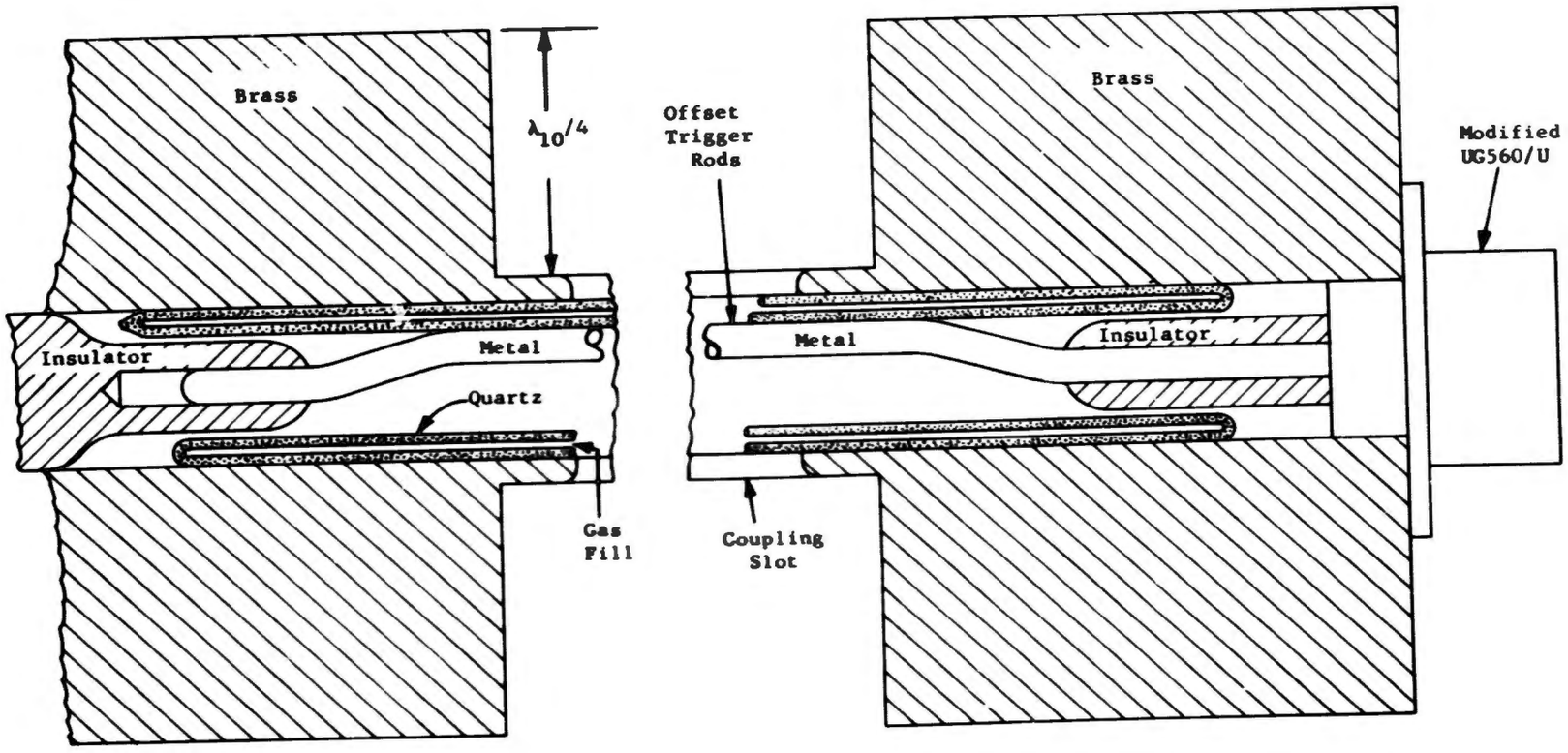

Figure 8.5 Details of Gas Tubes and Pre-Trigger Rods (Section B-B of Fig. 4).

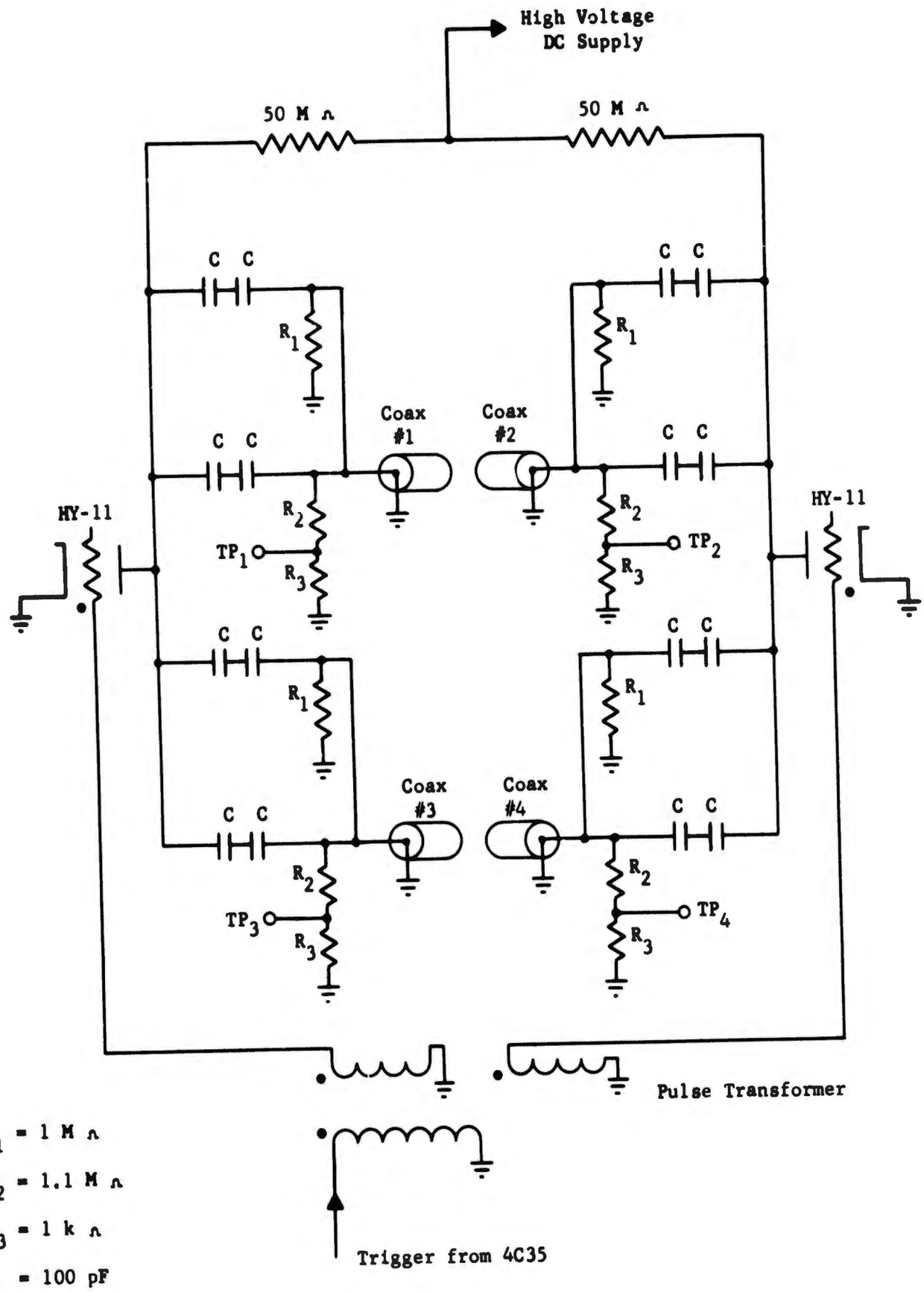

Figure 8.6 dc Pulse Generator Circuit for Duplexer.

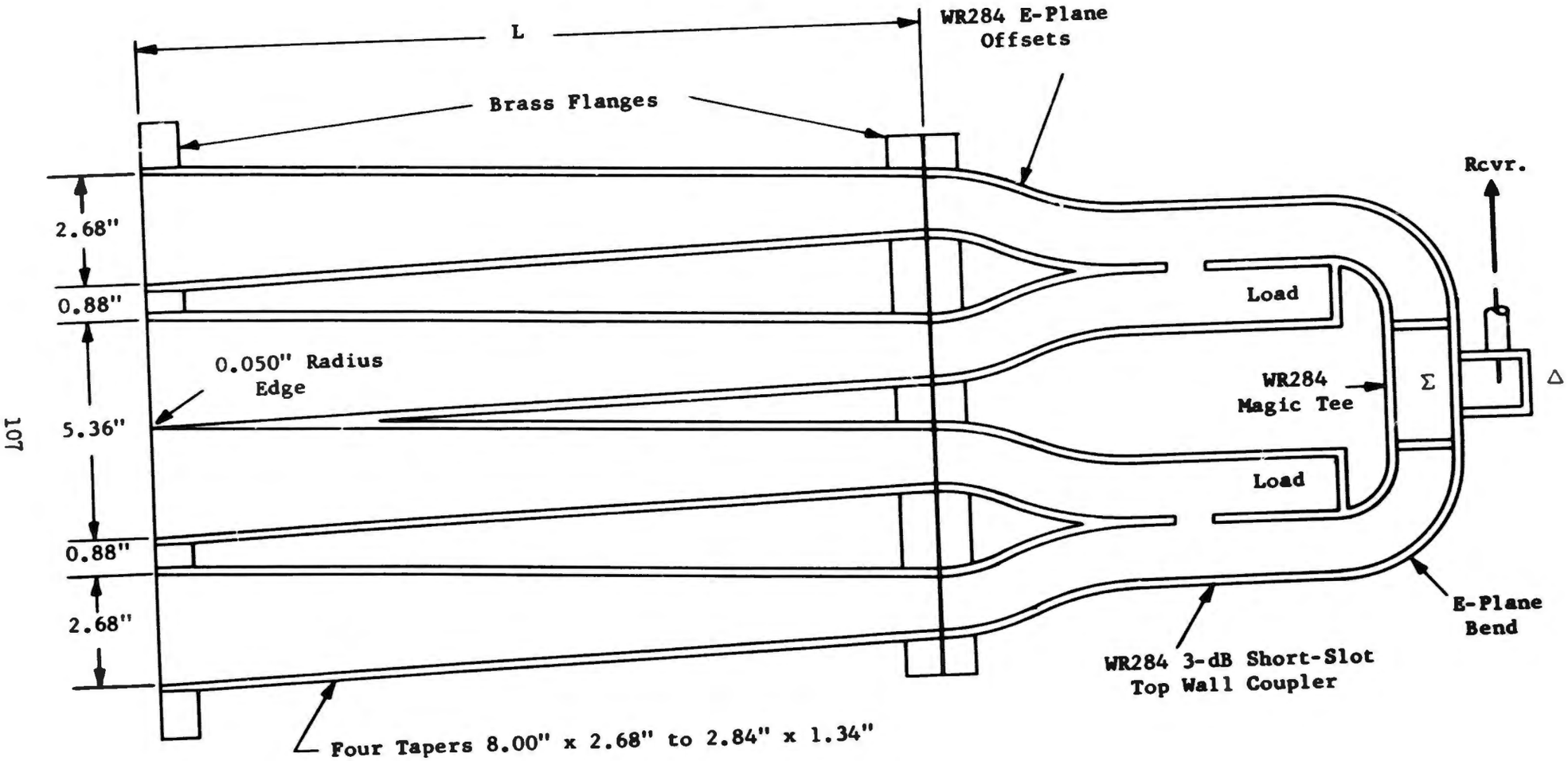

Figure 8.8 Low-Power Receiver-Output Section.

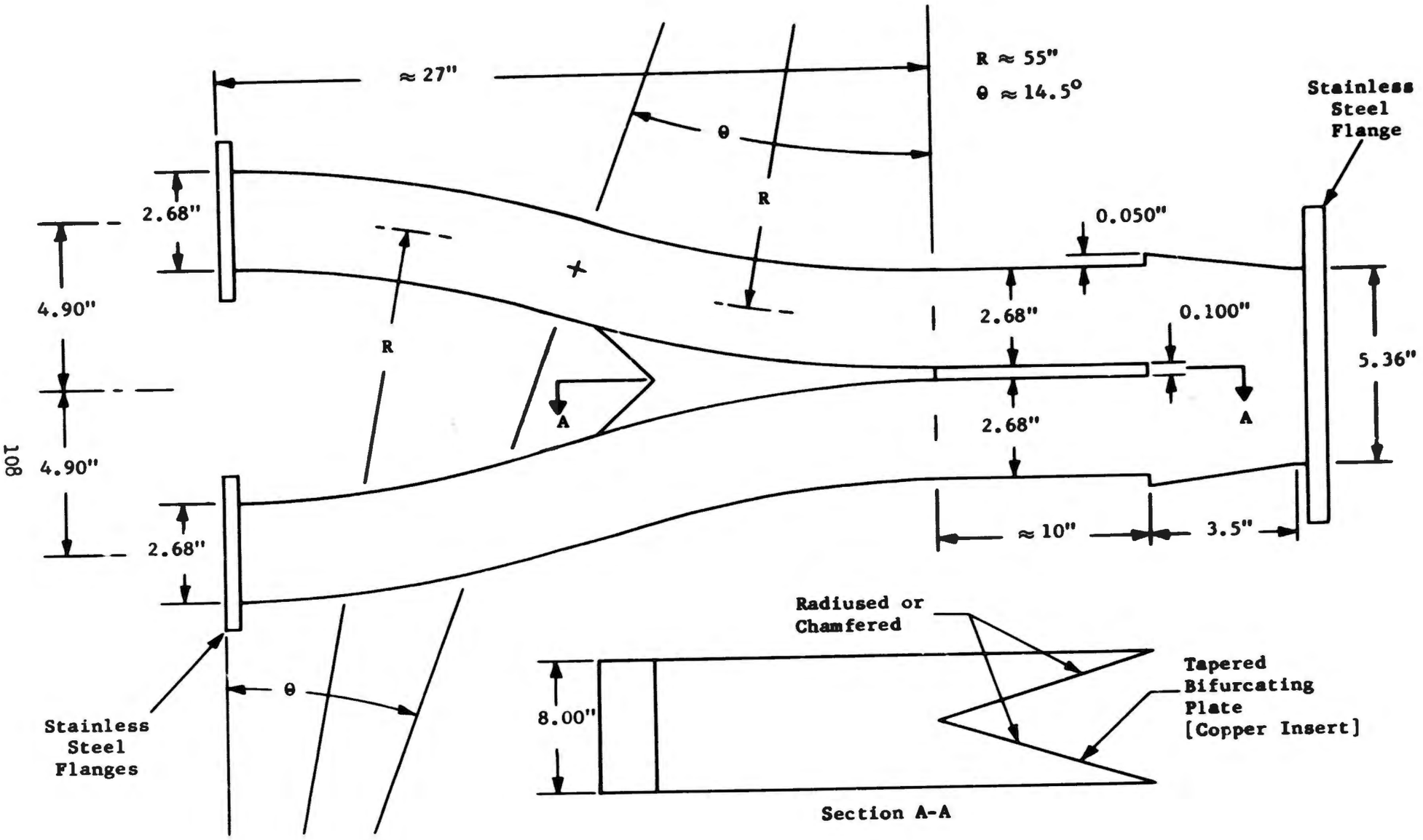

Figure 8.9 High-Power-Combiner Output Section.

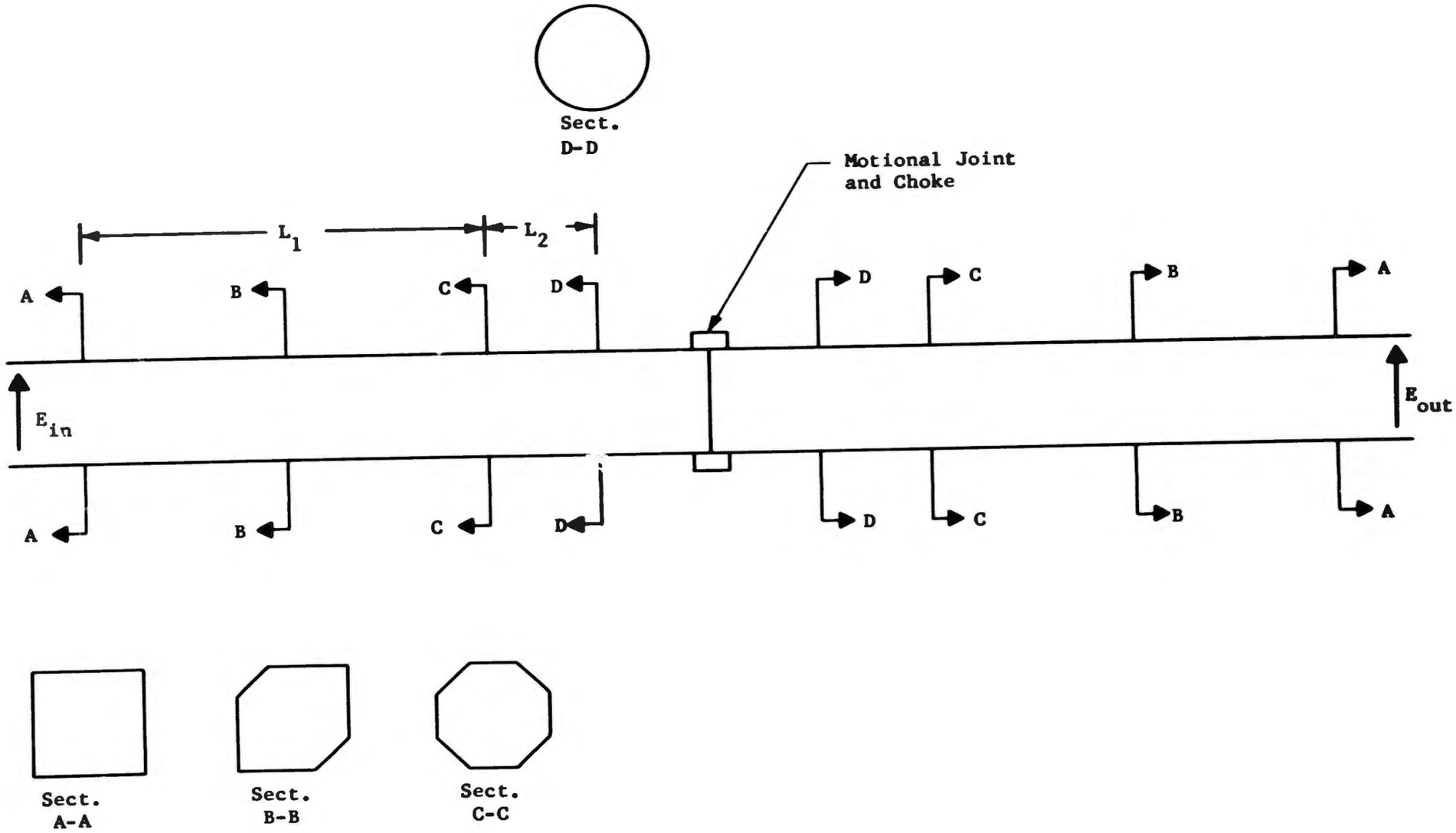

Figure 9.1 Circularly Polarized TE_{11}^{o} Mode Rotary Joint.

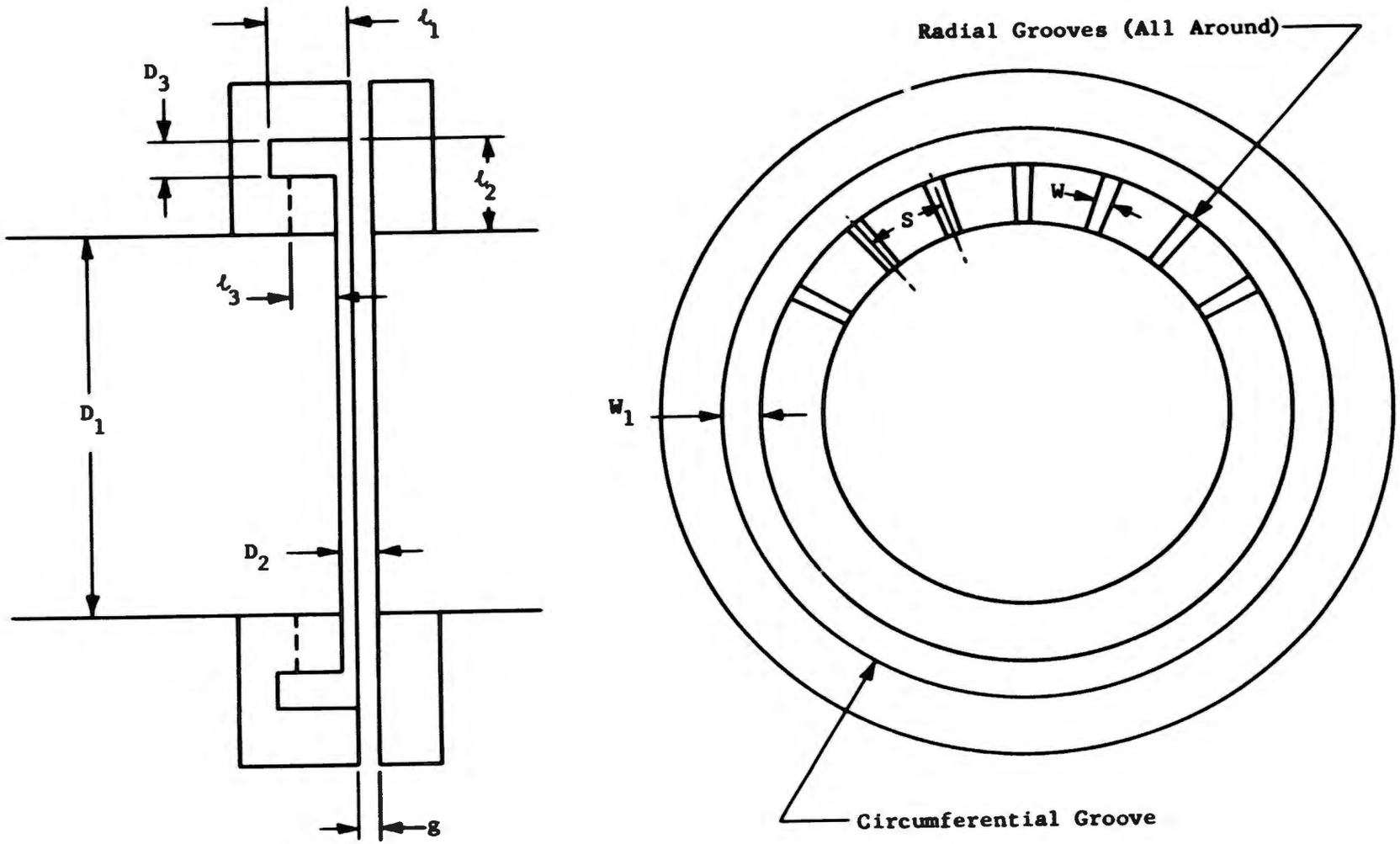

Figure 9.2 Reactive Choke Joint for Circular Waveguide.

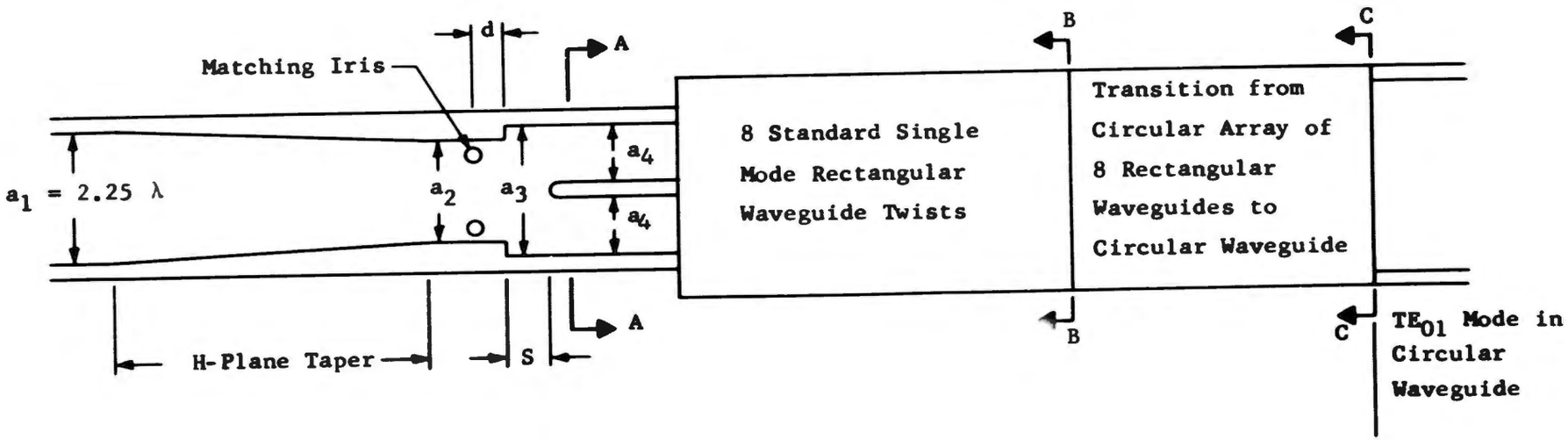

Arrows Indicate Direction of Electric Field

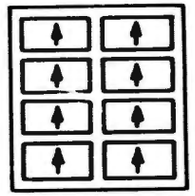

Section A-A
(E and H-Plane Bifurcation)

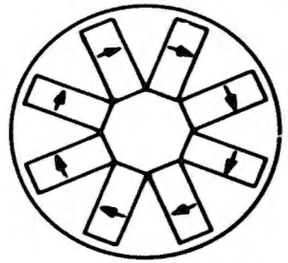

Section B-B

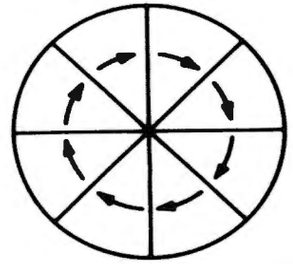

Section C-C

Figure 9.3 Transducer from $TE_{10}^{\square}$ Mode in Oversize Rectangular Waveguide to TE_{01}^{o} Mode in Circular Waveguide.

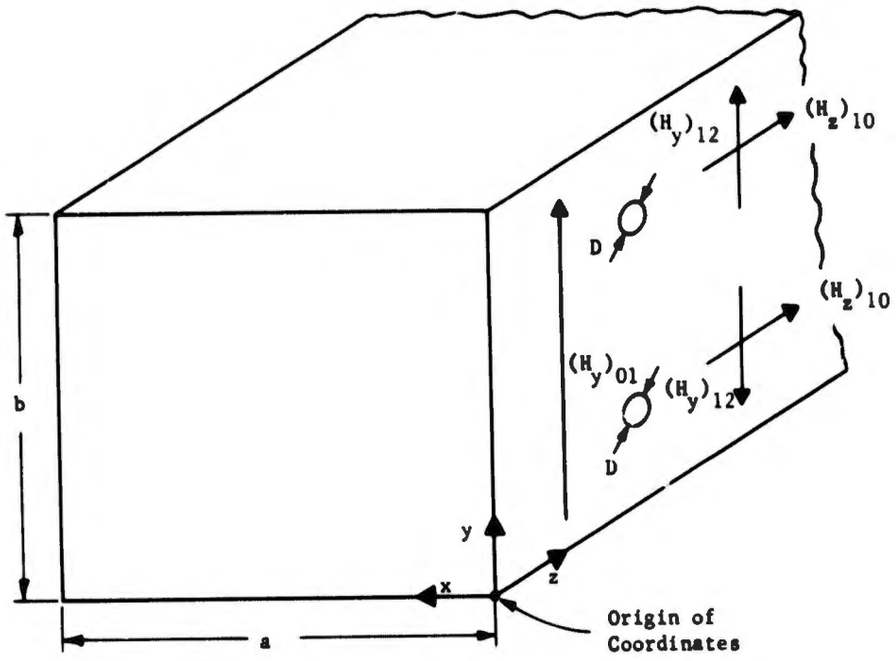

(a) Magnetic-Field Directions at Coupling Holes

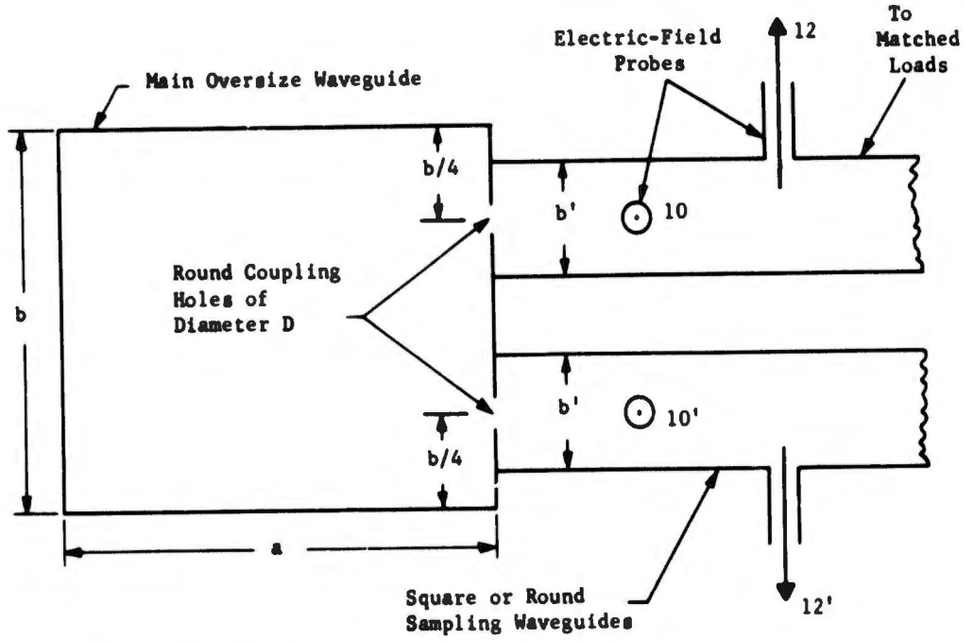

(b) Method of Coupling to Oversize Waveguide

Figure 10.1 Configuration for Measuring TE_{10} and LSE_{12} Modes.

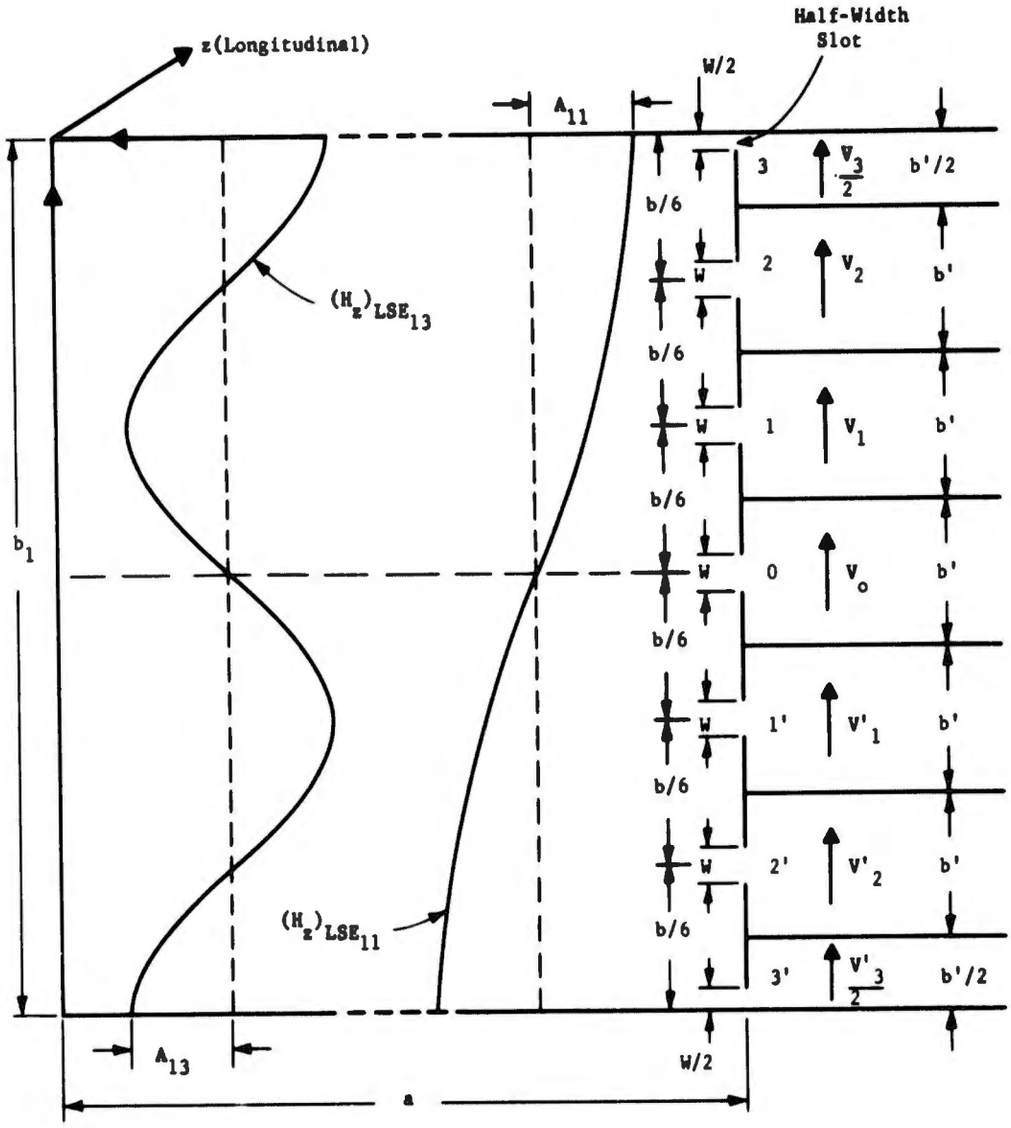

Figure 10.2 Method for Measuring the TE_{10}, LSE_{11} and LSE_{13} Modes.

UNCLASSIFIED

Security Classification

DOCUMENT CONTROL DATA - R & D

(Security classification of title, body of abstract and indexing annotation must be entered when the overall report is classified)

1. ORIGINATING ACTIVITY (Corporate author)
General Electric Co.
R&D Center
Schenectady, N.Y.

2a. REPORT SECURITY CLASSIFICATION
Unclassified

2b. GROUP

3. REPORT TITLE
NANOSECOND RADAR-OVERSIZE WAVEGUIDE SYSTEM (NAROWS)

4. DESCRIPTIVE NOTES (Type of report and inclusive dates)
Final Tech. Report 15 October 1968 to 15 May 1969

5. AUTHOR(S) (First name, middle initial, last name)
Cousby Younger John W. Maurer
John P. Quine
A. E. Blume

6. REPORT DATE
September 1969

7a. TOTAL NO. OF PAGES
127

7b. NO. OF REFS
27

8a. CONTRACT OR GRANT NO.
F30602-69-C-0066

b. PROJECT NO.
4506

Task No.
450602

d.

9a. ORIGINATOR'S REPORT NUMBER(S)

9b. OTHER REPORT NO(S) (Any other numbers that may be assigned this report)
RADC-TR-69-253

10. DISTRIBUTION STATEMENT
This document has been approved for public release and sale; its distribution is unlimited.

11. SUPPLEMENTARY NOTES

12. SPONSORING MILITARY ACTIVITY
Rome Air Development Center (EMATP)
Griffiss Air Force Base, New York 13440.

13. ABSTRACT

This report summerizes the results of a six month study to determine the optimum configurations for the components of a feed system for a high-power nanosecond-pulse high-resolution S-Band radar system. The system employs 8.00 X 5.36 inch oversize rectangular waveguide. Developmental model system components including power combiners, load switches, straight waveguides, H-plane, bends, horn radiators, and horn radomes are described. The breadboard model system consisting of duplexers rotory joints and sampling couplers is also described.

DD FORM 1 NOV 65 1473

UNCLASSIFIED

Security Classification

UNCLASSIFIED
Security Classification

14 KEY WORDS	LINK A		LINK B		LINK C	
	ROLE	WT	ROLE	WT	ROLE	WT
High Power						
Low Dispersion						
Oversize Waveguide						
Microwave Components						

UNCLASSIFIED
Security Classification

AFLC—Griffiss AFB NY 26 Sep 69-78